

DOUBLE RESONANCE SPECTROSCOPY AS A DIAGNOSTIC TOOL  
AND ANALYTICAL TECHNIQUE FOR ATOMIC SPECTROSCOPY

BY

MOI BON LEONG

A DISSERTATION PRESENTED TO THE GRADUATE SCHOOL  
OF THE UNIVERSITY OF FLORIDA IN  
PARTIAL FULFILLMENT OF THE REQUIREMENTS  
FOR THE DEGREE OF DOCTOR OF PHILOSOPHY

UNIVERSITY OF FLORIDA

1988

Dedicated to my father, my brother, and my sister for their undying support and trust in me. In memory of my mother who did not live to see the growth of her son but will always be remembered by him for the time she spent when she was here.

## ACKNOWLEDGMENTS

I would like to sincerely thank Dr. James D. Winefordner for his guidance, inspiration, and encouragement during my three and one half years in the finest spectroscopy group anywhere. It has been both a learning experience and a great joy to work with such a distinguished and friendly individual. I would like to thank you for the opportunity.

I would like to acknowledge Dr. Benjamin Smith and Dr. Nicolo Omenetto for their invaluable support and help as well as their wisdom and guidance.

Lastly, I would like to thank the friends that I have made during my quest, because without them it would not have been nearly as fun and enjoyable. Of this host of friends, I especially thank the clan for allowing me to eat with them. Thanks for the good times, and I hope we remain friends and not strangers. I hope to see you down the road: Brad, Tony, Benny, Jorge, Tom, Mark, Mike M., Mike R., Wellington, Richard, Chris, Joe, Ben, Andres, Doug, Leigh Ann, Tiing, the secretaries (Jeanne, Chris, Susan, and Robin), and Dave Berberich.

# TABLE OF CONTENTS

	<u>Page</u>
ACKNOWLEDGMENTS.....	iii
LIST OF TABLES.....	vi
LIST OF FIGURES.....	vii
ABSTRACT.....	xii
CHAPTERS	
1 INTRODUCTION.....	1
Basic Principles of Two-Photon Methods.....	1
Brief Review of Double Resonance Spectroscopy for Atomic Species.....	4
Intent of Dissertation.....	5
2 FLUORESCENCE DIP SPECTROSCOPY FOR THE MEASUREMENT OF ATOMIC PARAMETERS.....	8
Introduction to Fluorescence Dip Spectroscopy.....	8
Experimental Facilities and Considerations.....	17
Results and Discussion.....	25
Conclusions.....	55
3 ATOMIC FLUORESCENCE AND IONIZATION MECHANISM FOR LEAD IN AIR-ACETYLENE FLAME.....	61
Basic Principles of Atomic Fluorescence and Ionization Spectroscopies.....	61
Experimental Facilities and Considerations.....	64
Results and Discussion.....	69
Conclusions.....	79
4 MEASUREMENT OF ATOMIC FLUORESCENCE FOR LEAD IN A GRAPHITE TUBE ATOMIZER.....	81
Introduction to Graphite Tube Atomizers.....	81
Brief Review of Atomic Fluorescence Using Graphite Furnace Atomization.....	83

	Experimental Facilities and Considerations.....	85
	Results and Discussion.....	94
	Conclusions.....	108
5	FINAL COMMENTS AND FUTURE WORK.....	111
APPENDICES		
A	GLOSSARY OF TERMS AND SYMBOLS.....	114
B	LIMITING CASES FROM FIGURE 2-4.....	116
C	SAHA EQUATION.....	117
	REFERENCES.....	118
	BIOGRAPHICAL SKETCH.....	125

# LIST OF TABLES

<u>Table</u>	<u>Page</u>
2-1 Experimental Components for Fluorescence Dip Spectroscopy.....	19
2-2 Experimental Parameters for Fluorescence Dip Spectroscopy.....	23
2-3 Comparison of Gate Widths with Respect to Slope, Intercept, and $r^2$ Correlation Coefficient.....	30
2-4 Comparison of Relative (Ratio) of Atomic Parameters.....	43
2-5 Comparison of Steady State Saturation Dip Parameter with Respect to the Second Laser Excitation Wavelength....	54
3-1 Experimental Components for Laser Enhanced Ionization and Laser Excited Atomic Fluorescence Spectroscopies.....	66
3-2 Experimental Parameters for Laser Enhanced Ionization and Laser Excited Atomic Fluorescence Spectroscopies.....	70
4-1 Experimental Components for Double Resonance Laser Excited Atomic Fluorescence in a Graphite Tube Atomizer.....	87
4-2 Experimental Parameters for Double Resonance Laser Excited Atomic Fluorescence in a Graphite Tube Atomizer.....	93
4-3 Peak Fluorescence Signals for 100 pg of Lead and Related Noise Figures.....	103
4-4 Laser Excited Atomic Fluorescence of Lead in a Graphite Tube Atomizer: Absolute Detection Limits as Obtained by Single Step and Two-Step Excitation.....	105

## LIST OF FIGURES

<u>Figure</u>	<u>Page</u>
1-1	Diagrammatic Representations of (a-c) Two-Photon and (d) Double Resonance Excitation Schemes.....2
1-2	Double Resonance Excitation Schemes Followed by (a) Fluorescence or (b) Ionization Detection.....6
2-1	Generic Energy Level Diagram for Fluorescence Dip Spectroscopy.....9
2-2	Cross-Sectional Area of the Atomizer Including Excitation Beam and Fluorescence Geometry and Prefilter and Postfilter Effects.....11
2-3	Rate Expressions for a Three-Level System.....13
2-4	Expression for the Steady State Population of the First Excited State in Terms of the Radiative and Collisional Rate Coefficients.....14
2-5	Theoretical Expressions for Fluorescence Dip Spectroscopy for the Limiting Case of Optical Saturation of the First Transition.....15
2-6	Block Diagram of Experimental Setup for Fluorescence Dip Spectroscopy.....18
2-7	Partial Energy Level Diagram for Sodium.....21
2-8	Scan of the Second Excitation Laser Through the Upper Level Transitions of Sodium at 0.10 mJ per Pulse with the Fluorescence Wavelength at 589.6 nm.....26
2-9	Scan of the Second Excitation Laser Through the Upper Level Transitions of Sodium at 0.73 mJ per pulse with the Fluorescence Wavelength at 589.6 nm.....27
2-10	Scan of the Second Excitation Laser Through the Upper Level Transitions of Sodium at 8.33 mJ per pulse with the Fluorescence Wavelength at 589.6 nm.....28

2-11	Plot of the Relative Dip and the Relative Fluorescence Intensity as a Function of Observation Height Above the Load Coil.....	31
2-12	Measurement of the Relative Fluorescence Intensity at 588.995 nm With and Without the Second Laser at 568.266 nm as a Function of the Second Laser Irradiance...	33
2-13	Measurement of the Relative Fluorescence Intensity at 589.592 nm With and Without the Second Laser at 568.266 nm as a Function of the Second Laser Irradiance...	34
2-14	Reciprocal Plot of Relative Dip vs Spectral Energy Density with 2 ns Gate Width and 568.3 nm Transition.....	35
2-15	Reciprocal Plot of Relative Dip vs Spectral Energy Density with 2 ns Gate Width and 568.8 nm Transition.....	36
2-16	Reciprocal Plot of Relative Dip vs Spectral Energy Density with 4 ns Gate Width and 568.3 nm Transition.....	37
2-17	Reciprocal Plot of Relative Dip vs Spectral Energy Density with 4 ns Gate Width and 568.8 nm Transition.....	38
2-18	Reciprocal Plot of Relative Dip vs Spectral Energy Density with 600 ns Gate Width and 568.3 nm Transition....	39
2-19	Reciprocal Plot of Relative Dip vs Spectral Energy Density with 600 ns Gate Width and 568.8 nm Transition....	40
2-20	Theoretical Reciprocal Plot of Relative Dip vs Spectral Energy Density.....	41
2-21	Plot of Relative Dip vs Spectral Energy Density with 589.0 and 568.3 nm Excitation and Fluorescence Detection at 589.0 nm.....	44
2-22	Plot of Relative Dip vs Spectral Energy Density with 589.0 and 568.3 nm Excitation and Fluorescence Detection at 589.6 nm.....	45
2-23	Plot of Relative Dip vs Spectral Energy Density with 589.0 and 568.8 nm Excitation and Fluorescence Detection at 589.0 nm.....	46
2-24	Plot of Relative Dip vs Spectral Energy Density with 589.0 and 568.8 nm Excitation and Fluorescence Detection at 589.6 nm.....	47



2-25	Plot of Relative Dip vs Spectral Energy Density with 589.6 and 568.3 nm Excitation and Fluorescence Detection at 589.0 nm.....	48
2-26	Plot of Relative Dip vs Spectral Energy Density with 589.6 and 568.3 nm Excitation and Fluorescence Detection at 589.6 nm.....	49
2-27	Plot of Relative Dip vs Spectral Energy Density with 589.6 and 568.8 nm Excitation and Fluorescence Detection at 589.0 nm.....	50
2-28	Plot of Relative Dip vs Spectral Energy Density with 589.6 and 568.8 nm Excitation and Fluorescence Detection at 589.6 nm.....	51
2-29	Theoretical Plot of Relative Dip vs Spectral Energy Density.....	53
2-30	Partial Energy Level Diagram for Palladium.....	57
2-31	Measurement of Relative Fluorescence Intensity at 344.1 nm With and Without Laser Excitation at 565.5 nm as a Function of Laser Irradiance.....	58
2-32	Partial Energy Level Diagram for Calcium (II) Ion.....	60
3-1	The Three Basic Pathways of Atomic Fluorescence: a) Resonance Fluorescence, b) Direct Line Fluorescence, and c) Stepwise Line Fluorescence.....	62
3-2	Block Diagram of Experimental Setup for Laser Enhanced Ionization and Laser Excited Atomic Fluorescence Spectroscopies.....	65
3-3	Partial Energy Level Diagram for Connected Double Resonance Excitation and Ionization of Lead.....	67
3-4	Partial Energy Level Diagram for Connected Double Resonance Excitation of Lead.....	71
3-5	Scan of the Second Excitation Laser With the Fluorescence Wavelength at 239.379 nm and the First Excitation Laser at 283.306 nm for Lead.....	73
3-6	Scan of the Second Excitation Laser With the Fluorescence Wavelength at 261.418 nm and the First Excitation Laser at 283.306 nm for Lead.....	74

3-7	Temporal Behavior of the Ionization Signal as Recorded by the Oscilloscope With Full Laser Irradiance in Both Beams (283.306 and 600.193 nm).....	76
3-8	Temporal Behavior of the Ionization Signal as Recorded by the Oscilloscope with the Laser Irradiance at 600.193 nm Decreased by a 100-Fold and the 283.306 nm Laser Irradiance Unchanged.....	78
4-1	Graphite Furnace Designs.....	82
4-2	Block Diagram of the Double Resonance Laser Excited Atomic Fluorescence in a Graphite Tube Atomizer.....	86
4-3	Graphite Tube Atomizer Setup.....	90
4-4	Chart Recorder Tracings of the Furnace Emission Noise at the Four Fluorescence Wavelengths Investigated in this Work: a) 405.783 nm, b) 261.418 nm, c) 239.379 nm, and d) 216.999 nm.....	97
4-5	Boxcar Output for Laser Induced Noise into the Detector System for Single Resonance Excitation at 283.306 nm and Fluorescence Wavelength at 405.783 nm: a) 10% Transmission Neutral Density Filter Placed Between the Laser and the Graphite Furnace and b) 1% Transmission Neutral Density Filter Placed as in a.....	98
4-6	Boxcar Output for Laser Induced Noise into the Detector System for Double Resonance Excitation at 283.306 and 600.193 nm and Fluorescence Wavelength at 216.999 nm: a) Laser Operated at Full Power, b) 10% Transmission Neutral Density Filter Placed Between the First Laser (283.306 nm) and the Graphite Furnace, c) 1% Transmission Neutral Density Filter Placed as in b.....	99
4-7	Boxcar Output for Fluorescence of 100 pg of Lead With Excitation at 283.306 and 600.193 nm and the Fluorescence Wavelength at 216.999 nm: a) Both Laser Operated at Full Power, b) 10% Transmission Neutral Density Filter Placed Between the First Laser (283.306 nm) and the Graphite Furnace, and c) 1% Transmission Neutral Density Filter Placed as in b.....	102
4-8	Partial Energy Level Diagram for Disconnected Double Resonance Excitation of Lead.....	106

4-9	Comparison of Connected and Disconnected Double Resonance Excitation of Lead.....	108
-----	--	-----

Abstract of Dissertation Presented to the Graduate School  
of the University of Florida in Partial Fulfillment of the  
Requirements for the Degree of Doctor of Philosophy

DOUBLE RESONANCE SPECTROSCOPY AS A DIAGNOSTIC TOOL  
AND ANALYTICAL TECHNIQUE FOR ATOMIC SPECTROSCOPY

BY

MOI BON LEONG

April, 1988

Chairman: James D. Winefordner  
Major Department: Chemistry

Double resonance spectroscopy is a technique whereby two lasers (i.e., two-color) are used to excite two real and different atomic transitions in a species of interest. The first step of the excitation process is the absorption of photons by the atomic species to the first excited state from the ground state. This is subsequently followed by a secondary absorption of photons from the first excited state to the second excited state. Once the atomic species have reached the second excited state, there are several methods for monitoring the events that occur, among these are ionization and fluorescence measurements. In the present study, three different measurement methods are used with three different atomization cells. The measurements demonstrate the usefulness of double resonance excitation processes as a diagnostic tool for flames, plasmas, and possibly, graphite furnaces, as well as an analytical

method for the measurement of lead at femtogram levels in a graphite tube atomizer.

## CHAPTER 1 INTRODUCTION

### Basic Principles of Two-Photon Methods

The development of pump lasers such as the nitrogen, excimer (i.e., XeCl), and Nd:YAG (Neodymium:Yttrium Aluminum Garnet) together with the organic dye laser has opened up the realm of analytical atomic spectroscopy. Because organic dye lasers are not stand-alone instruments, they are always coupled with a pump laser such as the ones mentioned above. A majority of the analytical work to date has thus involved the use of a pump laser in conjunction with an organic dye laser. The addition of a second dye laser to this system has provided the opportunity to perform two-color experiments.

Two-photon excitation methods usually involve a minimum of three levels. These levels, however, are not necessarily real and well-defined (i.e., virtual levels and ionization continuum). Figure 1-1 illustrates several types of two-photon excitation schemes. Two-photon excitation taken in its basic form involves the utilization of the same wavelength twice. The energy from the two photons excites the atom from the ground state to a real excited state via a virtual level that is midway between the ground and real excited states. The real excited state must have the same symmetry and multiplicity as that of the ground state for it to be a two-photon allowed transition as shown in Figure 1-1a. However, as shown in Figures 1-1b and 1-1c,

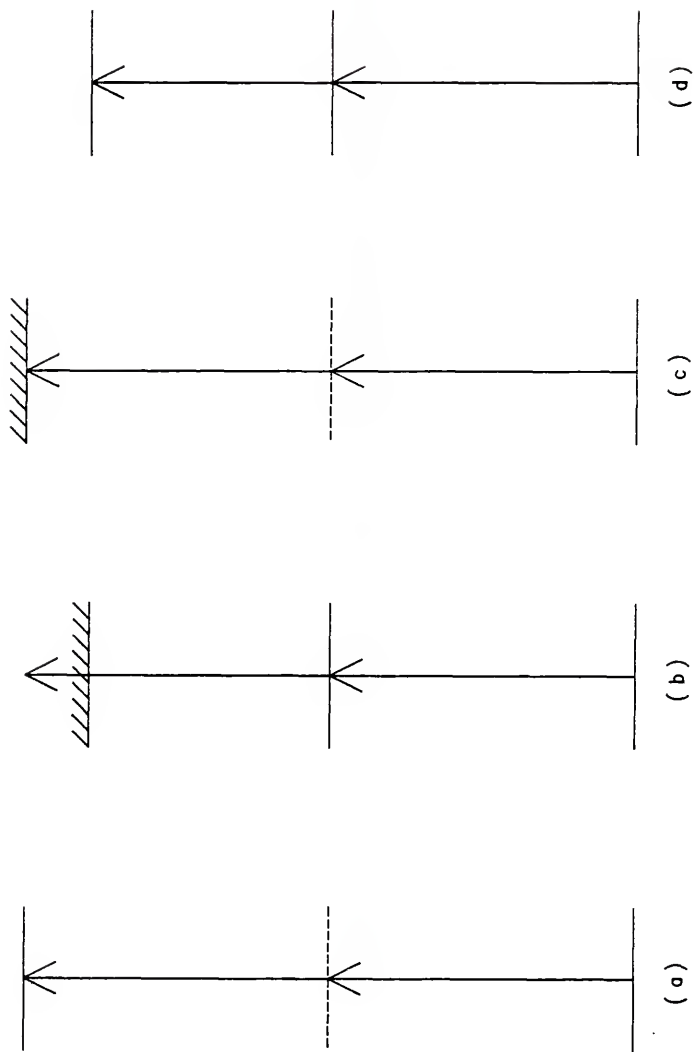


Figure 1-1 Diagrammatic Representations of (a-c) Two-Photon and (d) Double Resonance Excitation Schemes

the ionization continuum can be considered as a level. In both of these cases, the second photon promotes the species of interest from a real or virtual level to the continuum, but not a well-defined level in terms of the specific state (e.g., symmetry and multiplicity) to which the species has been promoted. These cases have been used to investigate atoms that are not easily accessible by one-photon excitation schemes (1-24).

Double resonance excitation is a limiting case of two-photon excitation (25). This excitation scheme incorporates three real, distinct levels. The species of interest absorbs photons of a discrete energy such that excitation occurs from the ground state to the first excited state. Once the species are in the first excited state, a second set of photons with a different and discrete energy than that of the initial excitation is absorbed such that promotion of the species occurs from the first excited state to the second excited state as shown in Figure 1-1d. Thus, all further discussion pertains to this specific excitation scheme.

To populate the first excited state, the wavelength of the first laser is tuned to a resonance transition of the atomic species. This first transition should be saturated; that is, there is an equal population in the ground state and the first excited state due to the laser irradiance. Once this has been attained, an increase in laser irradiance should have no or little effect on the overall distribution between the two states, and hence, fluctuations in laser irradiance have no effect. The second excited state is then populated when the wavelength of the second laser is tuned to the



transition that couples the first and second excited states. Again, saturation is desired but not always necessary because the laser irradiance of the second laser can be varied to provide the optimal performance characteristics of the experiment.

#### Brief Review of Double Resonance Spectroscopy for Atomic Species

The technique of double resonance excitation by two lasers has been growing primarily due to the development of more powerful lasers. With this development, more work has gone into the investigation of atoms in the ultraviolet (200 nm) to the near infrared (~900 nm) regions (26-38). The more powerful pulsed lasers have provided high pumping rates such that the rate of absorption exceeds the radiative and/or radiationless deactivations (25) (e.g., collisional de-excitation). The pumping rate of the first laser, that is, the rate at which the first excited state is populated, must exceed (i.e., beat) the deactivation processes from that first excited state. If this does not occur, then there is not a sufficient number of species in that first excited state to populate, to a great extent, the second excited state.

A majority of the publications to date have been studies of the high lying (Rydberg) states that are close to the ionization continuum (26-28,32,35,36) as well as studies of the fine and hyperfine structures of specific levels (29-31,33,34). More recently, fluorescence and ionization measurements have appeared in the literature with promising and exciting results (39-48).

Fluorescence monitoring from the second excited state to states below the first excited state or even to the ground state as well as those transitions that lie between the first and second excited states (Figure 1-2a) have provided several interesting advantages. These advantages include high selectivity, the detected fluorescence can be blue-shifted relative to both pumping wavelengths (reduction of laser scatter effects), and transition probabilities are generally greater for those transitions originating from the second excited state than the first excited state (39,40). Ionization measurements, e.g., two-color laser enhanced ionization in flames, have provided some of the best detection limits for several elements (41-48) in analytical atomic spectroscopy. The primary advantage was that the atoms were much closer to the ionization continuum than in a one-color situation (Figure 1-2b), and hence, the collisional processes that promoted the atoms into the continuum were significantly increased. In addition to this, there was increased selectivity as well as increased sensitivity by one to three orders of magnitude. Thus, double resonance excitation schemes have opened up new avenues of exploration in analytical spectroscopy.

#### Intent of Dissertation

In this dissertation, double resonance excitation schemes were investigated in three different atomization sources [i.e., flames, inductively coupled plasmas (ICPs), and graphite furnaces] to obtain information about the atomic parameters of elements, mechanistic

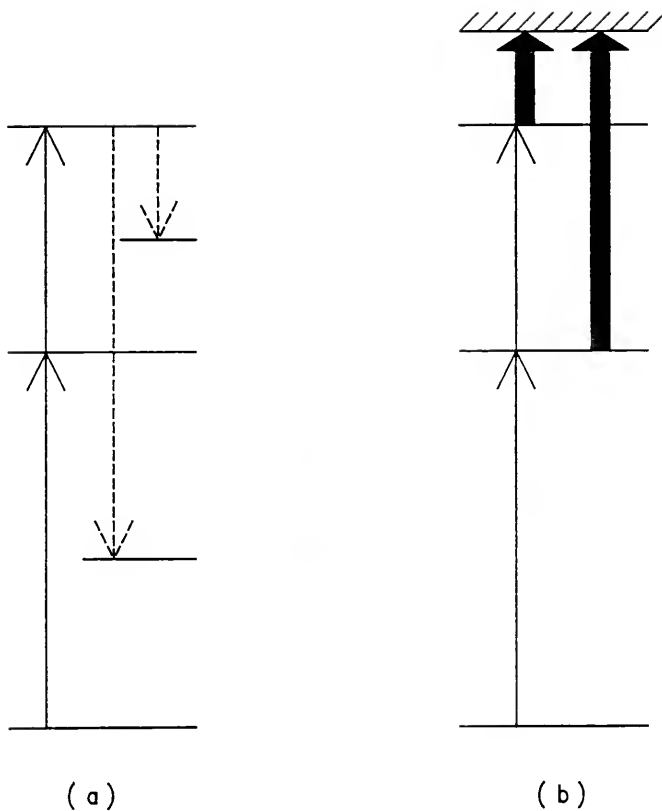


Figure 1-2 Double Resonance Excitation Schemes Followed by (a) Fluorescence or (b) Ionization Detection

studies in laser enhanced ionization (i.e., temporal separation of photoionization and collisional ionization), and the measurement of ultratrace levels of lead by atomic fluorescence. Three different techniques were used to gather this information, and they are discussed individually. These excitation schemes have demonstrated the usefulness and the viability for analytical atomic spectroscopy.

CHAPTER 2  
FLUORESCENCE DIP SPECTROSCOPY FOR THE  
MEASUREMENT OF ATOMIC PARAMETERS

Introduction to Fluorescence Dip Spectroscopy

Principles of Fluorescence Dip

Fluorescence dip is, as the term implies, a dip in the fluorescence. To better explain this phenomenon, it is best illustrated with a generic energy level diagram (Figure 2-1). Atoms are produced from the atomization of a liquid sample, converted to an aerosol and then to a dry particle and finally to submicroscopic species such that the species of interest are lying in their ground state. The first excitation laser is fixed to a resonance transition of the analyte such that the first excited state is populated. The extent of this population should be in an optical saturation mode; that is, both the ground and first excited states are equally populated assuming  $g_1 = g_2$ . The resulting fluorescence from the first excited state, whether it be a resonant or nonresonant situation, is monitored. The second excitation laser is allowed to pass such that this laser beam arrives at the center of the atomization cell temporally and spatially coincident with respect to the first excitation laser beam. This second laser excites atoms from the first to the second excited state.

A fluorescence dip occurs because the first excited state has been depleted. This depletion is a function of the average laser

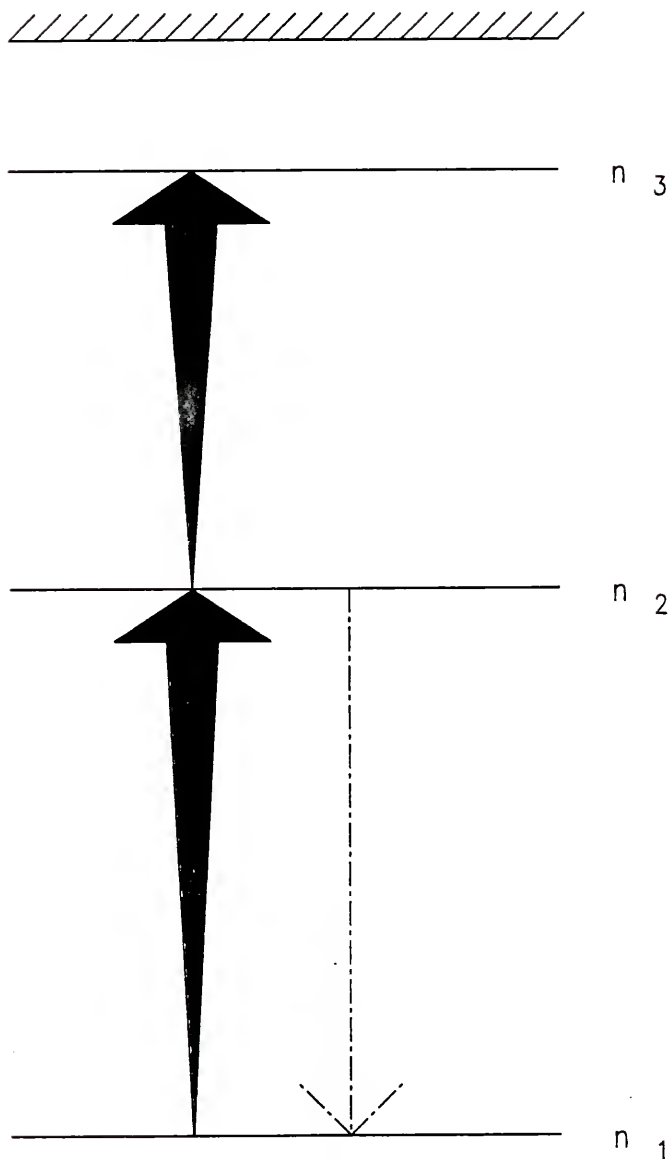


Figure 2-1 Generic Energy Level Diagram for Fluorescence Dip Spectroscopy

irradiance of the second excitation laser. It is important to note that the laser irradiance of the second excitation laser must exceed the radiative and radiationless deactivation pathways from the second excited state.

### Theoretical Considerations

The theory, as proposed by Omenetto et al. (49), was the first general treatment of the fluorescence dip as it pertained to atoms and/or ions in atomic spectroscopy. Several assumptions were made: 1) the time behavior of the laser pulses was approximated by a step-like function, i.e., with a rise time equal to zero; 2) the lasers were spatially homogeneous in the fluorescence volume; 3) the atomic vapor was dilute (no self-absorption, prefilter, and postfilter effects); 4) the spectral bandwidths of the excitation lasers were much greater than the absorption profiles; and 5) the rate equation approach was considered valid; i.e., coherence effects were neglected (49). More discussion of points 3 and 5 is presented below.

The atomic vapor is dilute if there are no self-absorption, prefilter, and postfilter effects. Self-absorption occurs from the reabsorption of fluorescence photons, within the excitation volume, as they traverse the atom reservoir (50). Prefilter effects are those regions in which the analyte of interest is present and is illuminated by the excitation beam but the resulting fluorescence is not viewed by the detector (Figure 2-2) (50). Postfilter effects are those regions in which the analyte of interest is present but the region is not illuminated by the excitation source (Figure 2-2) (50).

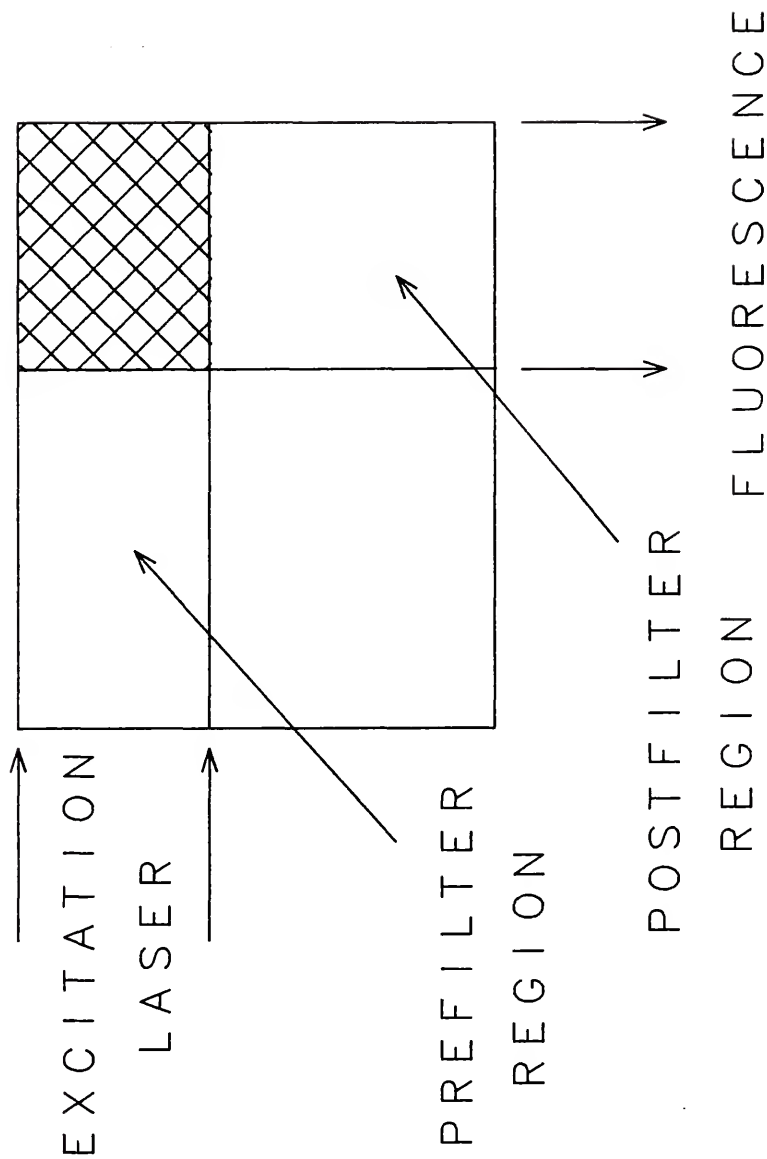


Figure 2-2 Cross-Sectional Area of the Atomizer Including Excitation Beam and Fluorescence Geometry and Prefilter and Postfilter Effects



The rate equation approach is considered valid if coherence effects are neglected. Coherence effects are interactions between the analyte of interest and the laser field. This usually occurs at very high pumping rates (i.e.,  $10^{10} \text{ s}^{-1}$  or greater). The high pumping rates result in short interaction times (i.e., less than 100 ps). At such short times, the rate equation approach fails because the atoms are oscillating between the first and second excited states. Thus, the atoms are not exclusively lying in the first excited state. At longer times, 1 ns or greater, the coherence effects are negligible because they have been damped out.

The rate equations for the system illustrated in Figure 2-1 (see Appendix A) are presented in Figure 2-3 (49). The time dependent solutions for the population of the levels can be obtained after many mathematical manipulations but are not shown here. However, the conclusions from these solutions indicate that when the radiatively induced rates significantly exceed the collisional rates, the attainment of the steady state population of the final level is also reached, and that when the first excitation laser is capable of optical saturation, the steady state population of the ground and first excited states depends upon the values of the radiatively induced rate of the second excitation laser (49).

From the time dependent solutions and further mathematical manipulations, it is possible to write an expression for the steady state population of the first excited state in terms of the radiative and collisional rate coefficients as shown in Figure 2-4 (see

$$\frac{dn_3(t)}{dt} = R_{23}n_2(t) - (R_{32} + R_{31})n_3(t) \quad (1)$$

$$\frac{dn_2(t)}{dt} = R_{12}n_1(t) + R_{32}n_3(t) - (R_{23} + R_{21})n_2(t) \quad (2)$$

$$n_1(t) + n_2(t) + n_3(t) = n_1 \quad (3)$$

Figure 2-3 Rate Expressions for a Three-Level System

$$\left[ \frac{(n_2)_{ss}}{n_T} \right] = \frac{B_{12} \rho(\nu_{12}) Z + g' B_{12} \rho(\nu_{12}) B_{23} \rho(\nu_{23})}{B_{23} \rho(\nu_{23}) [k_{31} + B_{12} \rho(\nu_{12}) + g' [Z_2 + B_{12} \rho(\nu_{12}) g]] + Z_3 [Z_2 + g B_{12} \rho(\nu_{12})]} \quad (4)$$

where the subscript means the second laser ( $2 \rightarrow 3$ ) is "on" as well as

the first laser ( $1 \rightarrow 2$ ) and

$$Z_3 \equiv A_{32} + k_{32} + k_{31} \quad (4a)$$

$$Z_2 \equiv A_{21} + k_{21} \quad (4b)$$

$$g' \equiv (g_2/g_3) \quad (4c)$$

$$g \equiv \left( 1 + \frac{g_1}{g_2} \right) \quad (4d)$$

Figure 2-4 Expression for the Steady State Population of the First Excited State in Terms of the Radiative and Collisional Rate Coefficients

Appendix A). Utilizing this equation, the limiting cases (i.e., absence of the second excitation laser; optical saturation of the first transition; optical saturation of the second transition but not the first transition; and optical saturation of both transitions) for the steady state population of the first excited state can be derived (see Appendix B). It can be shown that the atomic population is redistributed among the three states according to their respective statistical weights (39).

Knowing these equations, it is now possible to define the relative steady state fluorescence dip,  $\Delta'$ , as shown in equation 5, Figure 2-5, where (off) and (on) correspond to whether the second laser is off [i.e., limiting case of absence of the second excitation laser,  $B_{23}\rho(\nu_{23}) = 0$ ] or on. This expression can also be written explicitly as shown in equation 6, Figure 2-5 (see Appendix A). With this expression, two graphical representations are possible. The first is a reciprocal plot, i.e.,  $(\Delta')^{-1}$  vs  $[B_{23}\rho(\nu_{23})]^{-1}$ , and the second is a conventional plot of  $\Delta'$  vs  $B_{23}\rho(\nu_{23})$ . The reciprocal expression of equation 6 is equation 7 in Figure 2-5 (see Appendix A). It becomes apparent that a reciprocal plot as that described above is not practical because it assumes that certain atomic parameters are known (e.g., transition probabilities). However, the quantum efficiency of the second transition is shown as equation 8 in Figure 2-5 (see Appendix A) and the radiatively induced absorption rate is listed as equation 9 in Figure 2-5 (see Appendix A). By substituting equations 8 and 9 into equation 7, one obtains the expression shown in equation 10 (Figure 2-5) (see Appendix A). A

$$\Delta' = \frac{n_2(\text{off}) - n_2(\text{on})}{n_2(\text{off})} \quad (5)$$

$$\Delta' = \frac{B_{23}\rho(\nu_{23})}{[B_{23}\rho(\nu_{23})]\left[\frac{g_1 + g_2 + g_3}{g_3}\right] + \left[\frac{g_1 + g_2}{g_2}\right][A_{32} + k_{32} + k_{31}]} \quad (6)$$

$$\frac{1}{\Delta'} = \left[\frac{g_1 + g_2 + g_3}{g_3}\right] + \left[\frac{g_1 + g_2}{g_2}\right]\left[\frac{A_{32} + k_{32} + k_{31}}{B_{23}\rho(\nu_{23})}\right] \quad (7)$$

$$Y_{32} = \frac{A_{32}}{A_{32} + k_{32} + k_{31}} \quad (8)$$

$$B_{23}\rho(\nu_{23}) = \frac{g_3}{g_2} A_{32} \frac{c^3}{8\pi h \nu_{23}^3} \rho(\nu_{23}) \quad (9)$$

$$\frac{1}{\Delta'} = \left[\frac{g_1 + g_2 + g_3}{g_3}\right] + \left[\frac{g_1 + g_2}{g_2}\right]\left[\frac{8\pi h \nu_{23}^3}{c^3} \frac{1}{Y_{32}}\right][\rho(\nu_{23})]^{-1} \quad (10)$$

$$\Delta' = \left[\frac{g_3}{g_1 + g_2 + g_3}\right] + \left[\frac{g_3}{g_1 + g_2}\right]\left[\frac{c^3}{8\pi h \nu_{23}^3}\right]Y_{32}[\rho(\nu_{23})] \quad (11)$$

$$\rho^s(\nu_{23}) = \left[\frac{g_1 + g_2}{g_1 + g_2 + g_3}\right]\left[\frac{8\pi h \nu_{23}^3}{c^3}\right]\frac{1}{Y_{32}} \quad (12)$$

Figure 2-5 Theoretical Expressions for Fluorescence Dip Spectroscopy for the Limiting Case of Optical Saturation of the First Transition

plot of  $(\Delta')^{-1}$  vs  $[\rho(v_{23})]^{-1}$  would result in a straight line where the slope can be used to evaluate the quantum efficiency,  $Y_{32}$ . This is possible because there are only constants left in the expression for the slope.

A conventional plot of  $\Delta'$  vs  $B_{23}\rho(v_{23})$  is also not practical for the same reasons discussed above. With the substitutions previously made, an expression (reciprocal of equation 10) is obtained as shown in equation 11 (Figure 2-5) (see Appendix A). By plotting  $\Delta'$  vs  $\rho(v_{23})$ , a full steady state saturation dip curve can be obtained. Such a plot has two distinct features: the first is a linear portion and the second is a saturation plateau. The intersection point of these two asymptotes constitutes the steady state saturation dip parameter. The steady state saturation dip parameter is defined as the value of the spectral energy density for which the relative dip is equal to one half the maximum value of the relative dip (plateau region). Once this value has been determined, the quantum efficiency can then be calculated by equation 12 (Figure 2-5) (see Appendix A) (49).

### Experimental Facilities and Considerations

#### Instrumentation

A block diagram of the experimental setup is shown in Figure 2-6 and a detailed listing of the experimental components is described in Table 2-1. A frequency doubled Nd:YAG laser (i.e., 532 nm) operated at 30 Hz was used as the pumping source for a dual dye laser system. The pump laser beam was split equally to pump each dye laser.

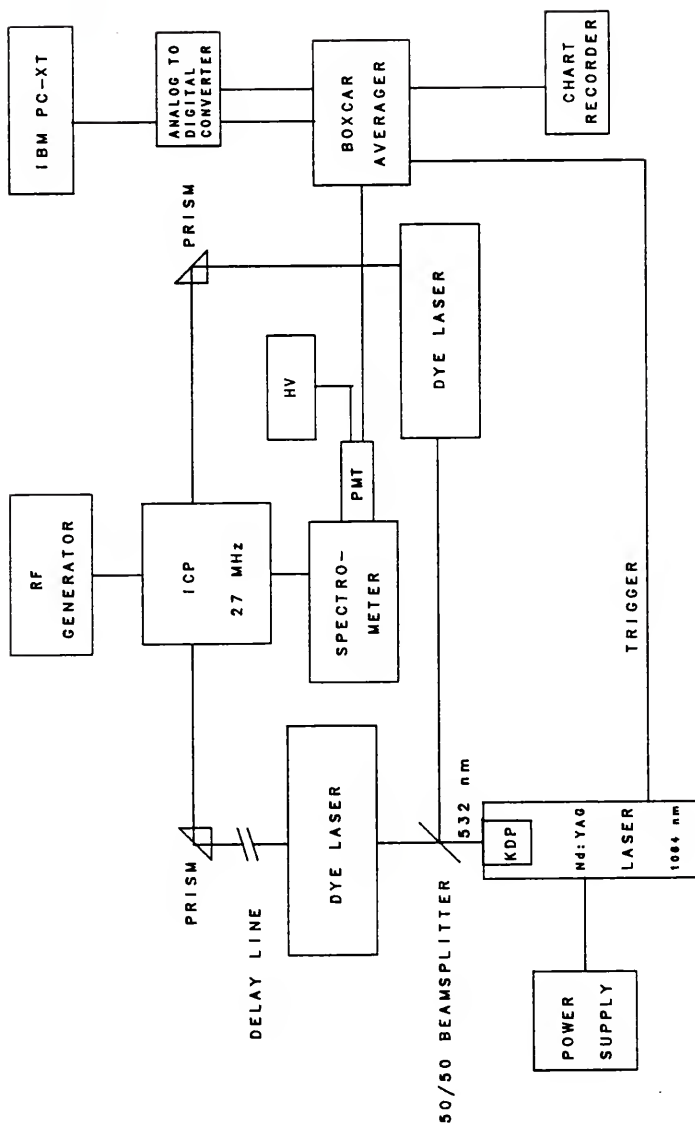


Figure 2-6 Block Diagram of Experimental Setup for Fluorescence Dip Spectroscopy

Table 2-1  
Experimental Components for Fluorescence Dip Spectroscopy

Component	Model No.	Manufacturer
Nd:YAG laser	YG 581-30	Quantel International, Santa Clara, CA
Dual dye lasers	TDL 50	Quantel International, Santa Clara, CA
RF generator	HFP 2500D	Plasma Therm, Inc., Kresson, NJ
Impedance matching network	AMN 2500E	Plasma Therm, Inc., Kresson, NJ
Glass concentric nebulizer	TR-30-C-3	J.E. Meinhard Assoc., Santa Ana, CA
Torch	T-1	Plasma Therm, Inc., Kresson, NJ
Spray chamber		Laboratory constructed
0.3 m Spectrometer	218	GCA/McPherson Instrument., Acton, MA
90° Quartz prisms		Esco Products, Inc., Oak Ridge, NJ
Quartz lens		Oriel Corp., Stratford, MA
Neutral density filters		Corion Corp., Holliston, MA
Photomultiplier tube	R 1547	Hamamatsu Corp., Bridgewater, NJ
High voltage power supply	226	Pacific Precision Instrum., Concord, CA
Boxcar averager, gated integrator	SR 250	Stanford Research Systems, Palo Alto, CA
Computer interface	SR 245	Stanford Research Systems, Palo Alto, CA
Computer	PC-XT	IBM Corp., Boca Raton, FL



Typical output irradiance from the frequency-doubled Nd:YAG laser was 250 mJ per pulse with a pulse duration of 12 ns. The first dye laser was operated with a dye mixture of Rhodamine 590 and Rhodamine 610 (i.e., solvent is methanol) in a 4:1 ratio, respectively. The second dye laser was operated with a pure Rhodamine 590 solution. The first dye laser was tuned to either of the sodium (Na) atomic resonance transitions (e.g., 588.995 nm or 589.592 nm) as shown in Figure 2-7. The second dye laser was tuned to either the 568.266 nm or 568.820 nm transition to probe the Na atom population in the first excited state. The second dye laser could also be scanned across these transitions to observe the dip shapes. Typical dye laser irradiances were 6 mJ per pulse for the first dye laser and 0.03 to 7 mJ per pulse for the second dye laser. For the second dye laser, the output irradiance was varied discretely with neutral density filters and/or selective amplification. Selective amplification meant that the dye laser could be amplified through the use of either a preamplifier or amplifier cell or both simultaneously. A delay line composed of prisms was arranged in such a manner that both laser beams arrived at the center of the atomization cell at the same time and in the same space, counterpropagating.

The inductively coupled argon (Ar) plasmas (ICPs) have been well documented as an excellent atomization cell for atomic fluorescence spectroscopy (AFS) (51-56). They possess several properties that make them attractive for AFS. First, the high temperature and chemically inert environment in Ar supported ICPs assure a high

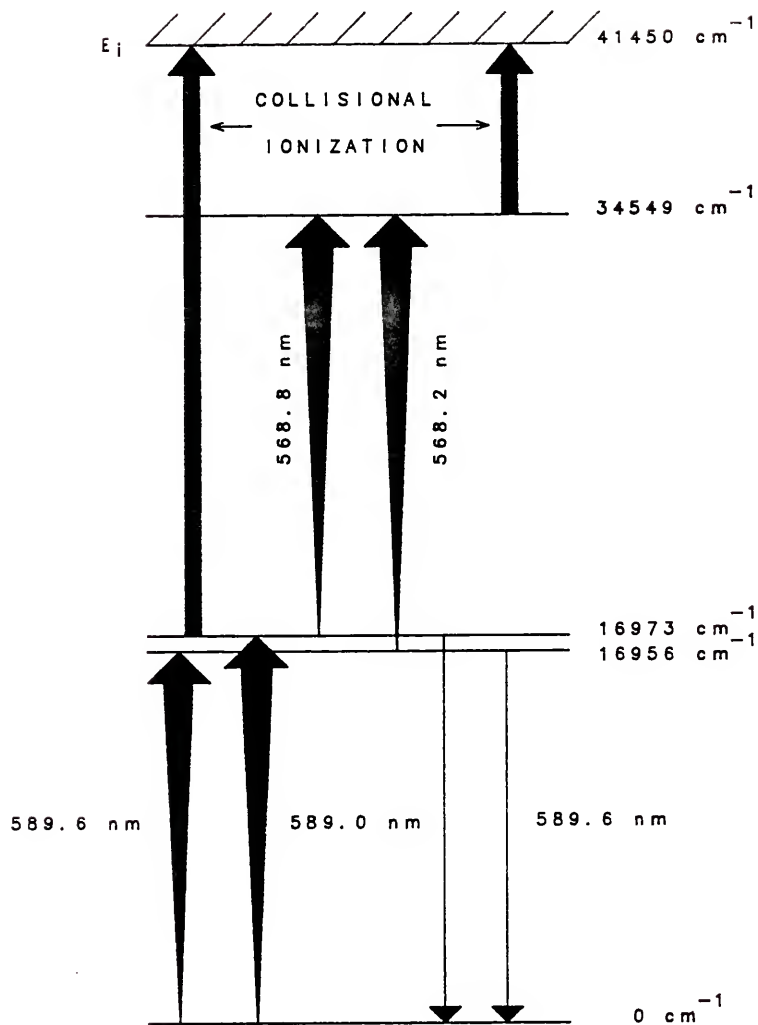


Figure 2-7 Partial Energy Level Diagram for Sodium

degree of conversion of the analyte into free atoms (51,56). Scattering of primary radiation by unvaporized analyte should, therefore, be negligible. Second, on a comparison basis, fluorescence quenching should be less in the predominantly Ar environment than those in many other vaporization-atomization cells, such as high temperature combustion flames (51,56,57).

The experimental operating conditions are listed in Table 2-2. The ICP was operated at low powers (i.e., 500 W) to minimize as much as possible the emission and/or ionization of Na. Sample solution was introduced through a concentric nebulizer into a spray chamber. The aerosol was then carried by argon into the center of the ICP. The observation height of the fluorescence volume was 15 mm above the load coil. This height is the most commonly used in atomic emission measurements in the ICP, and it does not appear to degrade the atomic fluorescence measurements as demonstrated in previous investigations (58,59).

Laser excited atomic fluorescence of Na was detected at 588.995 nm or at 589.592 nm depending on the situation (i.e., resonance or nonresonance fluorescence transitions) at a right angle to the laser beams using a 50.8 mm diameter, 111.6 mm focal length quartz lens to image (1:1) the plasma onto the entrance slit of a  $f/5.3$ , 0.3 m spectrometer. An iris diaphragm (38 mm diameter opening) was placed directly after the lens to prevent overfilling the grating. The entrance and exit slits were set at 50  $\mu\text{m}$  in order to fully resolve the Na doublet. A neutral density filter of 1.0 was

Table 2-2  
Experimental Parameters for Fluorescence Dip Spectroscopy

---

Forward RF power	500 W
Reflected power	0 W
Coolant Ar flow rate	15 L/min
Auxiliary Ar flow rate	0 L/min
Nebulizer Ar flow rate	0.7 L/min @ 32 psi
Solution uptake rate	2.0 mL/min
Observation height above load coil	15 mm
PMT high voltage	-900 VDC
Slit width	50 $\mu$ m
Slit height	10 mm
Neutral density filter	1.0
External trigger rate	30 Hz
Gate delay	818 ns
Gate width	2 ns, 4 ns, 600 ns
Sensitivity	5 - 50 mV/V
Input filter	>10 kHz
Number of pulses averaged	10 pulses
Terminating resistor	1.2 k $\Omega$ (600 ns), 50 $\Omega$ (2 ns, 4 ns)

---

placed in front of the entrance slit. The output of the photomultiplier tube was terminated either into a  $50\ \Omega$  or  $1.2\ \text{k}\Omega$  resistor depending on the gate widths employed. Signal averaging from the output of the photomultiplier tube was performed with a boxcar averager, gated integrator. The averaged fluorescence signal was inputted to an analog-to-digital converter which was interfaced with a computer for data acquisition, analysis, and storage.

#### Measurement of the Fluorescence Dip

The fluorescence dip was measured in two ways. The first was by scanning the second laser through the two upper transitions shown in Figure 2-7. In this manner, the intensity of the dip as well as the peak shape was observed. However, the overall measurement of the dip was not made this way because of the relatively poor signal-to-noise ratios. The alternative way to measure the dip was to tune the second laser to one of the upper transitions. In this manner, it was only necessary to block and unblock the second laser to obtain the desired measurement as a function of laser irradiance.

There are four possible combinations of primary excitation and fluorescence wavelengths, and for each combination of excitation and fluorescence wavelength, there are two possible secondary excitation wavelengths for which the dip will occur, i.e., there are eight possibilities. For example, a possible combination is primary excitation at 589.0 nm and fluorescence detection at 589.6 nm, and secondary excitation at 568.3 nm (see Figure 2-7). In this study, all possible combinations are investigated. In addition, there are three different gate widths used for each possibility.

All the measurements pertaining to the dip were blank corrected. A working solution of 120 mg/L of Na was prepared from a 2% stock solution which was diluted to the mark with deionized distilled water (i.e., Barnstead water filtration system).

### Results and Discussion

As shown in the energy level diagram (Figure 2-7), a resonant or nonresonant fluorescence transition was monitored to observe the dip in the fluorescence signal when the second dye laser was scanned through the upper level transitions. This was shown clearly in Figures 2-8 to 2-10. As can be seen, the dips became broadened as the second laser irradiance was increased; that is, the peak shapes (FWHM) were widened. This was primarily due to power broadening of the second laser. Another outcome was that the peak of the dip did not increase in a linear fashion with respect to the laser irradiance of the second laser. This was explained by the condition of optical saturation of the second transition. That is, increasing the laser irradiance after a certain threshold had no appreciable effect on the magnitude of the dip. The depletion of the first excited state was between 50 and 80% depending on the irradiance of the second laser.

Gate widths of 2, 4, and 600 ns were used to note the effect. The primary difference between the smaller (e.g., 4 ns) gate width and the larger gate width (e.g., 600 ns), besides the time scale, was that the pulse shape for the larger gate width was stretched through the use of a 1.2 k $\Omega$  terminating resistor as compared to a 50  $\Omega$

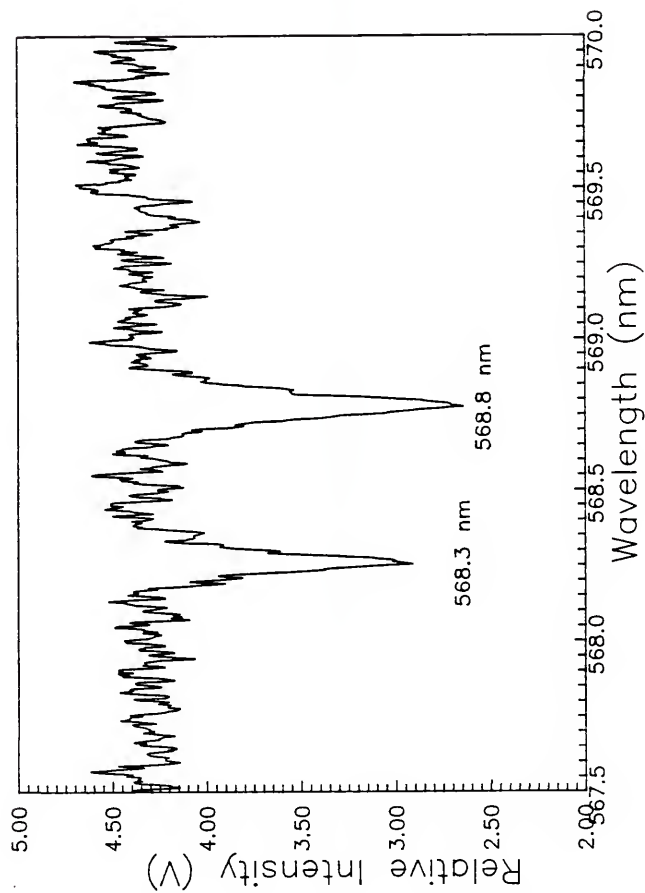


Figure 2-8 Scan of the Second Excitation Laser Through the Upper Level Transitions of Sodium at 0.10 mJ per pulse with the Fluorescence Wavelength at 589.6 nm

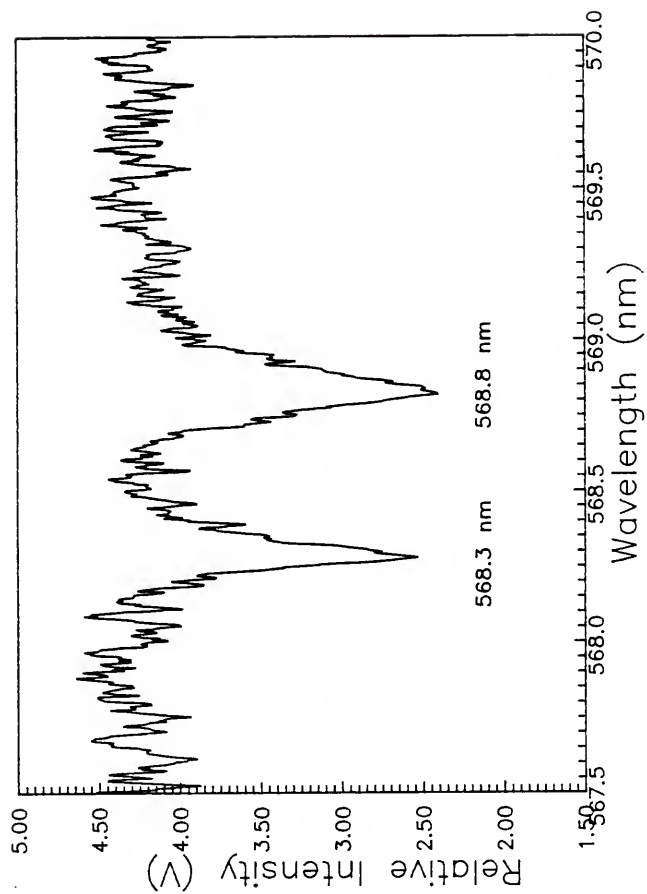


Figure 2-9 Scan of the Second Excitation Laser Through the Upper Level Transitions of Sodium at 0.73 mJ per pulse with the Fluorescence Wavelength at 589.6 nm



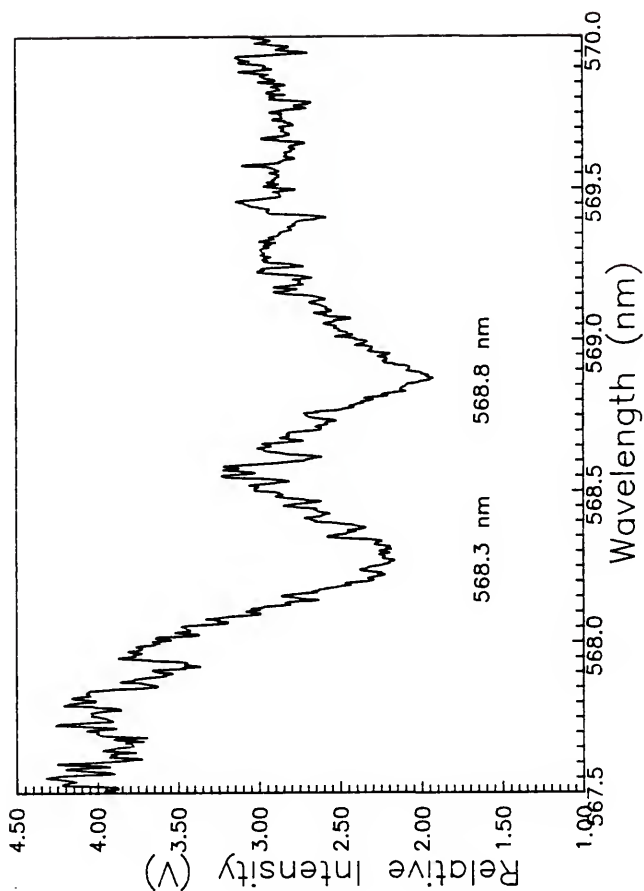


Figure 2-10 Scan of the Second Excitation Laser Through the Upper Level Transitions of Sodium at 8.33 mJ per pulse with the Fluorescence Wavelength at 589.6 nm

termination for the smaller gate widths. The smaller resistance termination allowed the integrity of the pulsed shape to be maintained. The major result of the larger gate width was that the intercepts of the reciprocal plots were greater than those employing the smaller gate widths (Table 2-3). This was probably due to the stretching of the signal pulse as mentioned earlier. The difference between the 2 and 4 ns gate width was that the 4 ns gate provided better signal-to-noise (S/N) and signal-to-background (S/B) ratios. An explanation of this occurrence was that as gate widths became narrower, the root mean square noise became greater. This was a result of the reduced sampling efficiency and wider bandwidth. The bandwidth was defined as approximately equal to 0.35 divided by the selected gate width (60).

The effect of the observation height above the load coil was investigated. As can be seen in Figure 2-11, the fluorescence signal did indeed behave as a function of the observation height, but the relative dip did not behave in an analogous manner. This was because the relative dip required two measurements (i.e., fluorescence signal with and without the second laser) so that the effect of observation height was present in both measurements. However, the relative dip was obtained by subtracting the fluorescence signal with the second laser from the fluorescence signal without the second laser, and hence, the effect of observation height was negated. An observation height of 15 mm above the load coil was chosen because it provided the greatest fluorescence signal.

Table 2-3  
Comparison of Gate Widths with Respect to Slope,  
Intercept, and  $r^2$  Correlation Coefficient

Wavelength (nm) ex/fl/ex	Gate Width (ns)	Slope $10^{-8} \text{ J/m}^3 \text{ Hz}$	Intercept	$r^2$
589.0/589.0/568.3	600	0.00345	2.499	0.990
	4	0.00264	1.574	0.986
	2	0.00342	1.483	0.996
589.6/589.0/568.3	600	0.00391	2.540	0.965
	4	0.00205	1.403	0.996
	2	0.00297	1.732	0.987
589.0/589.6/568.3	600	0.00325	2.475	0.975
	4	0.00357	1.748	0.992
	2	0.00390	1.973	0.984
589.6/589.6/568.3	600	0.00458	2.502	0.978
	4	0.00246	1.230	0.994
	2	0.00336	1.582	0.900
589.0/589.0/568.8	600	0.00219	2.244	0.987
	4	0.00150	1.465	0.980
	2	0.00164	1.384	0.984
589.6/589.0/568.8	600	0.00158	2.603	0.960
	4	0.00081	1.429	0.958
	2	0.00155	1.599	0.953
589.0/589.6/568.8	600	0.00223	2.382	0.975
	4	0.00148	1.608	0.929
	2	0.00193	1.680	0.975
589.6/589.6/568.8	600	0.00198	2.630	0.905
	4	0.00274	1.163	0.983
	2	0.00179	1.725	0.935

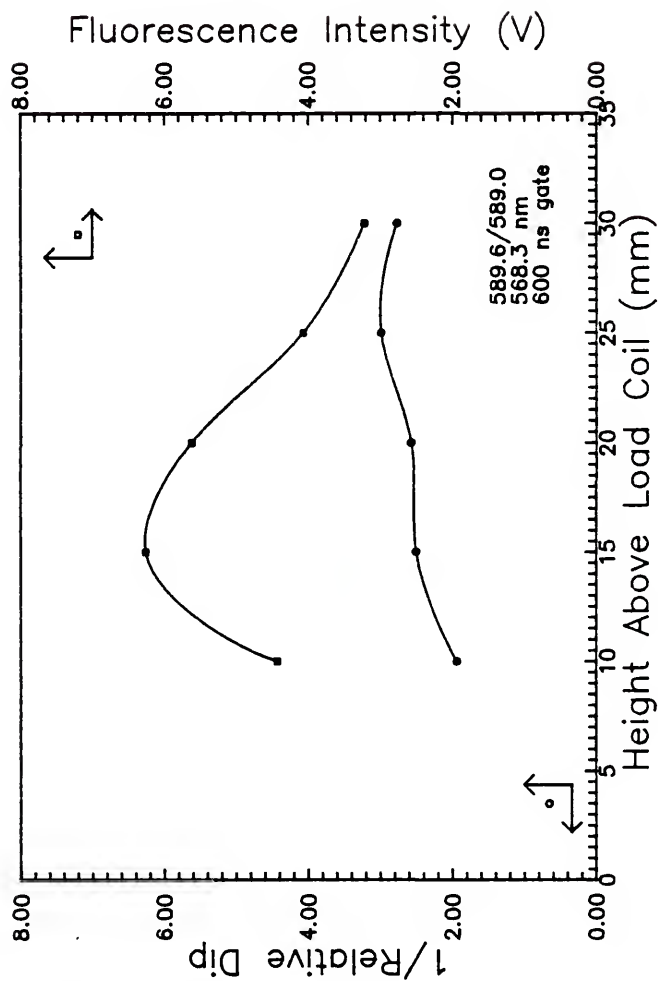


Figure 2-11 Plot of the Relative Dip and the Relative Fluorescence Intensity as a Function of Observation Height Above the Load Coil

The effect of monitoring resonance and nonresonance fluorescence transitions was studied. This was shown in Figures 2-12 and 2-13. The primary advantage of monitoring a nonresonance fluorescence transition was that scattering (e.g., laser) was reduced. To realize such a situation, the spectrometer had to have the capability of resolving the Na doublet (i.e., 589.0 and 589.6 nm). The spectrometer was a 0.3 m focal length with a reciprocal linear dispersion of 2.6 nm/mm. Thus employing 50  $\mu$ m slit widths ( $\delta\lambda_s = 0.13$  nm), the Na doublet was completely resolved. As can be seen, the nonresonance case (Figure 2-12) was not as noisy as the resonance case (Figure 2-13).

To extract information such as quantum efficiency and oscillator strength, a slope method for the steady state population of the first excited state is employed. The slope method employed the reciprocal plots as described earlier. The plots are shown in Figures 2-14 to 2-19 with each figure containing the four possible combinations of wavelength of first excitation laser and wavelength of fluorescence in addition to the gate width and the wavelength of the second laser.

From theoretical considerations, the reciprocal plot was a straight line as shown in Figure 2-20 with the slope that varied as the quantum efficiency,  $Y_{32}$ , varied. The reciprocal plots obtained from these experiments showed that indeed there were differences between the 568.3 nm and 568.8 nm transition probabilities. This was clearly indicated by the slopes for these two upper level transitions regardless what the lower level transitions (589.0 nm, 589.6 nm) were

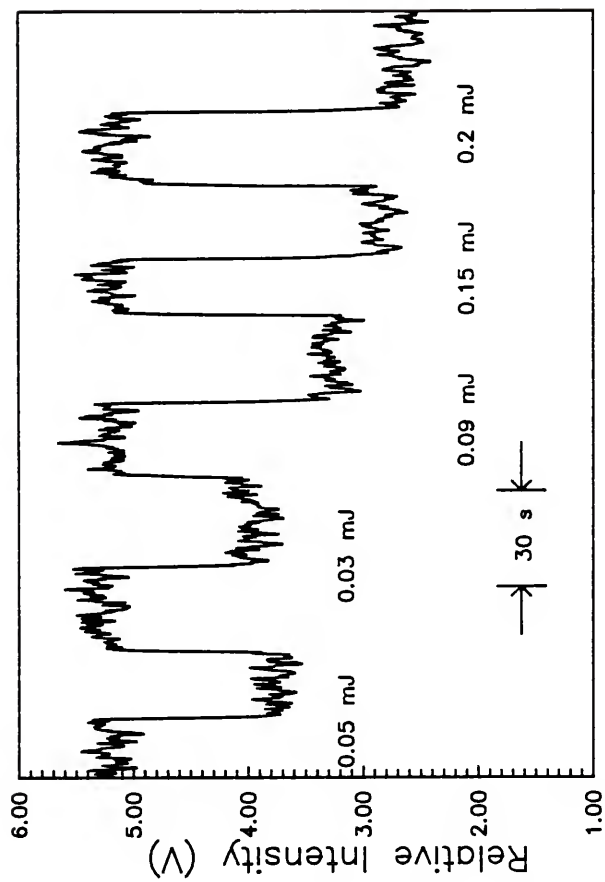


Figure 2-12 Measurement of the Relative Fluorescence Intensity at 588.995 nm With and Without the Second Laser at 588.266 nm as a Function of the Second Laser Irradiance

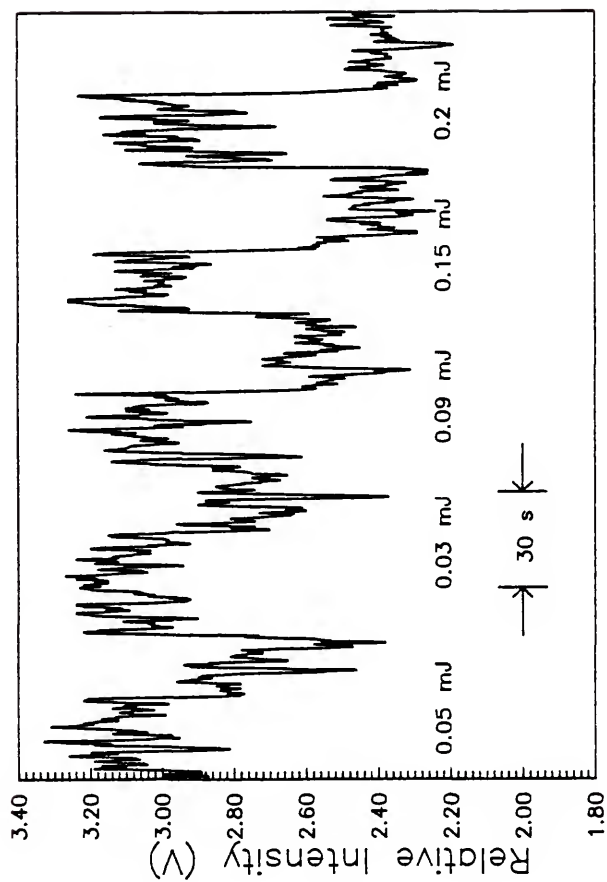


Figure 2-13 Measurement of the Relative Fluorescence Intensity at 589.592 nm With and Without the Second Laser at 568.266 nm as a Function of the Second Laser Irradiance

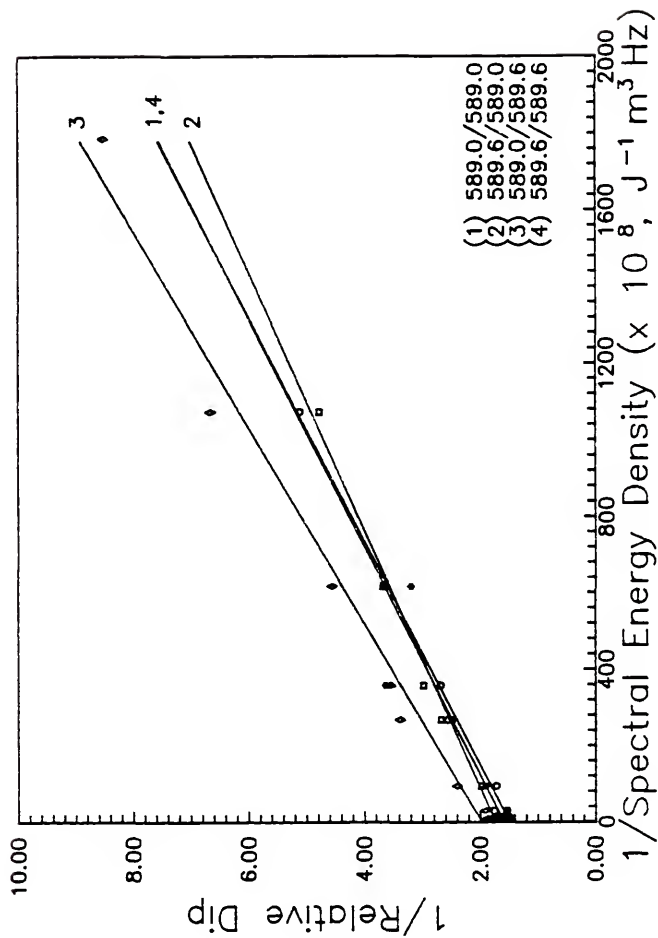


Figure 2-14 Reciprocal Plot of Relative Dip vs Spectral Energy Density with 2 ns Gate Width and 568.3 nm Transition



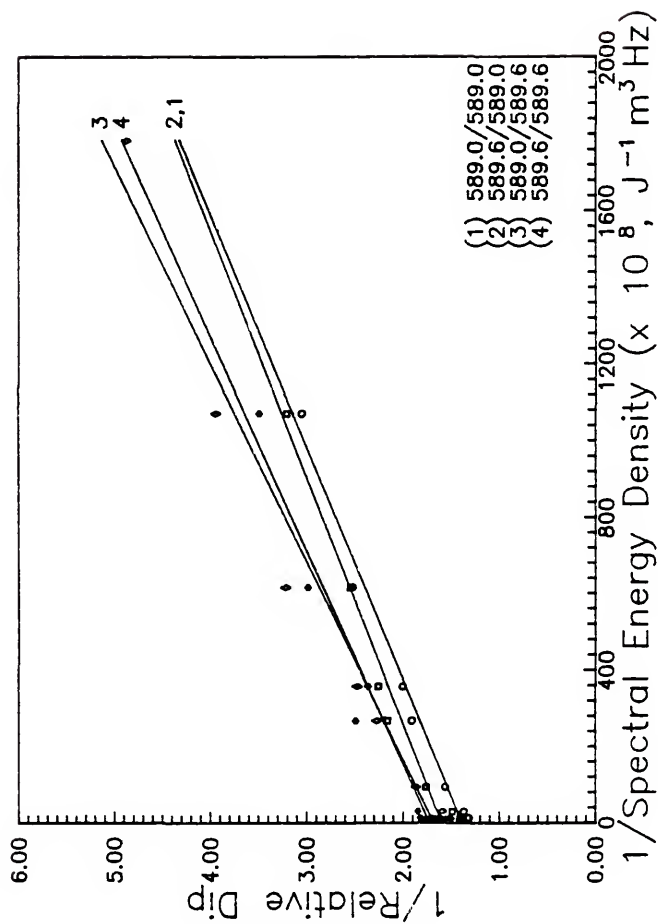


Figure 2-15 Reciprocal Plot of Relative Dip vs Spectral Energy Density with 2 ns Gate Width and 568.8 nm Transition

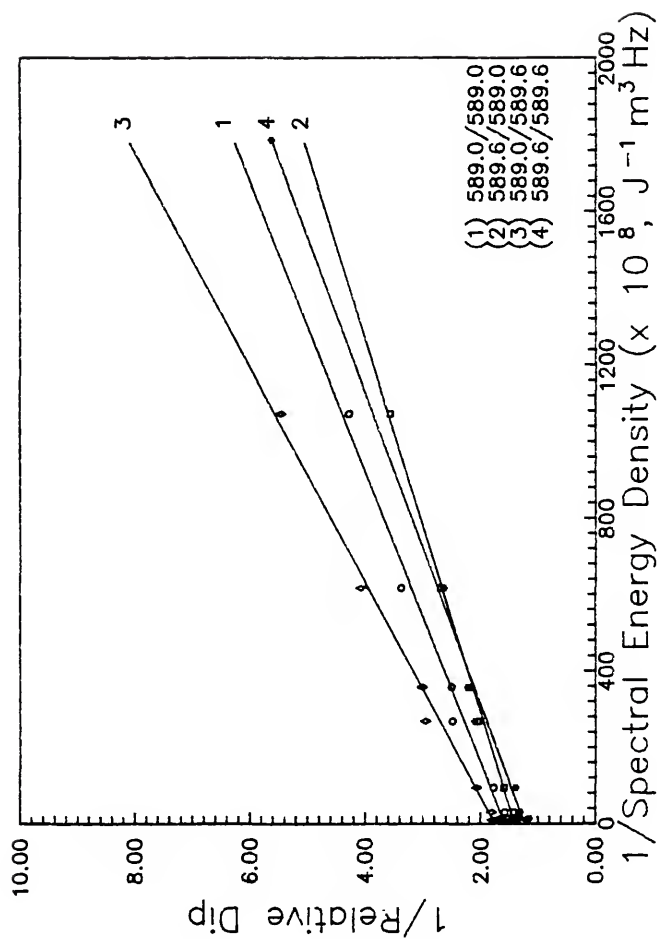


Figure 2-16 Reciprocal Plot of Relative Dip vs Spectral Energy Density with 4 ns Gate Width and 568.3 nm Transition

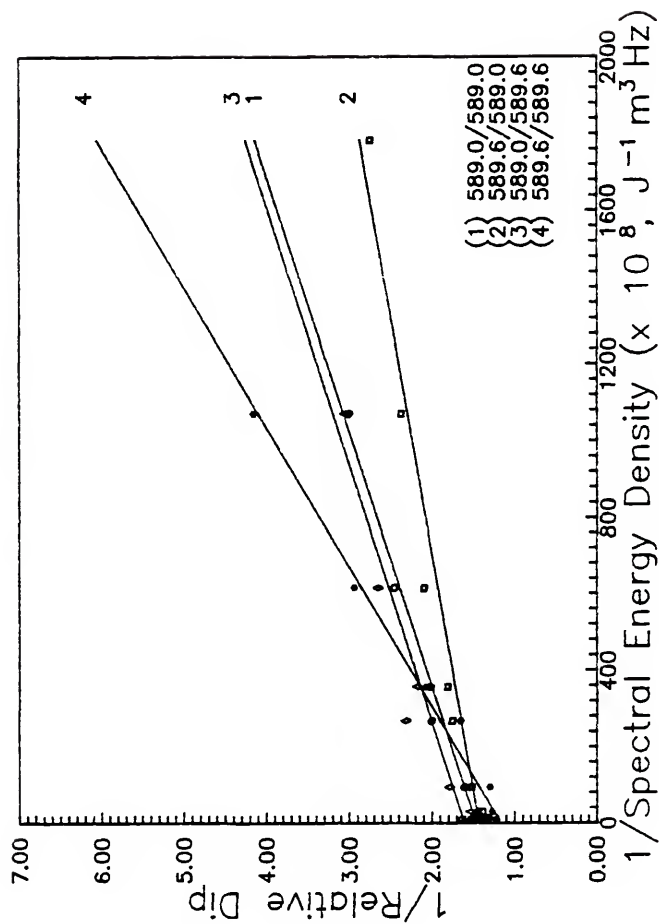


Figure 2-17 Reciprocal Plot of Relative Dip vs Spectral Energy Density with 4 ns Gate Width and 568.8 nm Transition

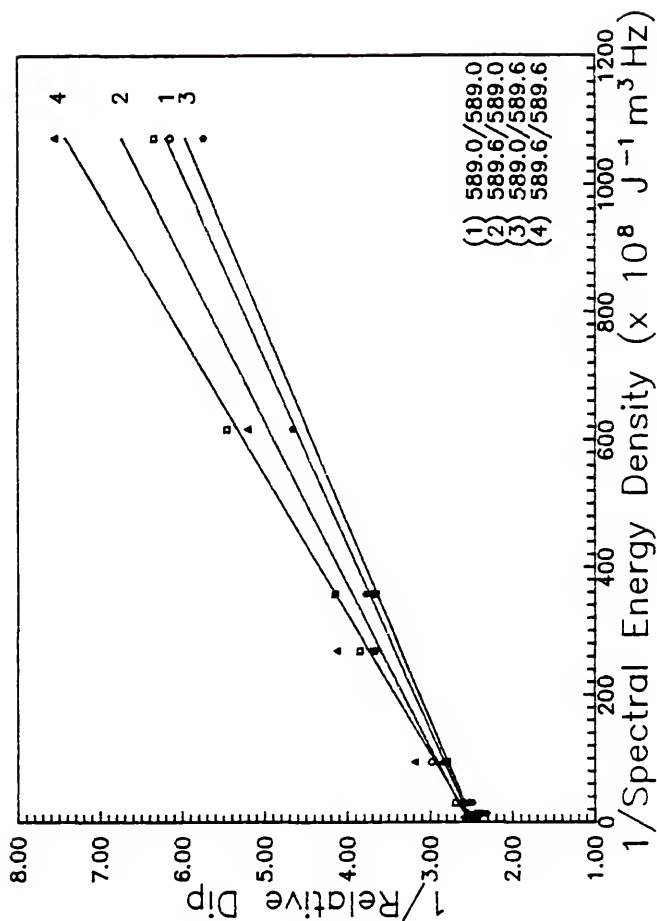


Figure 2-18 Reciprocal Plot of Relative Dip vs Spectral Energy Density with 600 ns Gate Width and 568.3 nm Transition

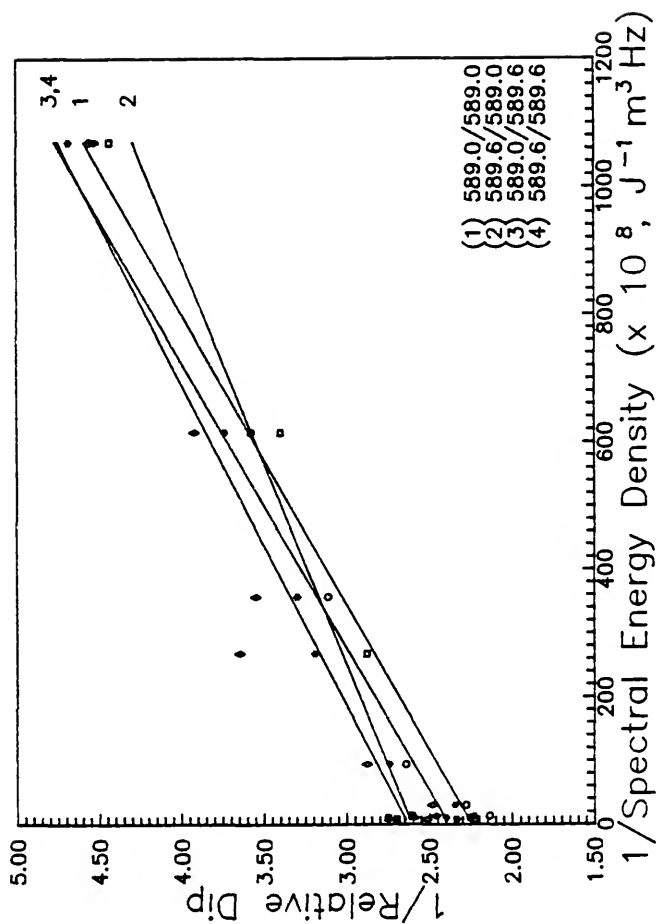


Figure 2-19 Reciprocal Plot of Relative Dip vs Spectral Energy Density with 600 ns Gate Width and 568.8 nm Transition

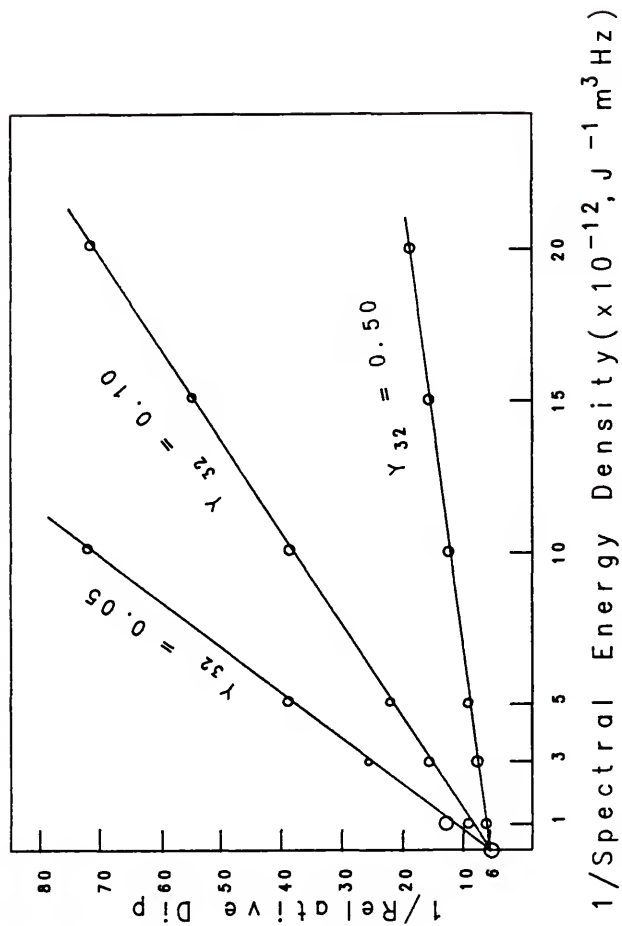


Figure 2-20 Theoretical Reciprocal Plot of Relative Dip vs Spectral Energy Density

(Table 2-3). It was evident that the gate widths and transitions monitored did not appreciably affect the slopes of these plots. The results indicated that the ratio between the average of the slopes for each gate width of the two upper level transitions was approximately two which was in good agreement with published results of the ratio of the transition probabilities (Table 2-4) (61,62). The calculation of an absolute quantum efficiency value using equation 10 (Figure 2-5) and the measured slopes (Table 2-3) for these two upper level transitions showed that the results were between 0.001 and 0.004. However, the ratios of the quantum efficiencies for the transitions showed that they were in good agreement with the literature value (Table 2-4) (62). A possible explanation for the such low values was that there were pronounced ionization losses in this particular system; i.e., Na is an easily ionizable element. The intercepts provide information about the statistical weights of the levels. The statistical weight,  $g$ , is equal to the number of superimposed levels, that is, the degeneracy of a state. In the case where two states are mixing and act as a single state, the statistical weight,  $g$ , is equal to the sum of the  $g$  values for each state. The intercepts from the reciprocal plots were in good agreement with the true value as shown in Table 2-4.

To extract the steady state saturation dip parameter, saturation dip curves were plotted (Figures 2-21 to 2-28). The experimental saturation dip curves showed a plateau region. The plateau region was obtained by averaging the last four points that showed a tendency to be constant. However, a linear portion was not as well-defined

Table 2-4  
Comparison of Relative (Ratio) of Atomic Parameters

Atomic Parameter	This Work	Literature <sup>a</sup>
Transition probabilities (568.8 nm/568.3 nm)	1.90 <sup>b</sup> 1.64 <sup>c</sup> 1.97 <sup>d</sup>	2.05
Quantum efficiency (568.8 nm/568.3 nm)	1.90 <sup>b</sup> 1.89 <sup>c</sup> 1.96 <sup>d</sup>	2.05
Statistical weights ( $g_1 + g_2$ )/ $g_3$	2.48 <sup>b</sup> 1.45 <sup>c</sup> 1.65 <sup>d</sup>	1.80

<sup>a</sup> Reference 62.

<sup>b</sup> 600 ns gate width.

<sup>c</sup> 4 ns gate width.

<sup>d</sup> 2 ns gate width.



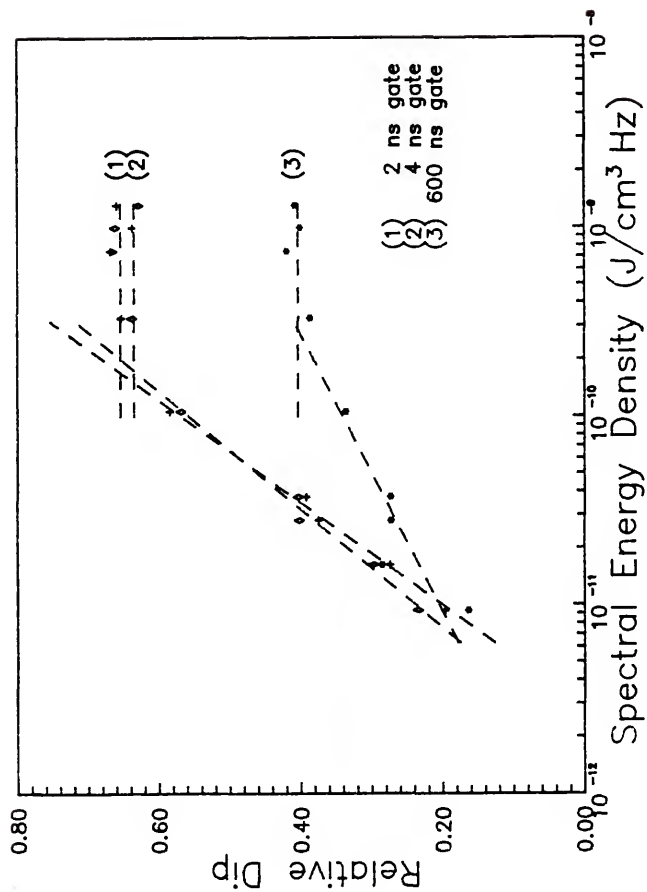


Figure 2-21 Plot of Relative Dip vs Spectral Energy Density with 589.0 and 568.3 nm Excitation and Fluorescence Detection at 589.0 nm

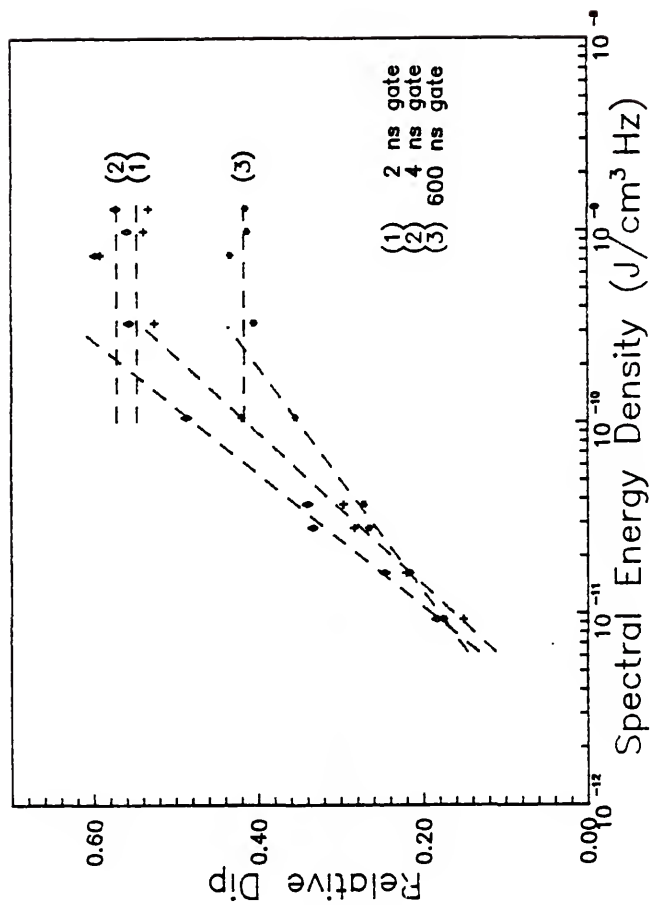


Figure 2-22 Plot of Relative Dip vs Spectral Energy Density with 589.0 and 568.3 nm Excitation and Fluorescence Detection at 589.6 nm

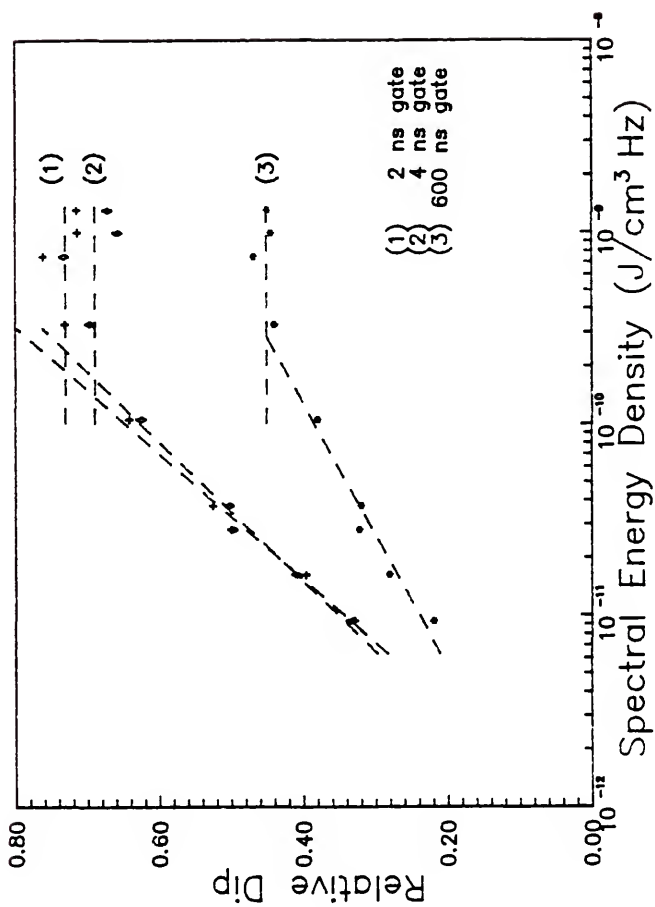


Figure 2-23 Plot of Relative Dip vs Spectral Energy Density with 589.0 and 568.8 nm Excitation and Fluorescence Detection at 589.0 nm

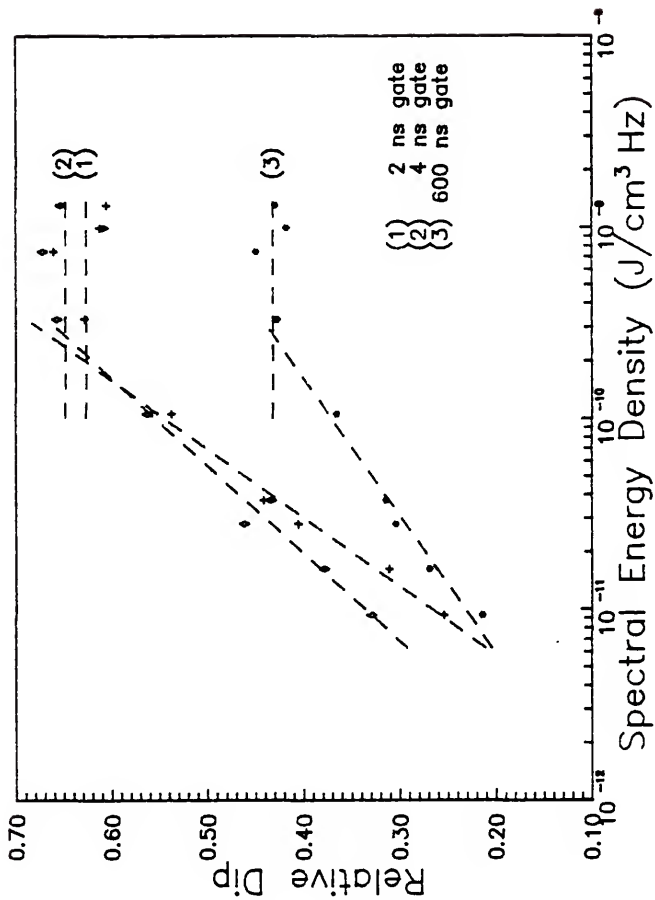


Figure 2-24 Plot of Relative Dip vs Spectral Energy Density with 589.0 and 568.8 nm Excitation and Fluorescence Detection at 589.6 nm

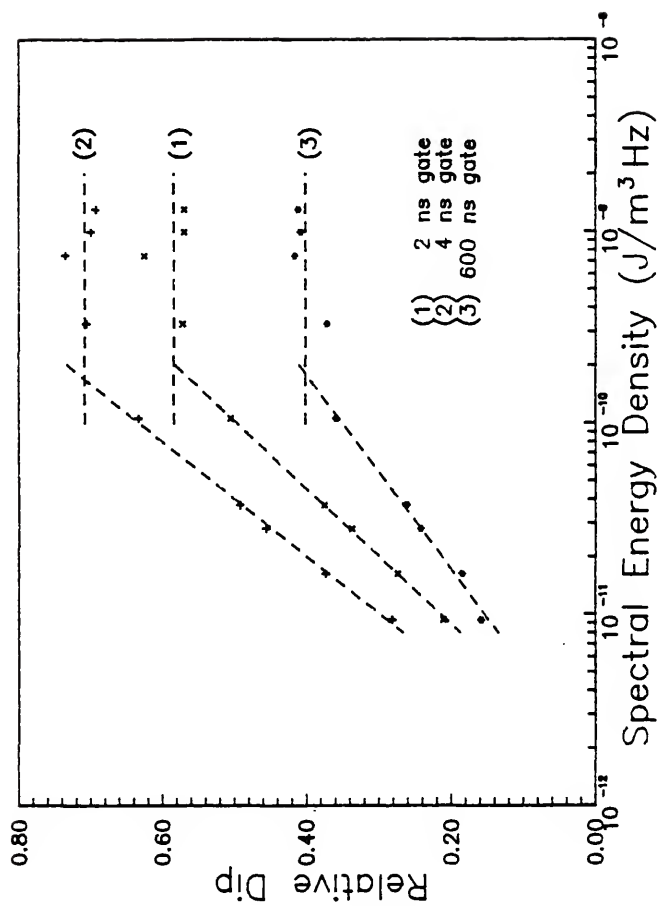


Figure 2-25 Plot of Relative Dip vs Spectral Energy Density with 589.6 and 568.3 nm Excitation and Fluorescence Detection at 589.0 nm

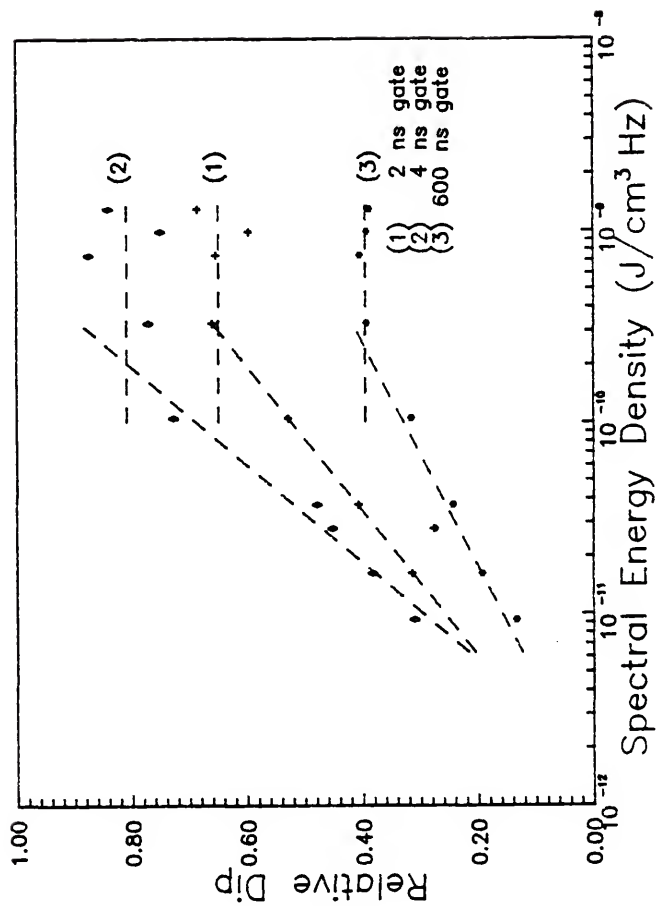


Figure 2-26 Plot of Relative Dip vs Spectral Energy Density with 589.6 and 568.3 nm Excitation and Fluorescence Detection at 589.6 nm

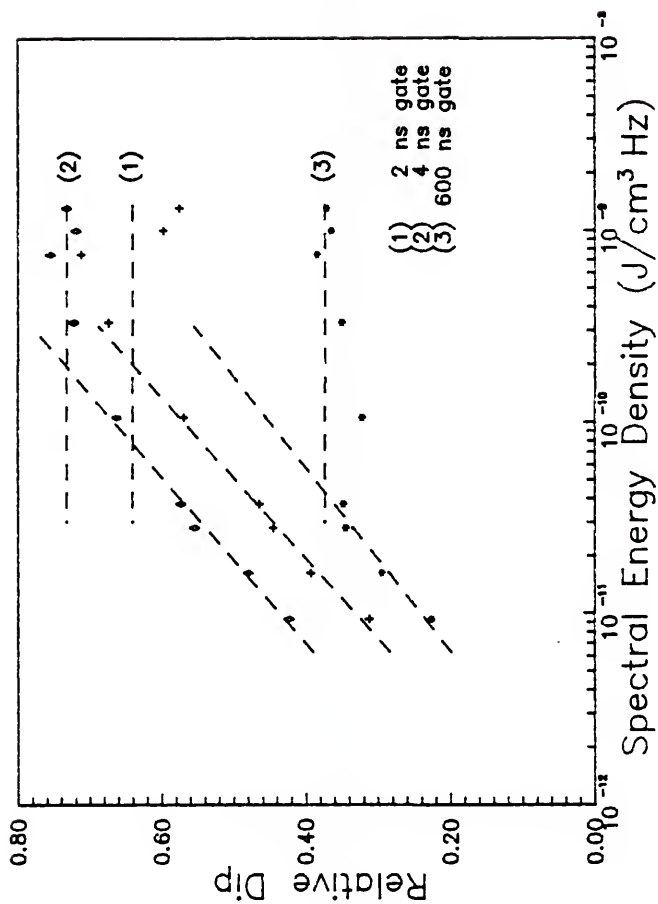


Figure 2-27 Plot of Relative Dip vs Spectral Energy Density with 589.6 and 568.8 nm Excitation and Fluorescence Detection at 589.0 nm

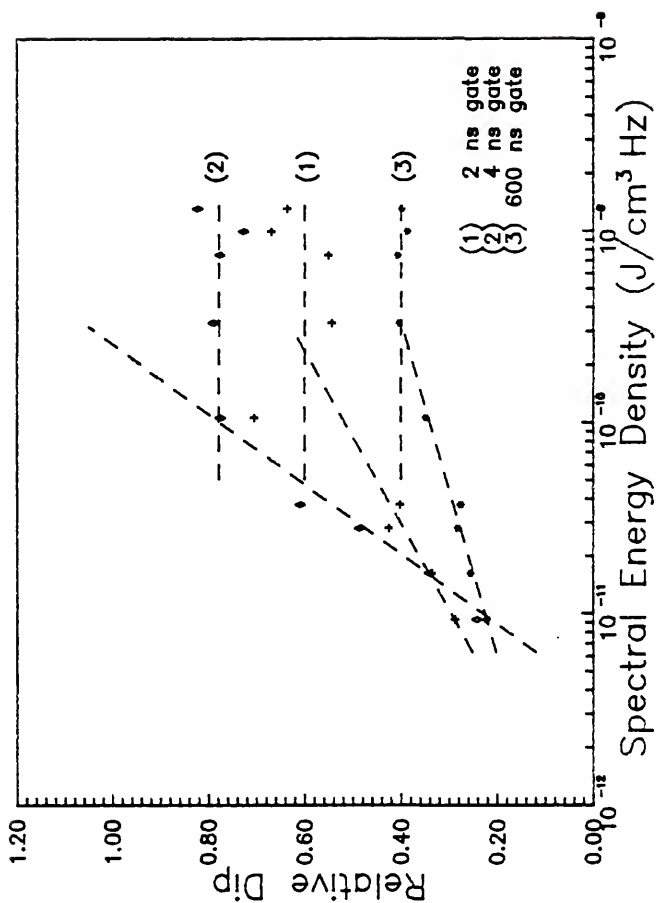


Figure 2-28 Plot of Relative Dip vs Spectral Energy Density with 589.6 and 568.8 nm Excitation and Fluorescence Detection at 589.6 nm



because the sensitivity of the measurement did not allow relative dips below 0.1 to be measured. As can be seen from Figure 2-29, the theoretical curve has a wide range of relative dip values. The plotted curves showed only a small range of relative dips (0.1 to 0.8), but the linear portion is assumed so that an intersection point can be obtained. The intersection of these two asymptotes provided a graphical method for the calculation of the steady state saturation dip parameter. Since the parameter had been defined on page 17, it was then possible to determine the spectral energy density at one half the maximum relative dip by graphical means. The figures shown were for a primary excitation wavelength (589.0 or 589.6 nm), a fluorescence wavelength (589.0 or 589.6 nm), and a secondary excitation wavelength (568.3 or 568.8 nm) for three gate widths. From these unextrapolated curves, it is evident that the saturation dip parameter was different depending upon which upper level transition was employed. The values for the steady state saturation dip parameter are tabulated in Table 2-5. Calculations were performed using equation 12 (Figure 2-5) to obtain the quantum efficiencies. Again the absolute values were low; however, the ratio of the quantum efficiencies for the upper level transitions produced similar values as that in Table 2-4. This served as a check for the reciprocal plots, and it showed consistency between the two types of plots.

From the published literature (61,62), it was clearly evident that agreement was certainly good on a relative basis and fair on an absolute basis (Table 2-4). On a relative basis, the ratios of the transition probabilities and quantum efficiencies agreed well with

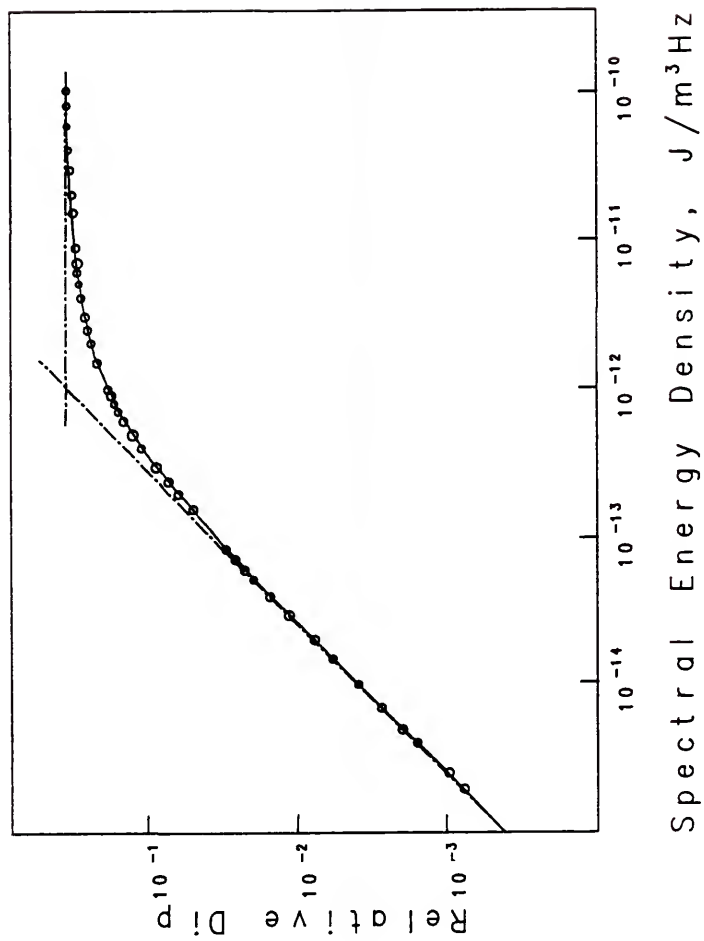


Figure 2-29 Theoretical Plot of Relative Dip vs Spectral Energy Density

Table 2-5  
Comparison of Steady State Saturation Dip Parameter with  
Respect to the Second Excitation Laser Wavelength

Wavelength, nm ex/fl/ex	Steady State Saturation Dip Parameter $10^{-11} \text{ J/m}^3\text{Hz}$		
	2 ns	4 ns	600 ns
589.0/589.0/568.3	2.20	1.77	0.93
589.0/589.6/568.3	1.78	1.46	1.75
589.6/589.0/568.3	1.78	1.90	1.69
589.6/589.6/568.3	2.76	2.16	1.46
589.0/589.0/568.8	1.05	1.78	0.63
589.0/589.6/568.8	1.47	0.88	0.77
589.6/589.0/568.8	1.18	1.44	0.80
589.6/589.6/568.8	0.89	0.63	0.63

the literature values. On an absolute basis, the  $g$  values for the levels that were obtained through the intercepts of the reciprocal plots were in good agreement. The absolute quantum efficiencies were apparently low to what was expected but quantum efficiencies have not been measured so it was uncertain whether the values were correct. However, the results were important because it provided the opportunity to investigate upper level transitions without knowing much information about those levels. Indeed, if the transition probability of one of the transitions was known, then other transitions can be determined in a qualitative manner in terms of its relative atomic parameters and its merits for atomic spectroscopy.

### Conclusions

Although this was a first attempt to apply fluorescence dip spectroscopy for the determination of atomic parameters, it was moderately successful as it was first envisioned, and certain conclusions were drawn. First, sodium was a good example, but it had its drawbacks. Sodium had been thoroughly investigated because of the wealth of information with which to compare the results of this technique. However, sodium also was a very easily ionizable element even at the low powers used in this investigation. There was approximately 80% of the initial atomic population lost through ionization without any benefit of laser excitation. This value was obtained by the Saha equation (see Appendix C) using rough estimates of the temperature and the electron number density in the ICP. A more accurate value can be calculated using the Saha equation and the

electronic partition functions (63) if more accurate measurements were made for the temperature and the electron number density. Other investigators have calculated that 98 to 99.9% of the sodium atoms are lost through ionization assuming a temperature of 7500 K and local thermodynamic equilibrium (64,65). In addition to direct ionization, there were losses due to laser excitation followed by collisions into the ionization continuum, a trap. Second, qualitative and some quantitative results were obtained, and comparisons were made that proved the technique was viable for the study of upper level transitions as well as a diagnostic tool for plasmas and flames with the possibility of graphite tube atomizers. Third, the first excited doublet states were strongly coupled with one another by collisions. This meant that the doublet acted as a "single" state. This was shown to be true because a dip was observed for the resonant as well as the nonresonant fluorescence wavelength situations. Fourth, the applicability to other elements for the investigation of their atomic parameters was investigated.

Other elements such as palladium (Pd) and calcium (Ca) were also investigated. The choice of palladium was made because it had an abundant number of energy levels near the first excited state (Figure 2-30). The main purpose, then, was to monitor different fluorescence transitions to note the observance of a dip, if any. There was the primary dip observed for the connected states (Figure 2-31), but no other dips were observed for several fluorescence transitions. This indicated that the levels were not strongly coupled with one another.

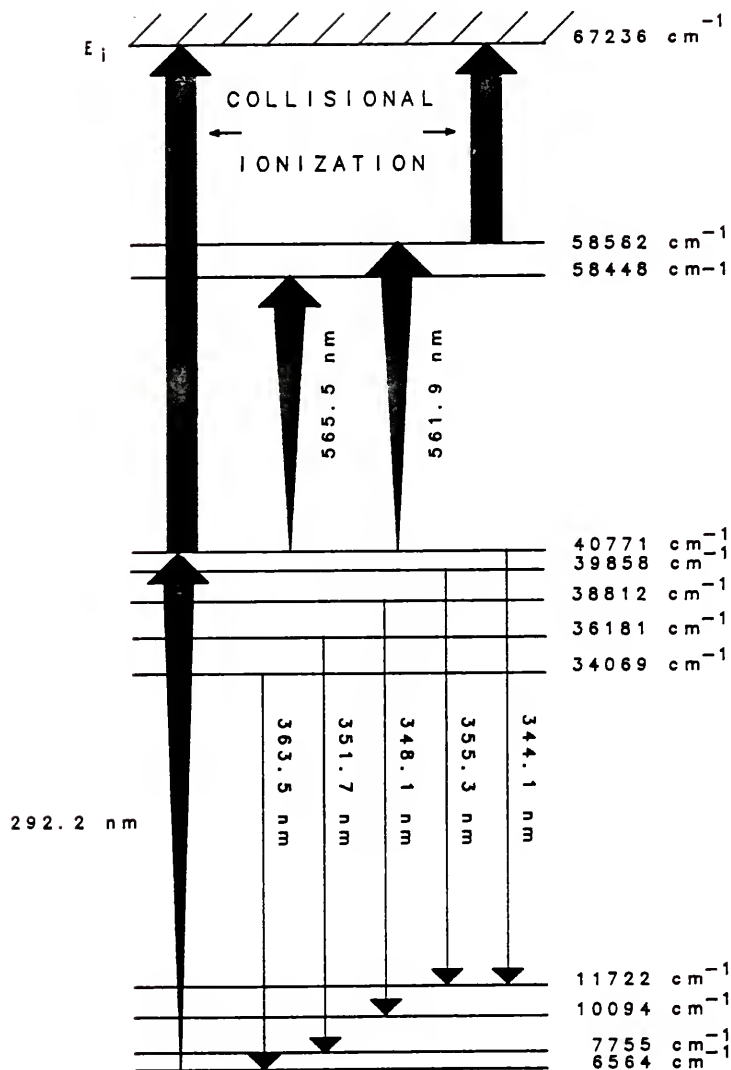


Figure 2-30 Partial Energy Level Diagram for Palladium

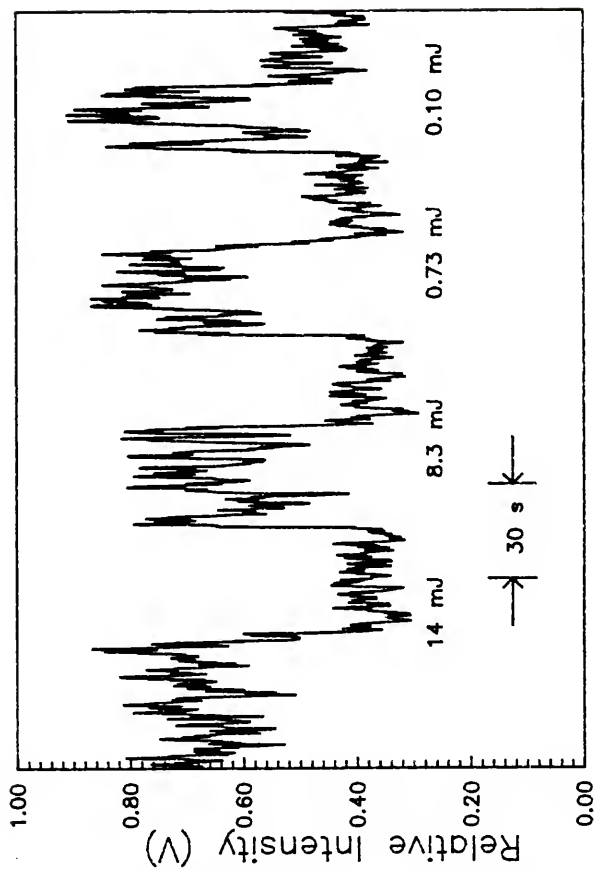


Figure 2-31 Measurement of Relative Fluorescence Intensity at 344.1 nm With and Without Laser Excitation at 565.5 nm as a Function of Laser Irradiance

The investigation of calcium was entirely different. To circumvent the losses due to ionization in the ICP, calcium ions ( $\text{Ca}^+$ ) were chosen as the target because the singly charged ions were prevalent and the possibility of creating the doubly charged ions was less than 1% (65). The second ionization potential was approximately 15 eV above the first ionization potential. In fact, the second excited state of the ionic transition was approximately 9 eV below the second ionization potential. With all these possibilities, it would appear that this would be an ideal situation for a dip. However, this was not the case because the necessary wavelengths (Figure 2-32) obtained from frequency conversion of the dye lasers were not able to saturate the transitions as well as not "beat" the deactivation processes. In addition, preliminary investigations of a fluorescence dip for lead (Pb) were done in a graphite tube atomizer. These experiments, along with the sodium dip experiments, demonstrated that fluorescence dip spectroscopy is indeed a viable diagnostic tool for qualitative and semi-quantitative information.



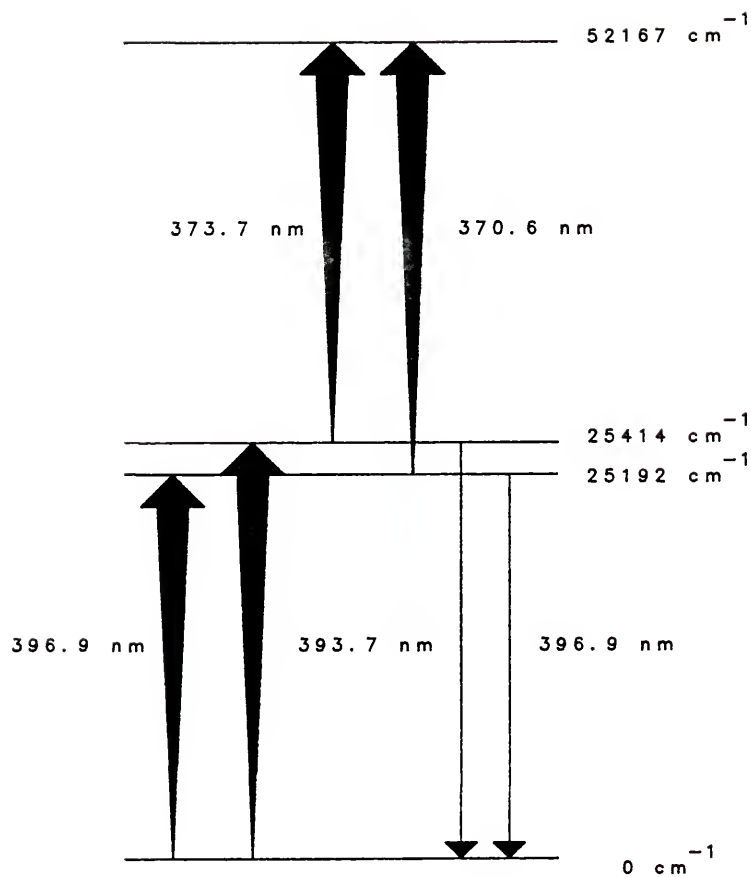


Figure 2-32 Partial Energy Level Diagram for Calcium (II) Ion

CHAPTER 3  
ATOMIC FLUORESCENCE AND IONIZATION MECHANISM  
FOR LEAD IN AIR-ACETYLENE FLAME

Basic Principles of Atomic Fluorescence and  
Ionization Spectroscopies

Atomic fluorescence spectroscopy (AFS) is based on the absorption of radiation by an atomic specie, thereby producing atoms in an excited electronic state, and the measurement of the light emitted when a fraction of the excited atoms undergoes radiational deactivation (66) from the excited electronic state. Of the several pathways for deactivation, the three most common are resonance fluorescence, in which the same lower and upper levels are involved in the excitation and deactivation processes (Figure 3-1a); direct line fluorescence, in which the same upper level is involved in the excitation and deactivation processes (Figure 3-1b); and stepwise line fluorescence, in which different upper levels are involved in the excitation processes (Figure 3-1c) (67). In stepwise line fluorescence, there are three steps. The first step is the absorption of photons to excite the atom to an excited level. This is subsequently followed by collisional processes where demotion or promotion of an electron to a nearby excited level occurs. The final step is the deactivation process from the new excited level to the lower level.

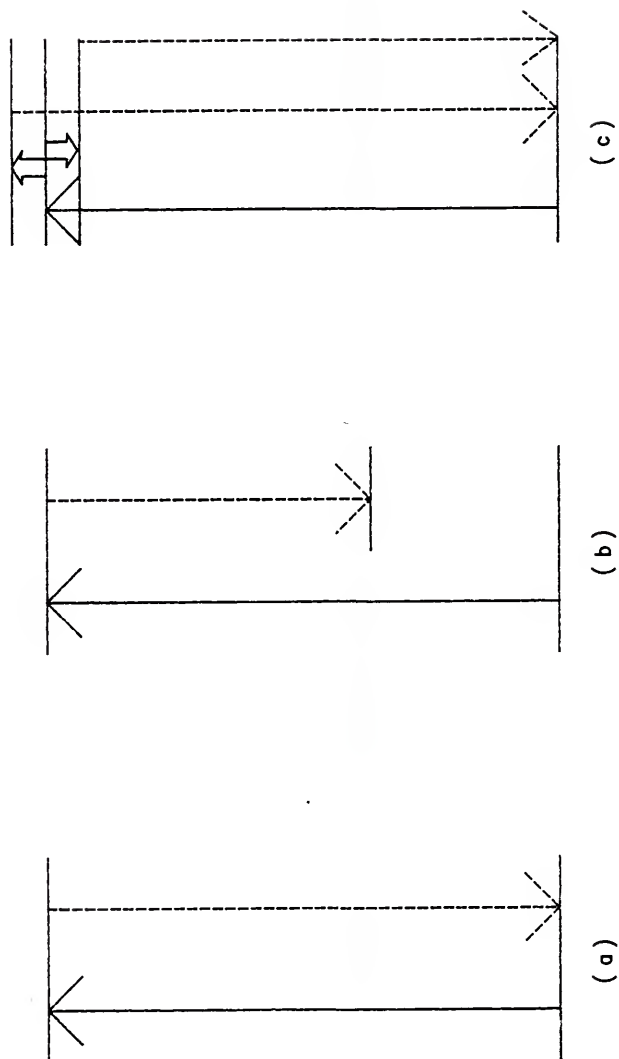


Figure 3-1 The Three Basic Pathways of Atomic Fluorescence: a) Direct Line Fluorescence, b) Resonance Fluorescence, and c) Stepwise Line Fluorescence

For double resonance excitation, resonance fluorescence is not possible because the transition from the second excited state to the ground state is a forbidden one-photon transition (i.e., the symmetries are incorrect). Thus, only direct and stepwise line (e.g., anti-Stokes) fluorescence schemes are considered.

Laser enhanced ionization is based on selectively populating a specific excited state of an analyte such that there is a decrease in energy required for ionization from the excited state relative to the ground state (41). Since the rate of collisional ionization increases as the energy required for ionization decreases, it is desirable to populate higher energy excited states (47). To this end, double resonance excitation schemes are ideal for this situation because they populate levels that are much closer to the ionization continuum than one-step processes (Figure 1-2b). Signal enhancements of 100-fold or greater are often achieved relative to that observed when the one-step processes are used (47).

It is apparent that the combination of two-color laser enhanced ionization and two-color laser excited atomic fluorescence is a powerful technique with which to study ionization mechanisms in the air-acetylene flame, traditionally the atomization cell of choice. The two-color laser enhanced ionization was more useful for diagnostic studies than the two-color laser excited atomic fluorescence because the primary investigation was the overall temporal features of the waveform for the electron pulse. However, the atomic fluorescence technique proved useful in the determination of the analytical wavelengths for the second transition as well as for later experiments involving the graphite tube atomizer.

### Experimental Facilities and Considerations

A block diagram of the experimental setup is shown in Figure 3-2 and a detailed listing of the experimental components is described in Table 3-1. The laser system has been previously described in this dissertation. There are two modifications of that laser system. The first difference was that the second dye laser was operated with a dye mixture of Rhodamine 610 and Rhodamine 640 in a 4:1 ratio, respectively. The second difference was that the first dye laser was frequency doubled to ultraviolet radiation through use of a potassium dihydrogen phosphate (KDP) crystal. The first dye laser was tuned to 566.612 nm and then frequency doubled to 283.306 nm, the atomic resonance transition of lead as shown in Figure 3-3. The second dye laser was either scanned through or tuned to three possible wavelengths (i.e., 600.193, 601.172, and 605.942 nm) (Figure 3-3). Typical laser irradiances were 1 mJ per pulse for the ultraviolet laser and 0.1 and 10 mJ per pulse for the second dye laser. For the second dye laser, the output irradiance was changed discretely by placing a neutral density filter at 2.0 in front of the laser beam.

The air-acetylene flame has been the stalwart for analytical flame atomic spectroscopy over the last twenty-five years. The air-acetylene flame has been studied in detail so that many of the mechanisms, and thus components in the flame, are known and understood (68). The primary limitations are the low temperature of the flame (e.g., 2500°K) and quenching of the fluorescence. To

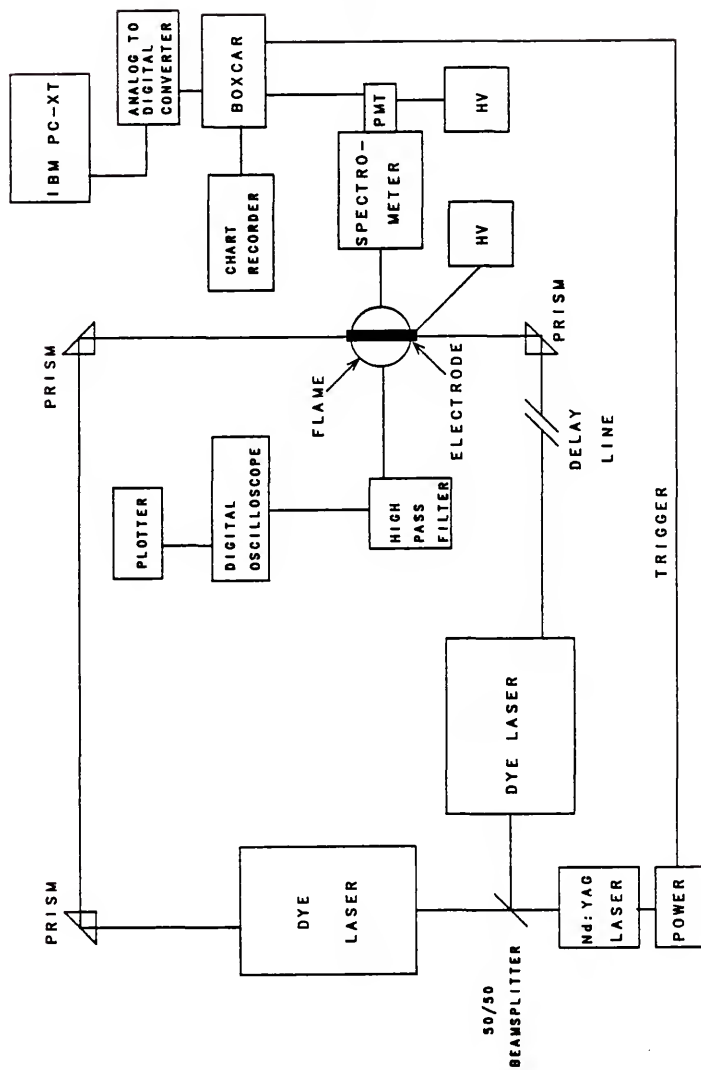


Figure 3-2 Block Diagram of Experimental Setup for Laser Enhanced Ionization and Laser Excited Atomic Fluorescence Spectroscopies

Table 3-1  
Experimental Components for Laser Enhanced Ionization  
and Laser Excited Atomic Fluorescence Spectroscopies

Component	Model No.	Manufacturer
Nd:YAG laser	YG 581-30	Quantel International, Santa Clara, CA
Dual dye lasers	TDL 50	Quantel International, Santa Clara, CA
Frequency doubler	HP 50	Quantel International, Santa Clara, CA
Slot burner, spray chamber, and nebulizer		Perkin Elmer Corp., Norwalk, CT
Stainless steel electrode		Laboratory constructed
90° Quartz prisms		Esco Products, Inc., Oak Ridge, NJ
Quartz lens		Oriel Corp., Stratford, CT
0.35 m Spectrometer	EU-700	Heath, <sup>a</sup> Acton, MA
Photomultiplier tube	R 1547	Hamamatsu Corp., Bridgewater, NJ
High voltage power supplies	226	Pacific Precision Instrum., Concord, CA
Boxcar averager, gated integrator	SR 250	Standard Research Systems, Palo Alto, CA
Computer interface	SR 245	Standard Research Systems, Palo Alto, CA
Chart recorder	D-5000	Houston Instrum., Austin, TX
Digital oscilloscope	2430A	Tektronix, Inc., Beaverton, OR
Plotter	HP 7470A	Hewlett Packard, Palo Alto, CA

<sup>a</sup> Now GCA/McPherson.

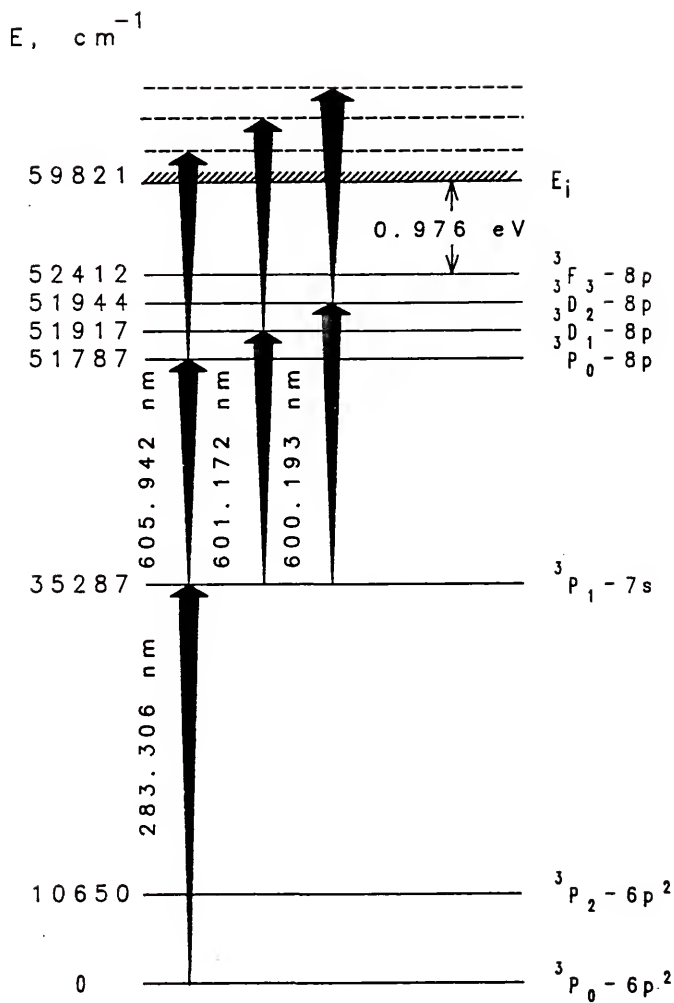


Figure 3-3 Partial Energy Level Diagram for Connected Double Resonance Excitation and Ionization of Lead



reduce some of the quenching, an argon sheath has been used to enclose the flame to prevent quenching from the surrounding air.

In these experiments, a 5 cm slot burner was used that did not have the necessary design for a protective sheath, but this was not a factor since quantitative measurements were not being made (i.e., limits of detection). The flame was mounted on a commercial atomic absorption spray chamber. An approximate stoichiometric air-acetylene flame was used for all studies. A water-cooled stainless steel tube that was flattened to increase the surface area was used as an electrode (i.e., cathode) with a negative bias voltage, -1300 VDC. This electrode was immersed into the center of the flame such that the electrode was 21 mm above the burner head and that the laser beam passed parallel to and 3 mm below the electrode, unless otherwise noted. The burner head was grounded (i.e., anode) through a 10 k $\Omega$  resistance so that it acted as a collector for electrons.

The ionization currents were capacitively coupled through 500 pF to reduce flame background leakage currents and then were converted to voltages using the 50  $\Omega$  termination mode in the digital oscilloscope. The waveform was acquired, displayed, and stored through the oscilloscope.

Laser excited atomic fluorescence of lead was monitored at several wavelengths (e.g., 216.999, 239.379, 261.418, or 405.783 nm) at a right angle to the laser beams using a 50.8 mm diameter, 111.6 mm focal length quartz lens to image (1:1) the flame volume onto the entrance slit of a f/6.8, 0.35 m spectrometer. This was done to insure that the lasers were properly tuned to the correct

transitions. An iris diaphragm (31 mm diameter opening) was placed directly after the lens to prevent overfilling the grating. The entrance and exit slits were set at 1 mm to collect as much fluorescence emission as possible. The output of the photomultiplier tube was terminated into a 50  $\Omega$  resistor. Data acquisition, analysis, and storage were the same as that described earlier.

The experimental parameters are listed in Table 3-2. All the measurements pertaining to the fluorescence and ionization signals were done with a solution of 100 mg/L of Pb unless otherwise noted. This solution was prepared from a 1 g/L stock solution which was diluted to the mark with deionized distilled water.

## Results and Discussion

### Atomic Fluorescence Study

Although the fluorescence study was not done to obtain analytical figures of merit, such as linear dynamic range and limits of detection, atomic fluorescence did serve a very important purpose in the outcome of the ionization studies. The fluorescence monitoring of the double resonance as well as the single resonance excitation schemes was important to the tuning of the lasers so that the transitions under investigation were indeed the correct ones being excited. To insure proper tuning, several fluorescence wavelengths were monitored as shown in Figure 3-4.

Laser enhanced ionization is a very powerful technique, and therefore, it was imperative that the centers of the atomic

Table 3-2  
Experimental Parameters for Laser Enhanced Ionization  
and Laser Excited Atomic Fluorescence Spectroscopies

---

Acetylene flow rate	1.2 L/min
Auxiliary air flow rate	7.5 L/min
Nebulizer air flow rate	2.8 L/min
Solution uptake rate	4.5 mL/min
Scan rate of second excitation laser	0.02 nm/s
Electrode potential	-1300 VDC
PMT high voltage	-900 VDC
Slit width	1 mm
Slit height	1 cm
External trigger rate	30 Hz
Gate delay	51 ns
Sensitivity	10 mV/V, 50 mV/V
Input filter	>10 kHz
Number of pulses averaged	3 pulses
Terminating resistor	50 $\Omega$

---

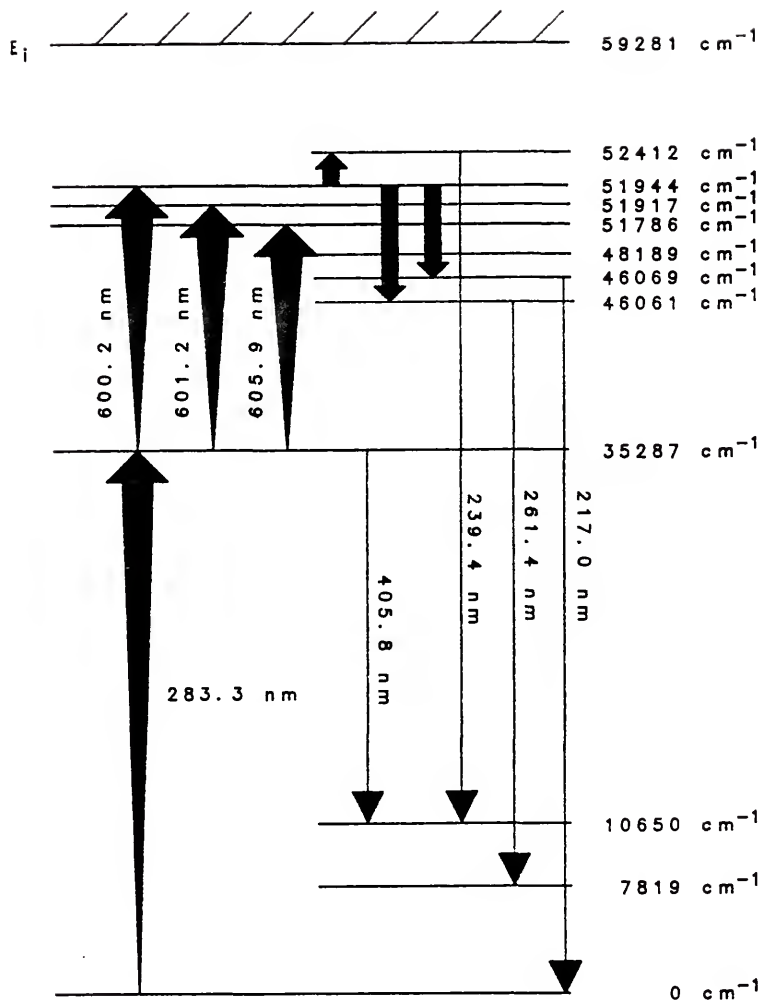


Figure 3-4 Partial Energy Level Diagram for Connected Double Resonance Excitation of Lead

resonance line was being excited and not the wings of the atomic lines. Excitation of the wings produced ionization signals. To achieve proper tuning, it was best to monitor fluorescence transitions so that fluorescence signals could be observed to unequivocally prove that the laser excitation schemes were indeed correct. This was done for the 283.306 nm excitation line by monitoring the 405.783 nm. For the double resonance excitation scheme, several fluorescence wavelengths were individually monitored. As the fluorescence wavelength was fixed, the second laser was scanned through the three upper level transitions as shown in Figures 3-5 and 3-6. It can be seen that the most intense transition was at 600.193 nm for both of these examples. This was further verified by other fluorescence wavelengths which ranged from 216.999 to 373.995 nm.

#### Ionization Study

Ionization currents were produced through the double resonance excitation scheme followed by collisional ionization or photoionization as illustrated in Figure 3-3. Lead was first excited with the ultraviolet radiation at 283.306 nm. It was then followed by the visible radiation at 600.193 nm, in most cases.

Amplification was desirable for our experiments, but could not be done because the available current-to-voltage amplifiers were too slow in their response. The waveform collected was distorted from the true waveform because of the speed with which these amplifiers

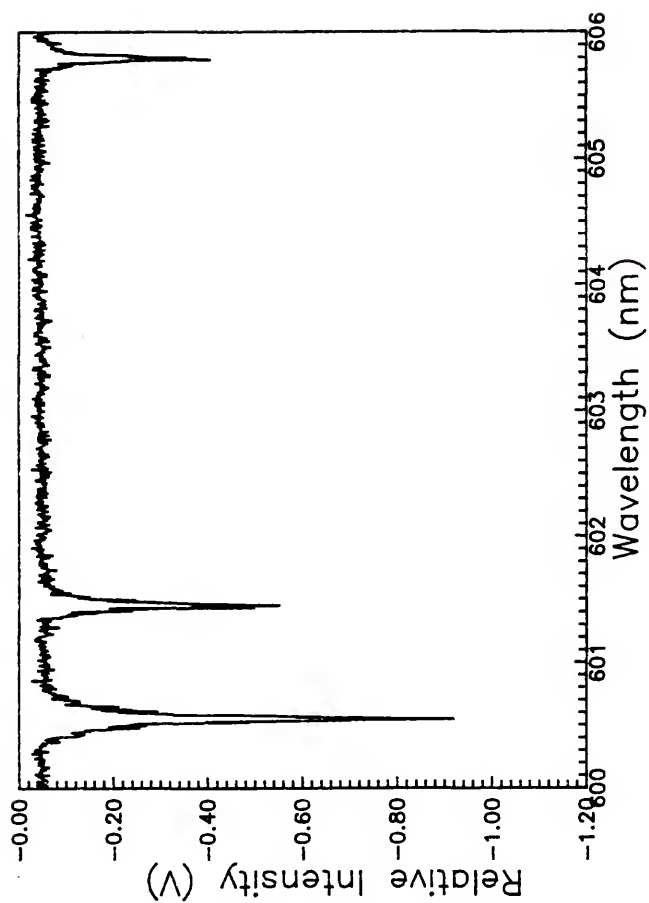


Figure 3-5 Scan of the Second Excitation Laser With the Fluorescence Wavelength at 239.379 nm and the First Excitation Laser at 283.306 nm for Lead

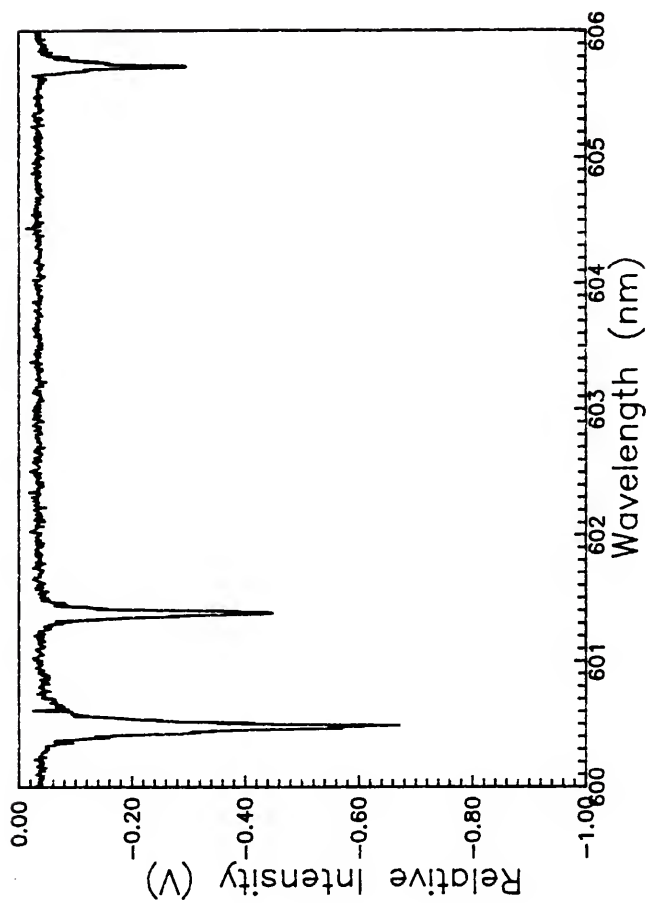


Figure 3-6 Scan of the Second Excitation Laser With the Fluorescence Wavelength at 261.418 nm and the First Excitation Laser at 283.306 nm for Lead

operate (e.g., 20 MHz). This is compared with that of the digital oscilloscope, 150 MHz. A voltage amplifier (X 10) was also tested, but not used because it added too much noise to our system. Therefore, it seemed that the best arrangement was also the simplest one [i.e., signal was directly connected into a digital oscilloscope (50  $\Omega$  termination mode) without amplification].

Since the best arrangement was setup to collect and store the waveforms for the two-color laser enhanced ionization of lead, we wished to determine whether it was possible to distinguish temporally the collisional ionization from the photoionization features of the electron pulse. The observation of two features in the electron pulse in Figure 3-7 was striking. It was clearly visible that a fast, sharp, and intense component (FWHM  $\sim$ 15 ns) and a slow, broadened component (FWHM  $\sim$ 200 ns) were there. The fast component was believed to be the photoionization feature whereby ground state lead atoms have absorbed three photons (i.e., 283.306, 600.193, and 600.193 nm) to reach the ionization continuum. The slow component was felt to be the collisional ionization feature whereby ground state lead atoms have absorbed two photons (283.306 and 600.193 nm) and then, through collisions, have been elevated into the ionization continuum.

Further investigation of the phenomenon was done. The 600.193 nm laser beam was attenuated with a neutral density filter of 2.0; that is, the output irradiance was decreased by 100-fold and was approximately 0.1 mJ. This lower energy was insufficient to cause



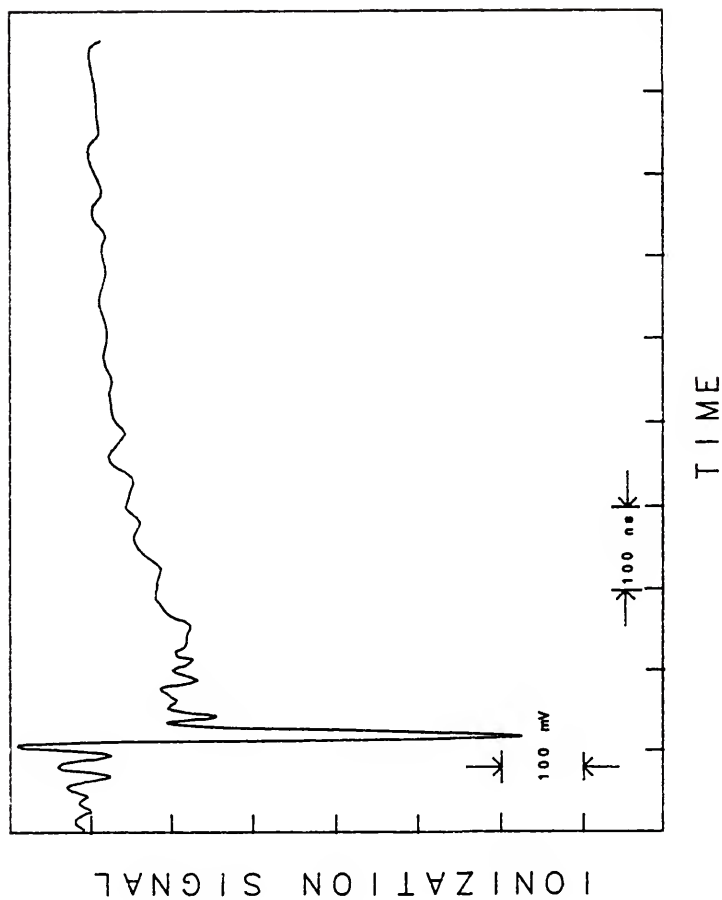


Figure 3-7 Temporal Behavior of the Ionization Signal as Recorded by the Oscilloscope With Full Laser Irradiance in Both Beams (283.306 and 600.193 nm)

photoionization (Figure 3-8) but still able to produce a collisional (i.e., ionization rate was lower than the radiative and quenching rates out from the 7s level) ionization feature. When Figures 3-7 and 3-8 were compared, it was apparent that the photoionization feature disappeared, but that the collisional feature was only reduced by a factor of two to three. This indicated that the upper 8d levels were under optical saturation. When the second excitation wavelength was changed to one of the other two transitions (e.g., 601.172 or 605.942 nm), similar ionization signals were observed with the only difference in the intensity. The intensity decreased as the second excitation wavelength became more shifted toward the red as shown in the fluorescence measurements (Figures 3-5 and 3-6).

Further experiments were performed as suggested by Turk of the National Bureau of Standards (69) to verify the shape of the waveform was real. Turk (69) felt the shape of the waveform was due to the detection process rather than the production of ions. The additional experiments included the effects of varying the bias voltage, the position of the laser beam relative to the burner head and the electrode, the variation of lead concentration, and the composition of the flame.

The effect of negative bias voltage was studied. Voltages were varied from -900 to -2000 VDC in increments of 100 V to note the effect, but no effect was observed with the exception of intensity. Since there was no effect, it was concluded that the waveform did not vary with the voltage in terms of its shape and behavior. This is in contrast to those results reported by Berthoud et al. (70).

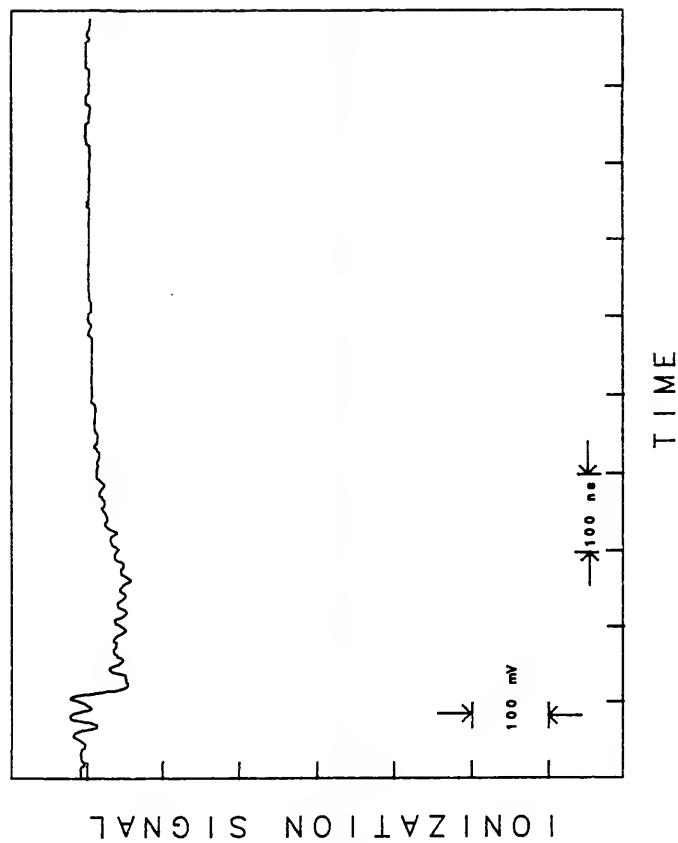


Figure 3-8

Temporal Behavior of the Ionization Signal as Recorded by the Oscilloscope with the Laser Irradiance at 600.193 nm Decreased by a 100-Fold and the 283.306 nm Laser Irradiance Unchanged

The position of the laser beam relative to the burner head and the electrode was investigated. The shape and behavior of the ionization waveform was identical with respect to the previous experiments at a laser position centered between the electrode and the burner (10 mm above the surface) except for a small decrease in magnitude. Measurements taken with the laser beams very close to the burner head (2 mm above the surface) showed a complete absence of the slower pulse component possibly due to a very low degree of collisional ionization within the flame reaction zone.

The effect of lead concentration and flame composition was considered. No dependence of the ionization waveform shape on lead concentration was noted. The concentration was varied from 10 to 500 mg/L. The normal air-acetylene flame that is used in everyday circumstances is composed of compressed air and acetylene. Since oxygen is the prime ingredient in compressed air for this type of flame, a gas cylinder containing a mixture of oxygen and argon in the ratio 1:4 was substituted for the compressed air. This flame has provided the identical shape and behavior of the ionization waveform.

### Conclusions

The ionization signal contained two distinct features in its waveform. It was concluded that the photoionization and the collisional ionization features were separated temporally as shown in Figure 3-7. Several experimental parameters were varied to note if the pulse shape and behavior changed, but none were observed. As mentioned earlier, Berthoud et al. (70) noticed extreme variations in

their pulse shape as the voltages were changed. This effect was not observed for these experiments.

However, these experiments were similar to those pointed out by Broglia et al. (71) in their investigation of the optogalvanic signal of uranium in a hollow cathode discharge lamp. By using a fast detection system, they showed that the temporal shape of the optogalvanic signal consisted of two components: a slow one, in a time scale typical of the relaxation time of the discharge, and a fast and more intense one, which occurred within the time scale of their laser pulse ( $\sim 5$  ns). The fast component was observed only when the difference in energy between the first excited state and the ionization limit was less than the energy required to excite atoms from the ground state to the first excited state, clearly pointing to a direct photoionization process caused by nonresonant absorption of a laser photon into the ionization continuum.

Much of the work in laser enhanced ionization spectroscopy was and is done with electronic detection systems that were not as fast (e.g., more than 50 ns in time scale) as the ones utilized here. The combination of fast detection electronics and of the simultaneous observation of the fluorescence and ionization signals seemed to be the best method for elucidating the excitation-ionization processes when atmospheric pressure flames are used as atom reservoirs.

CHAPTER 4  
MEASUREMENT OF ATOMIC FLUORESCENCE FOR  
LEAD IN A GRAPHITE TUBE ATOMIZER

Introduction to Graphite Tube Atomizers

Graphite tube atomizers are a part of a larger area known as electrothermal atomizers or graphite furnaces. Electrothermal atomizers have gained popularity through the years as an effective and efficient method for the production of atoms for atomic absorption spectroscopy (72-74). Besides graphite tube atomizers, there are rods, cups, and filaments all of which are made of graphite (Figure 4-1). Only in the last ten years have electrothermal atomizers found a place in atomic fluorescence spectroscopy.

Graphite furnaces are electrically heated devices that are heated through water-cooled contacts (e.g., copper, brass, or stainless steel). The heating is usually performed in three stages (drying, charring, and atomizing the sample). The drying stage,  $-110^{\circ}\text{C}$ , is used to evaporate the solvent as quickly as possible without spattering the material inside the furnace (74). Charring,  $350$  to  $1200^{\circ}\text{C}$ , is performed to remove volatile sample components at a temperature as high as possible without any effect or loss of the analyte (73). Atomization is accomplished by heating the furnace to  $1600$  to  $3000^{\circ}\text{C}$ , with a very rapid heating rate ( $800^{\circ}\text{C/s}$  or greater) so that analyte is quickly vaporized and atomized (74).

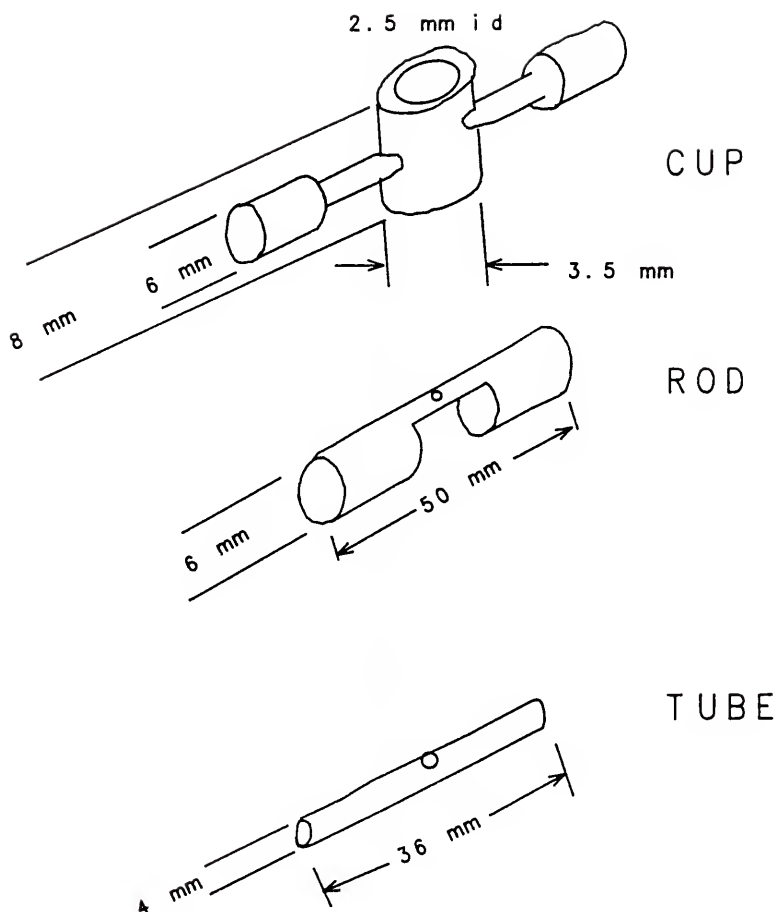


Figure 4-1 Graphite Furnace Designs

Over the years, graphite furnaces have been modified to improve the analytical performance. Among these modifications have been the L'vov platform (75) and treatment of the inner surface of the graphite furnace with coatings such as pyrolytic graphite (76), tantalum coating (77) or lining (78), and palladium (79).

The L'vov platform is a small graphite platform that is placed inside a graphite tube. The principle feature of the platform is that its temperature lags behind that of the walls because it is radiatively heated. This delay or lag in temperature causes the vaporation of the analyte to be delayed until the atmosphere reaches a high and quasi constant temperature. The platform results in a reduction of matrix interferences due to this constant atmosphere temperature (74). Modifiers, such as the ones mentioned, generally reduce or remove volatilization and vapor-phase interferences by allowing high enough pyrolysis temperatures to remove the bulk of concomitants during the charring stage (80).

#### Brief Review of Atomic Fluorescence Using Graphite Furnace Atomization

The vast majority of published literature employing graphite furnaces has been in atomic absorption spectroscopy. However, literature has appeared that has utilized graphite furnaces as atomization cells for laser excited atomic fluorescence spectroscopy (81-96). The graphite furnaces utilized have been either laboratory constructed or commercially available models. The mating of laser excited atomic fluorescence with graphite furnaces has provided



extremely low detection limits, in the range of sub-part per trillion to parts per trillion level or subfemtogram to picogram levels in terms of absolute amounts, for several elements, with linear dynamic ranges reaching six orders of magnitude (89,91,92).

Graphite furnaces possess several properties that make them attractive vaporization-atomization cells. First, the small volume consumption, typically 2 to 10 microliters per measurement, makes it well-suited for limited sample volumes as compared to the volume consumption of flame and plasma systems. Second, solid as well as liquid samples can be vaporized and atomized with no special adaptations to the furnace. Third, the nebulization stage is eliminated from the analytical sequence (75). Since the nebulization stage is eliminated, there is no need for sample introduction problems, and the sample is completely vaporized. Another advantage is that there is unlimited sample vaporization time (greater than 1 s) as compared to the limited vaporization time (less than 100 ms) for aerosol particles (75). Fourth, many of the matrix interferences have been greatly reduced due to the advent of matrix modifiers as first suggested by Ediger in 1975 (97). Fifth, graphite tube atomization (90,94,95) is preferred to graphite cup or carbon rod atomization despite the convenient optical geometry for observation of the fluorescence emission. Vapor phase interferences have existed with the carbon rod because of the strong temperature gradient between the atom formation and excitation zones. With graphite tube atomization, the atoms are contained in a hot environment while being excited by

the laser and, therefore, much better analytical performance results in the case of real samples (95).

Atomic fluorescence in graphite furnaces was first demonstrated for Pb by Neumann and Kriese (81) in 1974. Subsequently, other workers broadened the application to include a variety of elements, e.g., Bolshov et al. (85) (Ag, Co, Cu, Eu, Fe, Ir, Mn, and Pb) in 1981, Human et al. (88) (Pb and Tl) in 1984, Goforth and Winefordner (91,92) (Al, Cu, In, Li, Mn, Mo, Pb, Pt, Sn, and V) in 1986 and 1987, and Dittrich and Stark (95) (Al, Ga, In, Ir, and V) in 1987. Much of the work in this area has been performed by the Bolshov group in the Soviet Union as evidenced by their numerous publications (82,84,85, 89,98-102). It is also worth noting that only a couple of the published papers have delved into double resonance excitation schemes (86,96).

### Experimental Facilities and Considerations

#### Instrumentation

A block diagram of the experimental setup is shown in Figure 4-2 and a detailed listing of the experimental components is described in Table 4-1. The laser system has been previously described in this dissertation and is identical to the one used in the atomic fluorescence and ionization studies with two differences. The first difference was that the laser output irradiance of the first excitation laser, 283.306 nm, was changed discretely by placing a neutral density filter of 1.0 or 2.0 in front of the laser beam. The

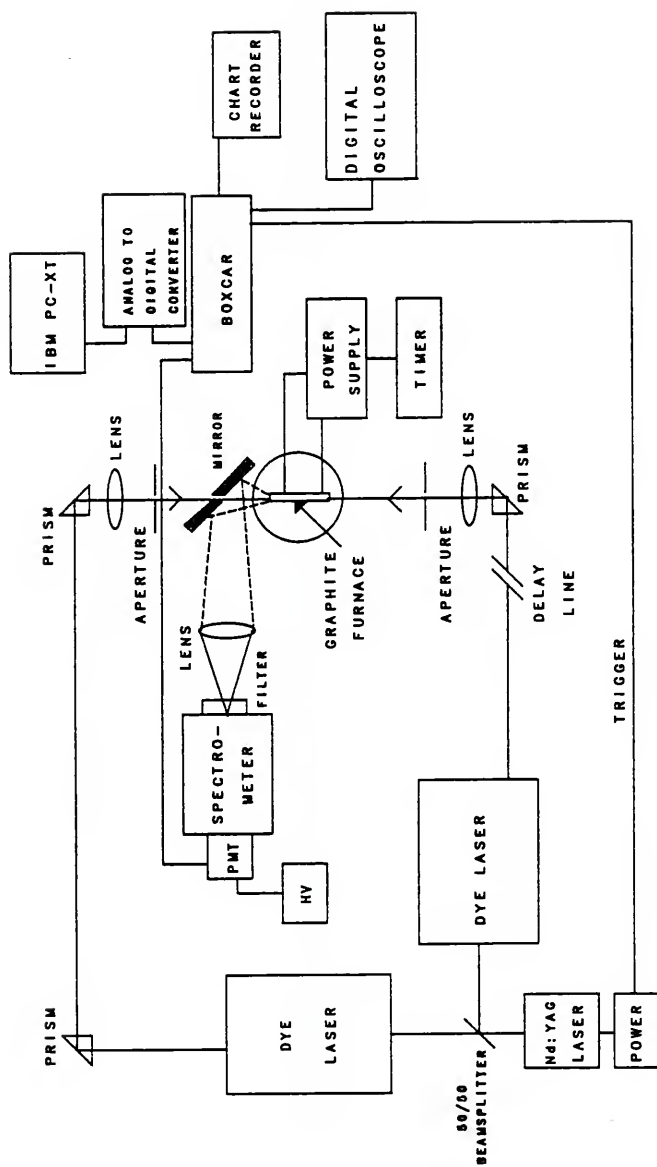


Figure 4-2 Block Diagram of the Double Resonance Laser Excited Atomic Fluorescence in a Graphite Tube Atomizer

Table 4-1  
Experimental Components for Double Resonance Laser Excited  
Atomic Fluorescence in a Graphite Tube Atomizer

Component	Model No.	Manufacturer
Nd:YAG laser	YG 581-30	Quantel International, Santa Clara, CA
Dual dye lasers	TDL 50	Quantel International, Santa Clara, CA
Frequency doublers	HP 50	Quantel International, Santa Clara, CA
Graphite tube and timing circuit		Laboratory constructed
Furnace power supply	SCR 20-250	Electronics Measurements, Neptune, NJ
Micropipette		Brinkmann Instrum. Co., Westbury, NY
90° Quartz prisms and quartz lenses		Esco Products, Inc., Oak Ridge, NJ
0.22 m Double monochromator with scan controller	1680B CD2A	Spex Industries, Inc., Methucen, NJ
Neutral density filters		Corion Corp., Holliston, MA
Photomultiplier tube	R 955	Hamamatsu Corp., Bridgewater, NJ
High voltage power supply	301	Bertan Assoc. Inc., Hicksville, NY
Amplifier	4131	Evans Assoc., Berkeley, CA
Boxcar averager, gated integrator	SR 250	Stanford Research Systems, Palo Alto, CA
Computer interface	SR 245	Stanford Research Systems, Palo Alto, CA
Computer	PC-XT	IBM Corp., Boca Raton, FL

Table 4-1--continued.

Component	Model No.	Manufacturer
Digital oscilloscope	2430A	Tektronix Inc., Beaverton, OR
Chart recorder	D-5000	Houston Instrum., Austin, TX

second difference was that the second excitation laser was either in the visible region ( $\sim 600$  nm) or the ultraviolet region ( $\sim 280$  nm). For the first set of experiments, the second excitation laser was operated with a dye mixture of Rhodamine 610 and Rhodamine 640 in a 4:1 ratio, respectively. For the second set of experiments, the second excitation laser was operated with pure Rhodamine 590 solution. The second dye laser was frequency doubled to ultraviolet radiation through the use of a potassium dihydrogen phosphate crystal. The second dye laser was tuned to 564.640 nm and then frequency doubled to 282.320 nm. Typical laser irradiances were 0.01, 0.1, and 1 mJ per pulse for the first excitation laser depending upon the neutral density filter and 1 or 10 mJ per pulse for the second excitation laser depending upon the excitation wavelength used.

Transfer of laser radiation into the graphite tube was accomplished with the use of prism reflectors and lenses. As previously mentioned, prisms were arranged in such a manner so that both laser beams arrived at the center of the tube at the same time and in the same space. Each beam, having approximately 3 mm diameter at each side of the tube, was separately focused with a suitable quartz lens (250 cm focal length) into a hole (2 mm diameter,  $45^\circ$ ) pierced in a plane mirror which was positioned near the furnace.

The graphite tube atomizer system (Figure 4-3) was similar to the one designed by Molnar et al. (103) and used by Goforth and Winefordner (92). The tube dimensions were 36 mm in length with an internal diameter of 4 mm. It consisted of two water-cooled copper

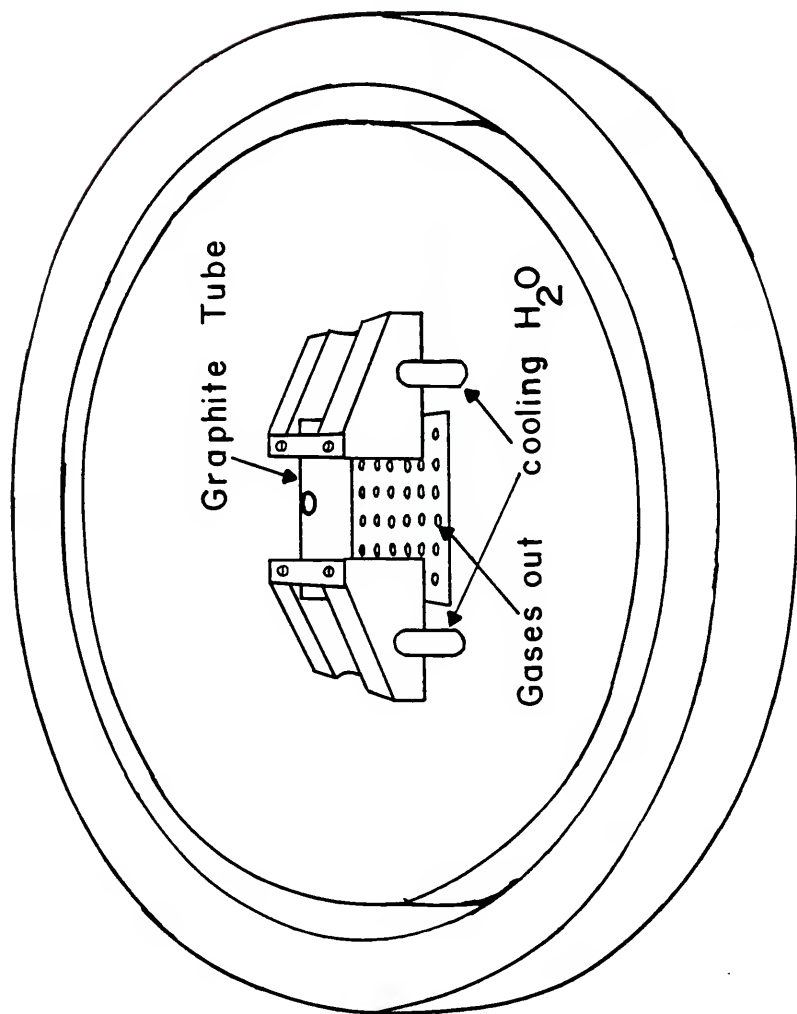


Figure 4-3 Graphite Tube Atomizer Setup

blocks mounted on a bakelite support serving the purpose of holding the graphite tube and providing the necessary electrical contact with two stainless steel plates screwed into the top of the copper blocks. A flow of argon gas was maintained around and above the tube. In order to obtain a small gas flow inside the tube, two small bore stainless steel tubes were positioned very close to each end of the tube. The flow rate was adjusted with calibrated flowmeters. The heating rate and the final temperature of the graphite were controlled by the voltage setting of the power supply and also by the timing circuit (104). In this way, the graphite tube could be reproducibly heated up to any specified temperature, which was measured with an optical pyrometer.

Laser excited atomic fluorescence of lead was detected at several wavelengths sequentially (i.e., 216.999, 239.379, 261.418, and 405.783 nm) at a right angle to the laser beams. A plane mirror placed near the graphite tube with a 2 mm diameter was employed to redirect the emitted fluorescence to a 50.8 mm diameter, 111.6 mm focal length quartz lens which formed a 1:1 image of the center of the tube onto the entrance slit of a  $f/4$ , 0.22 m double monochromator. The output from the photomultiplier tube was converted to a voltage with a 1.2 k $\Omega$  resistor amplified via an Evans amplifier, terminated into 50  $\Omega$ , and processed by a boxcar averager, gated integrator. Data acquisition, analysis, and storage were the same as that described earlier.

The spectral tuning of the dye lasers at the lead transitions investigated was accomplished by monitoring the atomic fluorescence



of lead atomized in air-acetylene flame as described in Chapter 3. The experimental parameters are listed in Table 4-2.

All the fluorescence measurements were made with a 10 ng/mL solution prepared from a freshly made acidic 1 mg/L stock solution which was diluted to the mark with deionized distilled water. Ten microliter samples were then introduced into the tube with a calibrated micropipette. It must be noted that the deionized distilled water had a Pb contamination of approximately 1 ng/mL.

#### Alignment and Laser Scatter Considerations

The alignment of the optics (e.g., prisms, lenses, and mirrors) was of the utmost importance because of laser scatter considerations. Great care was taken to align properly each optical component so that each was centered in terms of height and each was at 0° incidence with respect to the laser beams and the emitted fluorescence. Even with this much care taken, it was inevitable that there was still laser scatter. Several methods were utilized to further reduce laser scatter as well as stray light.

The use of iris diaphragms located between the graphite tube and the focusing lenses was instituted to reduce back reflections from the optical components and further minimize the laser scatter. The insertion of a neutral density filter in front of the first excitation laser was placed as close as possible to the output of the dye laser to further minimize scatter. The employment of an iris diaphragm was used in front of the entrance slit of the double monochromator so that only the center of the furnace was imaged. A double monochromator was used to reject stray light. Room lights

Table 4-2  
Experimental Parameters for Double Resonance Laser  
Excited Atomic Fluorescence in a Graphite Tube

---

Main argon flow rate	10 L/min
Auxiliary argon flow rate	50 mL/min
Furnace temperature	1800°C
PMT high voltage	-900 VDC
Slit width	2 mm
Slit height	7 mm
Neutral density filter	2.0
Amplifier gain	10
External trigger rate	30 Hz
Gate decay	81 ns
Gate width	300 ns
Sensitivity	5 mV/V - 1 V/V
Input filter	>10 kHz
Number of pulses averaged	last sample, 10 pulses
Terminating resistor	50 $\Omega$

---

caused an increase in noise as well as stray light reaching the detector. Room lights were, therefore, turned off and the room was darkened with shades to further reduce the stray light effects. Lastly, a piece of black tape (7 mm diameter) was placed onto the center of the imaging lens to mask the laser scatter from the optical components. Even with all these efforts, laser scatter was never eliminated.

## Results and Discussion

### Effect of Argon on the Fluorescence Signal

The fluorescence signal was enhanced by a factor of two when argon was flowing through the two small bore stainless steel tubes positioned very close to the graphite tube. The signal enhancement was a result of the improved quantum efficiency (i.e., inert atmosphere) and the prolonged period of time that the cloud of atoms resided in the graphite tube. No appreciable increase in signal was obtained when the flow was more than 50 mL/min. Thus, an argon flow was maintained at 50 mL/min for all of the fluorescence measurements. This argon flow was in addition to the argon flow (10 L/min) that provided an inert atmosphere around the graphite tube.

### Connected Double Resonance Excitation

The scheme, where the second excitation transition starts from the level reached by the first excitation step, is referred here as connected double resonance excitation. As shown in Figure 3-4, the first laser beam is tuned to the strongest resonance transition at

283.306 nm originating from the ground state of the atom. Within the spectral range of the second dye laser used, three transitions (600.193, 601.172, and 605.942 nm) can be chosen to allow further excitation of the atoms into several levels lying approximately  $52000\text{ cm}^{-1}$  above the ground state. Due to collisional coupling of these levels and the nearby levels at lower energy ( $46069$  and  $46061\text{ cm}^{-1}$ ), several fluorescence transitions have been readily observed at wavelengths lower than the first excitation step, i.e., lower than 283.306 nm.

From the different combinations of excitation and fluorescence transitions investigated, two simultaneous excitation wavelengths (283.306 and 600.193 nm) and three fluorescence wavelengths (261.418, 239.370, and 216.999 nm) were selected as those providing the most intense signals. As shown in Figure 3-4, these signals are due to stepwise and thermally assisted anti-Stokes fluorescence processes (105), as the fluorescence emission occurs at a wavelength which is lower than either laser excitation wavelength. Obviously, the most useful combination of excitation/fluorescence transitions in the case of lead is the single step excitation at 283.306 nm and the observation of the direct line fluorescence at 405.783 nm. This is indeed the universal excitation/detection scheme reported in all fluorescence literature (106).

One of the predicted advantages of measuring ultraviolet fluorescence transitions following double resonance excitation is that furnace emission and its associated noise will be negligible since the blackbody spectral radiance decreases by several orders of

magnitude from 400 nm to 200 nm. These results are clearly shown in Figure 4-4. Here, the furnace was operated without lead and the output of the boxcar averager, gated integrator was directly displayed on the chart recorder. Since the boxcar input was AC coupled, only the emission noise was observed. The noise shown at the wavelengths 261.418, 239.379, and 216.999 nm, i.e., tracings (c) and (d) in Figure 4-4, are due primarily to the electronics and the detector system, i.e., it is the ideal noise with no contribution from the laser source (with firing of the laser but both beams blocked) and from the atomizer. By acquiring every laser shot during the overall atomization time, the resulting standard deviation was found to be 205  $\mu$ V. The standard deviation improved by a factor of four when the boxcar was set to average ten laser pulses and its average output was sent to the computer. For these operating conditions, i.e., in the absence of laser induced noise and furnace emission noise, the value of three times the standard deviation of the noise of the detection system at the three ultraviolet wavelengths was 150  $\mu$ V. It is worth emphasizing here that the noise shown in Figure 4-4 at 405.783 nm is not that occurring during the atomization stage of lead (performed at 1800°C) but during the final cleaning stage (2500°C). Therefore, the lead peak is well separated from the noise shown.

However, when the laser beams were admitted into the system, without operating the furnace, the noise is increased considerably as shown in Figures 4-5 and 4-6. The limiting noise shown in these figures was a result of leakage of some laser radiation into the

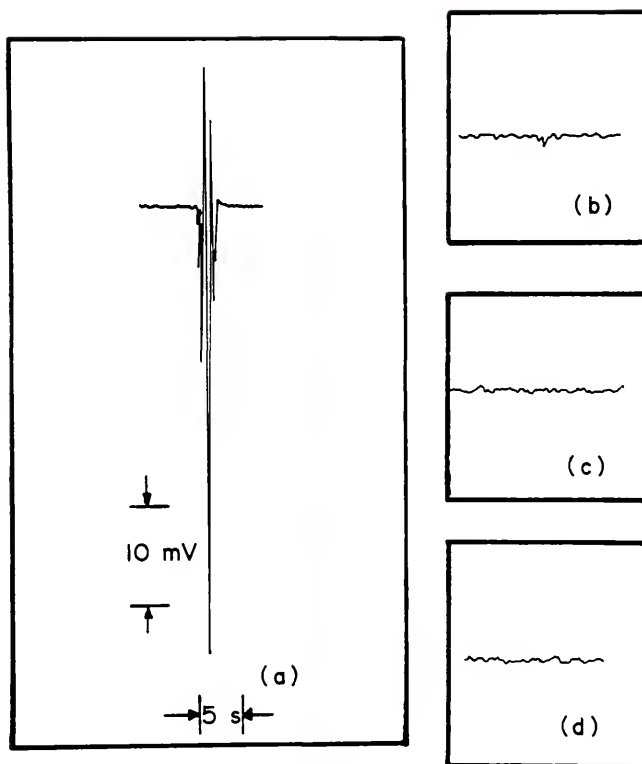


Figure 4-4 Chart Recorder Tracings of the Furnace Emission Noise at the Four Fluorescence Wavelengths Investigated in this Work: a) 405.783 nm, b) 261.418 nm, c) 239.379 nm, and d) 216.999 nm

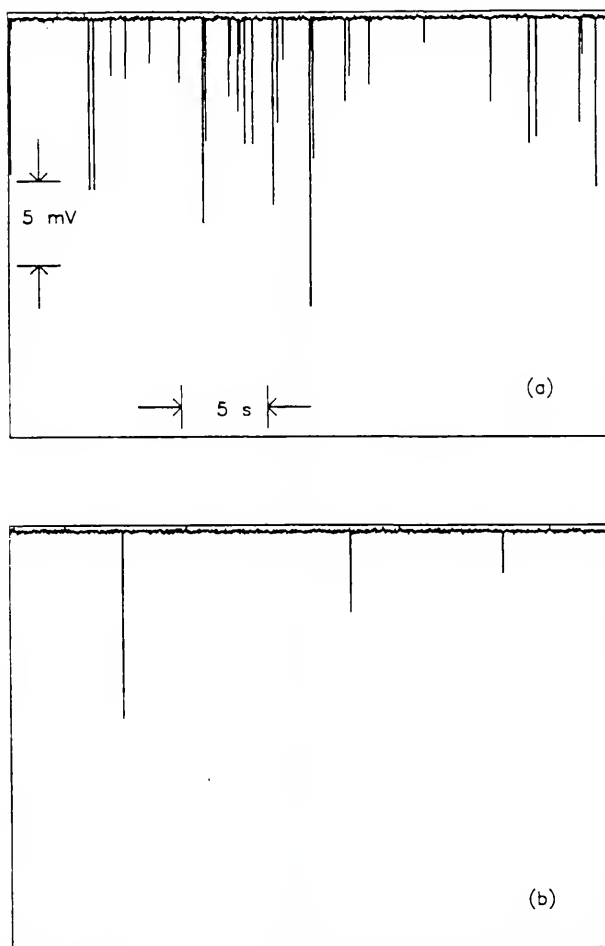


Figure 4-5 Boxcar Output for Laser Induced Noise into the Detector System for Single Resonance Excitation at 283.306 nm and Fluorescence Wavelength at 405.783 nm: a) 10% Transmission Neutral Density Filter Placed Between the Laser and the Graphite Furnace and b) 1% Transmission Neutral Density Filter Placed as in a

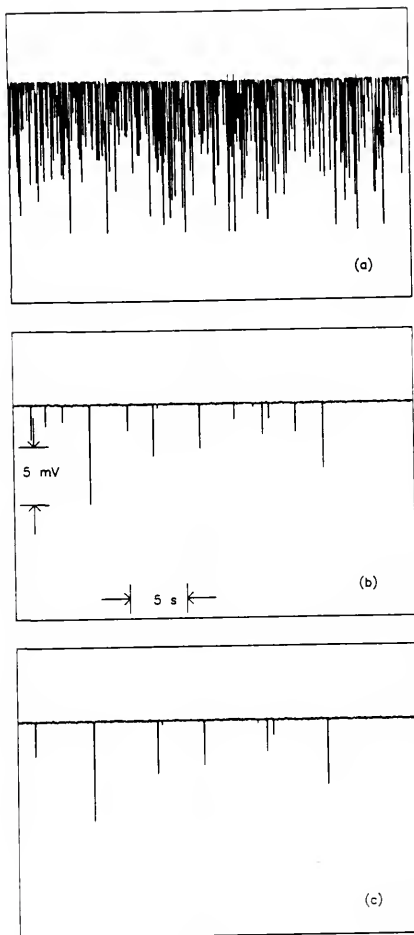


Figure 4-6 Boxcar Output for Laser Induced Noise into the Detector System for Double Resonance Excitation at 283.306 and 600.193 nm and Fluorescence Wavelength at 216.999 nm: a) Laser Operated at Full Power, b) 10% Transmission Neutral Density Filter Placed Between the First Laser (283.306 nm) and the Graphite Furnace, c) 1% Transmission Neutral Density Filter Placed as in b



fluorescence monochromator. Such leakage was a result of diffraction effects at the hole in the plane mirror and/or of reflections at the lenses and/or prisms, and atmospheric and furnace scattering. Because the magnitude of the spikes shown in Figures 4-5 and 4-6 were low (less than 10 mV), the signal levels in the experiments approach single photoelectron pulses. As a result, the frequency or rate of their occurrence can be decreased significantly by inserting suitable neutral density filters in front of the lasers as shown in Figures 4-5 and 4-6. It was found that the major leakage was caused by the laser tuned at 283.306 nm since the noise disappeared by blocking this beam. The laser tuned at 600.193 nm did not contribute to the noise level. In addition, it was found that the noise caused by the ultraviolet beam had different origins depending upon the settings of the fluorescence monochromator. In fact, when the monochromator was set at 405.783 nm, the signal in the absence of lead could be attributed to environmental fluorescence, as previously reported in the literature (88). Environmental fluorescence did not disappear when a cut-off filter, rejecting the 283.306 nm line, was placed in front of the monochromator. On the other hand, with the monochromator set at either of the ultraviolet fluorescence transitions, the signal was a result of stray light at 283.306 nm. At this stage of the work, no additional filters were available to isolate the ultraviolet fluorescence lines. Therefore, there is still ample room left for improvement in the noise level at these wavelengths and thus in the detection limits.

In order to improve the signal-to-noise ratio, one should take advantage here of the saturation of the absorption transitions, since in this case, unlike the noise, the fluorescence signal will not decrease by decreasing the laser irradiance. As shown in Figure 4-7, this was indeed the case for our laser system. In fact, the peak of the fluorescence signal at 216.999 nm obtained at full laser power did not change for a ten-fold decrease of the irradiance of the ultraviolet laser while it decreased by a factor of approximately six for a 100-fold decrease of the irradiation.

In Table 4-3, signals are given for both single resonance and double resonance excitation of 100 pg of lead introduced into the furnace as well as the standard deviation calculated by running the furnace without any sample injections. Operation of the furnace without any sample injections was necessary since the purest water available resulted in an easily observed signal. The blank signal was due to lead, since it disappeared by detuning the laser from the 283.306 nm line in the case of single resonance excitation and by simply blocking either laser beam in the case of double resonance excitation. As stated previously, it can be seen that the laser induced noise is the limiting noise with the present experimental setup. Only when the fluorescence is measured at 216.999 nm and a neutral density filter of 2.0 is inserted into the laser beam does the standard deviation of the blank approach the ideal level of 150  $\mu$ V (detector and electronics noise level). It is, therefore,

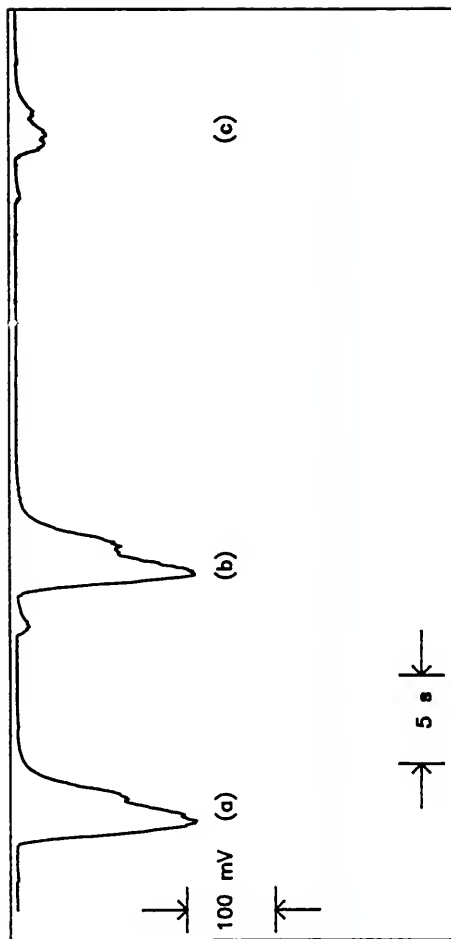


Figure 4-7 Boxcar Output for Fluorescence of 100 pg of Lead With Excitation at 283.306 and 600.193 nm and the Fluorescence Wavelength at 216.999 nm: a) Both Laser Operated at Full Power, b) 10% Transmission Neutral Density Filter Placed Between the First Laser (283.306 nm) and the Graphite Furnace, and c) 1% Transmission Neutral Density Filter Placed as in b

Table 4-3  
Peak Fluorescence Signals for 100 pg of Lead  
and Related Noise Figures

Excitation Wavelength (nm)	Fluorescence Wavelength (nm)	Signal (mV)		Standard Deviation (mV)	
		ND1 <sup>a</sup>	ND2 <sup>b</sup>	ND1 <sup>a</sup>	ND2 <sup>b</sup>
283.306	405.783	62,598	10,642	0.61	0.17
283.306 + 600.193	261.418	1,583	269	1.08	0.17
283.306 + 600.193	239.379	773	131	0.33	0.39
283.306 + 600.193	216.999	405	69	0.36	0.06

Note: Average output of the boxcar (10 pulses averaged) sent to the computer. Compared to no averaging, this procedure results in a loss in the peak of the signal of 25%.

<sup>a</sup> Neutral density filter (10% transmission in front of the 283.306 nm beam.

<sup>b</sup> Neutral density filter (1% transmission) in front of the 283.306 nm.

therefore, clear that one needs to improve the capability of the optical system to reject unwanted radiation scattered into the monochromator-detector. Additional filters transmitting below 270 nm will also prove useful but careful alignment and baffling is believed to be more important.

In Table 4-4, calculated experimental detection limits are given for all the combinations of excitation/fluorescence wavelengths used. It is evident that there is roughly one order of magnitude between the detection limits predicted and those actually achieved. The detection limits designated as achievable are under ideal conditions, i.e., no laser scatter, detector and electronic noise only and no averaging of pulses. Also, even though detection limits by the double resonance scheme are about two orders of magnitude worse than those obtained with the single resonance scheme, they are still one order of magnitude better than the best atomic absorption value (107).

These results are considered to be very promising and certainly point to a more general use of double resonance fluorescence technique. A very probable explanation of the loss of sensitivity for the double resonance scheme compared to the single resonance one consists in the pronounced ionization losses occurring during the interaction time between the atoms and the laser beams. As shown in Figure 3-4, the second excitation step ( $\sim 600$  nm) brings the atoms to a level which is  $\sim 7000 \text{ cm}^{-1}$  (less than 1 eV) below the ionization level and therefore collisional ionization out of this and the nearby collisionally mixed levels occurs at a much faster rate than that of

Table 4-4  
Laser Excited Atomic Fluorescence of Lead in a  
Graphite Tube Atomizer: Absolute Detection Limits  
as Obtained by Single Step and Two-Step Excitation

Excitation Scheme (wavelengths, nm)	Detection Limits (fg)			
	Literature AA <sup>a</sup>	Literature AF <sup>b</sup>	This work	
			f	g
$\lambda_{\text{exc}} = 283.306$ $\lambda_{\text{fl}} = 405.783$	5000	$5^c$ $10^d$	0.2	3
$\lambda_1 = 283.306$ $\lambda_2 = 600.193$ $\lambda_{\text{fl}} = 261.418$	----	$210^e$	9	200
$\lambda_1 = 283.306$ $\lambda_2 = 600.193$ $\lambda_{\text{fl}} = 261.418$	----	---	19	130
$\lambda_1 = 283.306$ $\lambda_2 = 600.193$ $\lambda_{\text{fl}} = 261.418$	----	---	37	270
$\lambda_1 = 283.306$ $\lambda_2 = 600.193$ $\lambda_{\text{fl}} = 261.418$	----	---	60	800
$\lambda_1 = 283.306$ $\lambda_2 = 600.193$ $\lambda_{\text{fl}} = 261.418$	----	---	200	2000

Note: S/N = 3, off line.

<sup>a</sup> Reference 107.

<sup>b</sup> Data refers to graphite tube atomization.

<sup>c</sup> Reference 96.

<sup>d</sup> Reference 94.

<sup>e</sup> Reference 86, recalculated for S/N = 3, 1-cm<sup>3</sup> atomizer volume, and equivalent time constants, assuming white noise.

<sup>f</sup> Predicted to be obtainable under ideal conditions, i.e., standard deviation of 150  $\mu$ V and no averaging, i.e., no loss of the peak signal.

<sup>g</sup> Obtained under our experimental conditions (laser irradiance attenuated 10X).

the level at  $35287\text{ cm}^{-1}$  which is reached with single step excitation at  $283.306\text{ nm}$ . In addition, there is the possibility of direct photoionization due to the simultaneous absorption of two laser photons at each of the three transitions shown in Figure 3-4, since their energy is greater than half the energy required to ionize the atoms present in the  $35287\text{-cm}^{-1}$  level. The laser enhanced ionization technique does indeed provide very low detection limits for lead both in flames (40,108) and in a graphite furnace (109) but inferior to those obtained here.

#### Disconnected Double Resonance Excitation

In the early studies of the laser excited fluorescence of lead atoms in flames and furnaces, it was soon recognized (110) that, because of the metastable character of the level lying at  $10650\text{ cm}^{-1}$  above the ground state, a significant fraction of the atoms will accumulate in this level during the excitation pulse, despite short interaction time. In an air-acetylene flame, the lifetime of this Pb level was measured by a modified ionization technique and found to be  $360\text{ ns}$  (42). It was, therefore, felt that one could tune the second excitation step to a transition originating from the metastable level (Figure 4-8). In this way, two advantages were predicted. First, direct line fluorescence could be measured at  $261.418\text{ nm}$  following excitation at  $282.320\text{ nm}$ . In this way, there was no need for collisions to populate the fluorescence level as it was in the case of connected double resonance excitation (see Figure 4-9). Second, the levels reached by the second step are located approximately  $1.6\text{ eV}$  below the ionization continuum, and therefore, the collisional

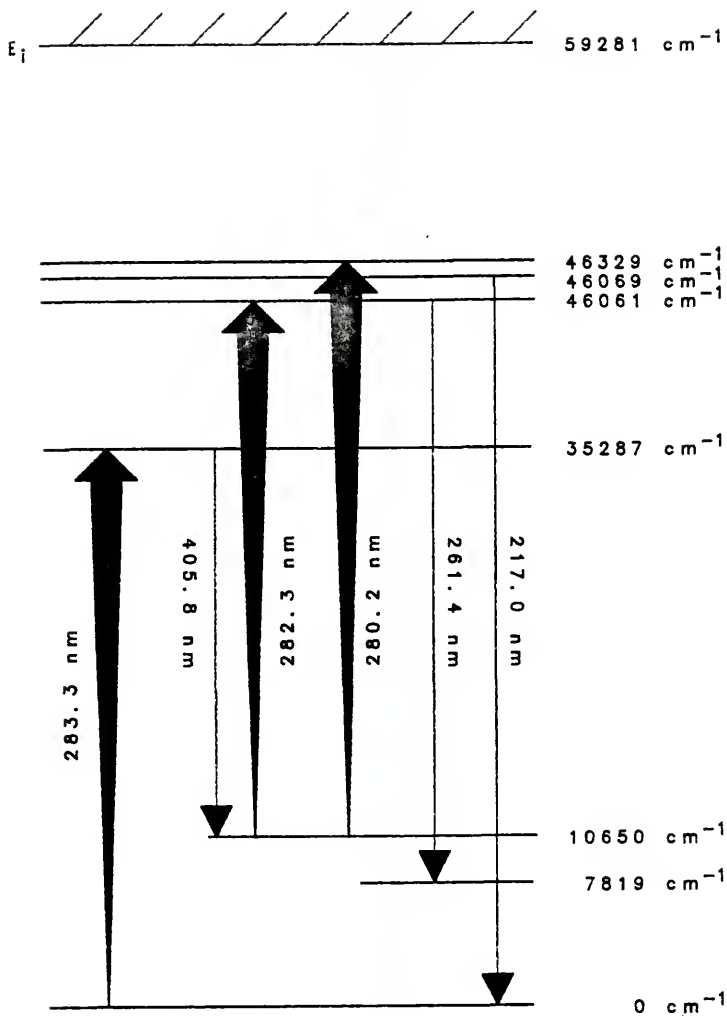


Figure 4-8 Partial Energy Level Diagram for Disconnected Double Resonance Excitation of Lead



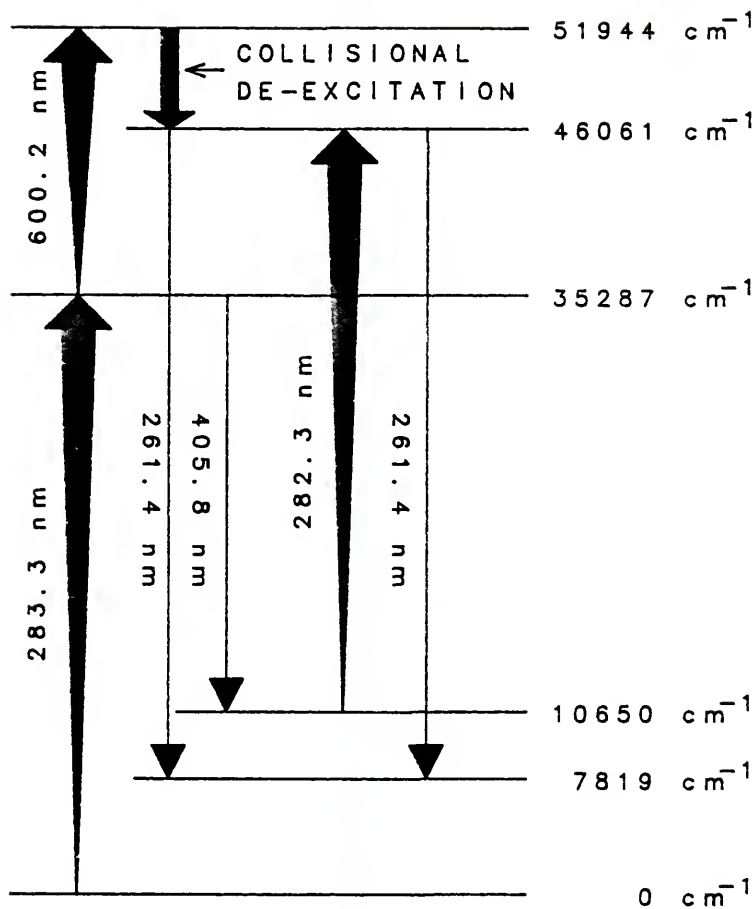


Figure 4-9 Comparison of Connected and Disconnected Double Resonance Excitation of Lead

ionization losses were expected to be much less than before. In addition, the second excitation step being also in the ultraviolet, the laser had to be frequency doubled, with a power loss of  $\sim 10$  times. As a consequence, the possibility of direct photoionization losses should have been negligible.

The experiment was performed with the second step tuned to 282.320 nm and the fluorescence collected at 261.418 nm and at 216.999 nm (Figure 4-8). As predicted, the signal level was larger (approximately 2 to 3 times) than that obtained for the connected double resonance scheme and disappeared when either of the two laser beams was blocked. Unfortunately, the increase in the noise level, now due to stray light caused by both ultraviolet laser beams, was even larger, resulting in an overall degradation of the detection limits. In fact, with the same procedure used for the values reported in Table 4-4, the detection limits for the disconnected excitation scheme were found to be 0.8 pg for the 261.418 nm fluorescence and 2 pg for the 216.999 nm fluorescence. These results stress once more the need for improving the rejection efficiency of the optical system.

### Conclusions

From the experiments described, the following conclusions can be given. First, double resonance excitation followed by the observation of the fluorescence at a wavelength lower than either laser excitation wavelength provided excellent detection limits in a graphite tube atomizer, lower than the best atomic absorption values

by more than one order of magnitude. Second, the sensitivity of the double resonance scheme compared to that of single resonance excitation/direct line fluorescence was worse by about two orders of magnitude. Therefore, the single resonance excitation/direct line fluorescence scheme still remained the preferred excitation/detection scheme for lead. Third, the loss of sensitivity for the double resonance scheme reported in these experiments was partially attributed to the ionization losses occurring from the excited levels reached in the second excitation step. Such losses of atoms might be significant despite the short interaction time, about 12 ns, between the atoms and the laser pumping. Fourth, the efficiency of the optical system in rejecting unwanted scattered laser radiation into the fluorescence monochromator needs to be improved and/or high quality interference filters and cut-off filters have to be added. Fifth, lead was chosen because a comparison of these results could be made with those of Miziolek and Willis (86) and because the double resonance scheme could also be directly compared with the single resonance scheme. In this respect, however, lead was not a good choice, since its atomization temperature (about 1600°C) was still low enough to minimize furnace emission noise. As a result, the double resonance scheme with low ultraviolet fluorescence detection must be more rigorously tested with those elements requiring the furnace to be run at or above 2700°C.

## CHAPTER 5

### FINAL COMMENTS AND FUTURE WORK

The future of double resonance excitation is open for consideration. Certainly, there are many experiments to be performed. However, as to the immediate future with the techniques described in this dissertation, there are several experiments which should be performed.

Fluorescence dip spectroscopy needs to be continued for the calcium ion dip. This could be accomplished by increasing the laser irradiance from the dual dye lasers, thus improving the frequency conversion process necessary for the generation of these wavelengths (see Figure 3-32). After the evaluation of calcium, several more elements should be investigated (e.g., Pb, the rare earths) to provide further information on the high lying levels as well as applying the information for use in double resonance excitation/fluorescence or ionization schemes. Also it is desirable to determine the waveform of the dip, the pulse shape, and behavior and to evaluate any similarity to the results obtained for laser enhanced ionization.

There is no doubt that double resonance laser enhanced ionization is a very powerful technique for the measurement of trace elements. It is felt that further study needs to be performed on the ionization mechanism. This is evidenced by our present results.

This is not saying our results are the definitive answer, but more experiments must be considered and performed as suggested by Turk (69). These include the effect of low laser irradiances combined with low bias voltages (e.g., -100 VDC), the use of the fundamental wavelength (566.612 nm) of the frequency doubled dye laser as a photoionizing laser, and the use of the fundamental wavelength from the Nd:YAG laser (532 nm).

As for double resonance laser excited atomic fluorescence in a graphite tube atomizer, there are several modifications and experiments to be performed. The first of these, as previously mentioned, is reduction of laser scatter. This problem must be addressed and minimized through the use of baffling, colored glass filters, and/or liquid filters. Second, there should be replacement of the present furnace system with a commercially available unit because these have better control of temperature, higher temperature rates,  $dT/dt$ , and higher temperatures. They would improve the overall figures of merit for this technique. Third, further investigations for other elements (e.g., Cd, Tl, Ir, V, Fe, and Ga) are needed to ascertain the viability of this technique for ultra-trace analysis and femtogram detection limits. Both connected and disconnected levels should be investigated. Fourth, the coupling of laser enhanced ionization with graphite tube atomizers should further promote double resonance excitation schemes as versatile as well as sensitive. Lastly, the construction of clean room facilities such that the furnace system and any ancilliary items are enclosed to

prevent contamination from the environment. For example, lead is present in the air and thus causes contamination at ultratrace levels. The construction of clean room facilities could lead to the inevitable single atom detection.

# APPENDIX A GLOSSARY OF TERMS AND SYMBOLS

Here, it is designated that the lower level of the transition by the subscript l and the upper level by the subscript u.

$B_{lu}\rho(\nu_{lu})$  = radiatively induced absorption rate,  $s^{-1}$

$B_{ul}\rho(\nu_{ul})$  = radiatively induced emission rate,  $s^{-1}$

$B_{lu}(B_{ul})$  = Einstein coefficient for induced absorption (emission),  $m^3Hz/Js$

$g_l, g_u$  = statistical weights of the levels, dimensionless

$\rho(\nu_{lu})$  = spatially homogeneous, spectral energy density of the radiation field,  $J/m^3Hz$

$R_{lu}(R_{ul})$  = total rate of excitation (de-excitation) of the levels considered,  $s^{-1}$

$A_{ul}$  = Einstein coefficient for spontaneous emission,  $s^{-1}$

$k_{ul}$  = collisional de-excitation (quenching) rate coefficient,  $s^{-1}$

$Y_{ul}$  = quantum efficiency of the fluorescence process  $u \rightarrow l$ , dimensionless

$r_{lu} = B_{lu}\rho(\nu_{lu}), s^{-1}$

$R_{ul} = B_{ul}\rho(\nu_{ul}) + A_{ul} + k_{ul}, s^{-1}$

$R_{12} = B_{12}\rho(\nu_{12})$

$R_{21} = B_{21}\rho(\nu_{12}) + A_{21} + k_{21}$

$R_{32} = B_{32}\rho(\nu_{23}) + A_{32} + k_{32}$

$R_{23} = B_{23}\rho(\nu_{23})$

$$R_{31} = k_{31}$$

$$n_i(t) = \text{time dependent population of level } i \text{ when both} \\ \text{excitation transitions at } \nu_{12} \text{ and } \nu_{23} \text{ are present,} \\ m^{-3}$$

$$(n_i)^{ss} = \text{steady state population of level } i, m^{-3}$$

$$(n_i)_{sat}^{ss} = \text{saturated steady state population of level } i, m^{-3}$$

$$(n_2)_{off}^{ss} = \text{steady state population of level } 2, \text{ in absence of} \\ \text{excitation transition at } \nu_{23}, m^{-3}$$

$$\Delta' = \text{relative steady state resonance fluorescence dip,} \\ \text{dimensionless}$$

$$h = \text{Planck's constant, Js}$$

$$c = \text{velocity of light, m/s}$$

$$\nu(\nu_{lu}) = \text{central frequency of transition between levels } l \text{ and} \\ u, \text{ Hz}$$



APPENDIX B  
LIMITING CASES FROM FIGURE 2-4

In the absence of the second laser, i.e., when  $B_{23} \rho(\nu_{23}) = 0$ , the steady state population of level 2 reads

$$\left( \frac{n_2}{n_T} \right)_{\text{off}}^{\text{ss}} = \frac{B_{12} \rho(\nu_{12}) Z_3}{Z_3 [Z_2 + g B_{12} \rho(\nu_{12})]} .$$

If the first laser is able to saturate the transition between levels 1 and 2, i.e., if  $B_{12} \rho(\nu_{12})$  is much greater than  $Z_2$ , the maximum population of level 2 is given by

$$\left( \frac{n_2}{n_T} \right)_{\text{off}}^{\text{ss sat}} = \frac{g_2}{g_1 + g_2} .$$

If the second laser is present and is capable of saturating the transition between levels 2 and 3, i.e., when  $B_{23} \rho(\nu_{23})$  is much greater than  $Z_3$  and the first laser does not saturate the transition between levels 1 and 2, then the population of level 2 is

$$\left[ \frac{n_2}{n_T} \right]_{\text{on}}^{\text{ss}} = \frac{g' B_{12} \rho(\nu_{12})}{k_{31} + B_{12} \rho(\nu_{12}) + g' Z_2 + g g' B_{12} \rho(\nu_{12})}$$

When both lasers are saturating, the population of level 2 is

$$\left[ \frac{n_2}{n_T} \right]_{\text{on}}^{\text{ss sat}} = \frac{g_2}{g_1 + g_2 + g_3}$$

# APPENDIX C SAHA EQUATION

The degree of ionization of an element can be calculated from the Saha equation:

$$\frac{n_M^+}{n_M} = \frac{1}{n_e} \frac{(2 m_e kT)^{3/2}}{h^3} \frac{Q^+}{Q^0} \exp(-IP/kT)$$

where  $n_e$  is the electron density,  $m_e$  is the mass of the electron,  $k$  is Boltzmann's constant,  $T$  is the temperature of the plasma,  $h$  is Planck's constant,  $Q^+$  and  $Q^0$  are partition functions of the ion and neutral atom, and  $IP$  is the ionization potential of the element. Assuming local thermodynamic equilibrium (LTE),  $n_e = 1 \times 10^{21} \text{ m}^{-3}$  and  $T = 5000 \text{ K}$  and with the following values for  $m_e = 9.11 \times 10^{-31} \text{ kg}$ ,  $k = 1.38 \times 10^{-23} \text{ J/K}$ ,  $h = 6.626 \times 10^{-34} \text{ Js}$ ,  $IP (\text{Na}) = 8.22 \times 10^{-19} \text{ J}$ ,  $Q^+ = 1.0000$ , and  $Q^0 = 2.0472$  (63), the percentage of Na atoms existing as ions in the ICP is approximately 80%.

# REFERENCES

1. W.K. Bischel, B.E. Perry, and D.R. Crosley, Chem. Phys. Lett. 82, 85 (1981).
2. W.K. Bischel, B.E. Perry, and D.R. Crosley, Appl. Opt. 21, 1419 (1982).
3. J. Bokor, R.R. Freeman, J.C. White, and R.H. Storz, Phys. Rev. 24A, 612 (1981).
4. P. Brewer, N. van Veen, and R. Bersohn, Chem. Phys. Lett. 91, 126 (1982).
5. P. Brewer, P. Das, G. Ondrey, and R. Bersohn, J. Chem. Phys. 79, 720 (1983).
6. P. Das, G. Ondrey, N. van Veen, and R. Bersohn, J. Chem. Phys. 79, 724 (1983).
7. T.W. Hansch, S.A. Lee, R. Wallenstein, and C. Wieman, Phys. Rev. Lett. 34, 307 (1975).
8. M. Heaven, T.A. Miller, R.R. Freeman, J.C. White, and J. Bokor, Chem. Phys. Lett. 86, 458 (1982).
9. C.H. Muller, III, D.R. Eames, and D.H. Burrell, Bull. Amer. Phys. Soc. 26, 1031 (1981).
10. A.W. Miziolek and M.A. DeWilde, Opt. Lett. 9, 390 (1984).
11. R.P. Lucht, J.T. Salmon, G.B. King, D.W. Sweeney, and N.M. Laurendeau, Opt. Lett. 8, 365 (1983).
12. M. Alden, H. Edner, P. Grafstrom, and S. Svanberg, Opt. Commun. 42, 244 (1982).
13. C. Brechignac and Ph. Cahuzac, Opt. Commun. 43, 270 (1982).
14. H. Wakata, S. Saikan, and M. Kimura, Opt. Commun. 38, 271 (1981).
15. M.Y. Mirza and W.W. Duley, Opt. Commun. 25, 185 (1978).

16. M.Y. Mirza and W.W. Duley, Proc. R. Soc. Lond. 364A, 255 (1978).
17. M.Y. Mirza and W.W. Duley, Opt. Commun. 28, 179 (1979).
18. N.M. Shen and S.M. Curry, Opt. Commun. 20, 392 (1977).
19. R. Beigang and D. Schmidy, Phys. Lett. 87A, 21 (1981).
20. M. Alden, H.M. Hertz, S. Svanberg, and S. Wallin, Appl. Opt. 23, 3255 (1984).
21. S. Arepalli, N. Presser, D. Robie, and R.J. Gordon, Chem. Phys. Lett. 118, 88 (1985).
22. T.J. McIlrath, R. Hudson, A. Aikin, and T.D. Wilkerson, Appl. Opt. 18, 316 (1979).
23. J.J. Tiee, M.J. Ferris, G.W. Loge, and F.B. Wampler, Chem. Phys. Lett. 96, 422 (1983).
24. K. Scofield and M. Steinberg, Opt. Eng. 20, 501 (1981).
25. J.I. Steinfeld and P.L. Houston in "Laser and Coherence Spectroscopy," J.I. Steinfeld, Ed., Plenum Press, New York, (1978), Chapter 1.
26. D.J. Bradley, G.M. Gale, and P.D. Smith, J. Phys. B3, L11 (1970).
27. D.J. Bradley, P. Ewart, J.V. Nicholas, J.R.D. Shaw, and D.G. Thompson, Phys. Rev. Lett. 31, 263 (1973).
28. D.J. Bradley, P. Ewart, J.V. Nicholas, and J.R.D. Shaw, J. Phys. B6, 1594 (1973).
29. S. Haroche, M. Gross, and M.P. Silverman, Phys. Rev. Lett. 33, 1063 (1974).
30. H.T. Duong, S. Liberman, J. Pinaud, and J.-L. Vaille, Phys. Rev. Lett. 33, 339 (1974).
31. K. Takagi, R.F. Curl, Jr., and R.T.M. Su, Appl. Phys. 7, 181 (1975).
32. W. Gornik, D. Kaiser, W. Lange, J. Luther, H.-H. Radloff, and H.H. Schulz, Appl. Phys. 1, 285 (1973).
33. T.F. Gallagher, S.A. Edelstein, and R.M. Hill, Phys. Rev. A11, 1504 (1975).

34. T.F. Gallagher, S.A. Edelstein, and R.M. Hill, Phys. Rev. Lett. 35, 644 (1975).
35. T.W. Ducas, M.G. Littman, R.R. Freeman, and D. Kleppner, Phys. Rev. Lett. 35, 366 (1975).
36. W. Gornik, Z. Physik A283, 231 (1977).
37. R. Shuker, A. Ben-Amar, and G. Erez, Opt. Commun. 39, 51 (1981).
38. M.O. Rodgers, J.D. Bradshaw, K. Liu, and D.D. Davis, Opt. Lett. 7, 359 (1982).
39. N. Omenetto, B.W. Smith, L.P. Hart, P. Cavalli, and G. Rossi, Spectrochim. Acta 40B, 1411 (1985).
40. N. Omenetto, B.W. Smith, and L.P. Hart, Fresenius Z. Anal. Chem. 324, 683 (1986).
41. G.C. Turk, J.R. DeVoe, and J.C. Travis, Anal. Chem. 54, 643 (1982).
42. N. Omenetto, T. Berthoud, P. Cavalli, and G. Rossi, Appl. Spectrosc. 39, 500 (1985).
43. L.P. Hart, B.W. Smith, and N. Omenetto, Spectrochim. Acta 40B, 1637 (1985).
44. N. Omenetto, T. Berthoud, P. Cavalli, and G. Rossi, Anal. Chem. 57, 1256 (1985).
45. G.C. Turk, F.C. Ruegg, J.C. Travis, and J.R. DeVoe, Appl. Spectrosc. 40, 1146 (1986).
46. G.J. Havrilla and K.-J. Choi, Anal. Chem. 58, 3095 (1986).
47. B.W. Smith, L.P. Hart, and N. Omenetto, Anal. Chem. 58, 2147 (1986).
48. G.J. Havrilla and C.C. Carter, Appl. Opt. 26, 3510 (1987).
49. N. Omenetto, G.C. Turk, M.J. Rutledge, and J.D. Winefordner, Spectrochim. Acta 42B, 807 (1987).
50. M.J. Rutledge, Ph.D. Dissertation, University of Florida, Gainesville, FL (1987).
51. A. Montaser and V.A. Fassel, Anal. Chem. 48, 1490 (1976).

52. M.S. Epstein, S. Nikdel, J.D. Bradshaw, M.A. Kosinski, J.N. Bower, and J.D. Winefordner, *Anal. Chim. Acta* 113, 221 (1980).
53. D.R. Demers and C.D. Allemand, *Anal. Chem.* 53, 1915 (1981).
54. M.A. Kosinski, H. Uchida, and J.D. Winefordner, *Anal. Chem.* 55, 688 (1983).
55. H. Uchida, M.A. Kosinski, and J.D. Winefordner, *Spectrochim. Acta* 38B, 5 (1983).
56. S. Greenfield, "ICP-OES, HCL-ICP-AFS or AA?," Paper No. 345, Federation of Analytical Chemistry and Spectroscopy Societies, Philadelphia, PA (1982).
57. M.A. Kosinski, H. Uchida, and J.D. Winefordner, *Talanta* 30, 339 (1983).
58. N. Omenetto, H.G.C. Human, P. Cavalli, and G. Rossi, *Spectrochim. Acta* 39B, 115 (1984).
59. M.B. Leong, A.P. D'Silva, and V.A. Fassel, *Anal. Chem.* 58, 2594 (1986).
60. Fast Gated Integrators and Boxcar Averagers, Stanford Research Systems, Palo Alto, CA.
61. A. Lindgard and S.E. Nielsen, *Atomic Data and Nuclear Data Tables* 19, 533 (1977).
62. C.H. Corliss and W.R. Bozman, NBS Monograph 53 (1962).
63. L. deGalan, R. Smith, and J.D. Winefordner, *Spectrochim. Acta* 23B, 521 (1968).
64. D.J. Douglas and R.S. Houk, *Prog. Anal. At. Spectrosc.* 8, 8 (1985).
65. R.S. Houk, *Anal. Chem.* 58, 97A (1986).
66. L.M. Frazer and J.D. Winefordner, *Anal. Chem.* 44, 1444 (1972).
67. B.W. Smith, M.B. Blackburn, and J.D. Winefordner, *Can. J. Spectrosc.* 22, 57 (1977).
68. C.Th.J. Alkemade, T. Hollander, W. Snelleman, and P.J.Th. Zeegers, "Metal Vapours in Flames," Pergamon Press, New York (1982).
69. G.C. Turk, private communication (1987).

70. T. Berthoud, J. Lipinsky, P. Camus, and J.-L. Stehle, *Anal. Chem.* 55, 959 (1983).
71. M. Broglia, F. Catoni, and P. Zampetti, in P. Camus, Ed., "International Colloquium on Optogalvanic Spectroscopy and Its Applications," *J. de Physique* 44, Suppl. 11, C7-479 (1983).
72. B.V. L'vov, "Atomic Absorption Spectrochemical Analysis," Adam Hilger, London, England (1970).
73. R.E. Sturgeon, *Anal. Chem.* 49, 1255A (1977).
74. S.R. Koirtiyohann and M.L. Kaiser, *Anal. Chem.* 54, 1515A (1982).
75. B.V. L'vov, *Spectrochim. Acta* 33B, 153 (1978).
76. R.E. Sturgeon and C.L. Chakrabarti, *Anal. Chem.* 49, 90 (1977).
77. D.C. Gregoire and C.L. Chakrabarti, *Spectrochim. Acta* 37B, 11 (1982).
78. V.J. Zatzka, *Anal. Chem.* 50, 538 (1978).
79. G. Weibust, F.J. Langmyhr, and Y. Thomassen, *Anal. Chim. Acta* 128, 23 (1981).
80. G. Schlemmer and B. Welz, *Spectrochim. Acta* 41B, 1157 (1986).
81. S. Neumann and M. Kriese, *Spectrochim. Acta* 29B, 127 (1974).
82. M.A. Bolshov, A.V. Zybin, L.A. Zybina, V.G. Koloshnikov, and I.A. Majorov, *Spectrochim. Acta* 31B, 493 (1976).
83. J.P. Hohimer and P.J. Hargis, Jr., *Appl. Phys. Lett.* 30, 344 (1977).
84. M.A. Bolshov, A.V. Zybin, V.G. Koloshnikov, and M.V. Vasnetsov, *Spectrochim. Acta* 36B, 345 (1981).
85. M.A. Bolshov, A.V. Zybin, and I.I. Smirenkina, *Spectrochim. Acta* 36B, 1143 (1981).
86. A.W. Miziolek and R.J. Willis, *Opt. Lett.* 6, 528 (1981).
87. P.K. Wittman, Ph.D. Dissertation, University of Florida, Gainesville, FL (1982).
88. H.G.C. Human, N. Omenetto, P. Cavalli, and G. Rossi, *Spectrochim. Acta* 39B, 1345 (1984).

89. M.A. Bolshov, A.V. Zybin, V.G. Koloshnikov, I.A. Mayorov, and I.I. Smirenkina, *Spectrochim. Acta* 41B, 487 (1986).
90. K. Dittrich and H.-J. Stark, *J. Anal. Atom. Spectrom.* 1, 237 (1986).
91. D. Goforth and J.D. Winefordner, *Anal. Chem.* 58, 2598 (1986).
92. D. Goforth and J.D. Winefordner, *Talanta* 34, 290 (1987).
93. J.P. Dougherty, F.R. Preli, Jr., and R.G. Michel, *J. Anal. Atom. Spectrom.* 2, 429 (1987).
94. F.R. Preli, Jr., J.P. Dougherty, and R.G. Michel, *Anal. Chem.* 59, 1784 (1987).
95. K. Dittrich and H.-J. Stark, *J. Anal. Atom. Spectrom.* 2, 63 (1987).
96. N. Omenetto, P. Cavalli, M. Broglia, P. Qi, and G. Rossi, *J. Anal. Atom. Spectrom.* in press (1988).
97. R.D. Ediger, *At. Absorpt. Newslett.* 14, 127 (1975).
98. M.A. Bolshov, A.V. Zybin, V.G. Koloshnikov, A.V. Pisarskii, and A.N. Smirnov, *J. Appl. Spectrosc. USSR* 28, 31 (1978).
99. M.A. Bolshov, A.V. Zybin, and V.G. Koloshnikov, *Sov. J. Quantum Electron.* 10, 1042 (1980).
100. M.A. Bolshov, A.V. Zybin, L.N. Kolonina, I.A. Maiorov, I.I. Smirenkina, and O.A. Shiryayeva, *J. Anal. Chem. USSR* 39, 253 (1984).
101. M.A. Bolshov, A.V. Zybin, Yu.R. Kolomiiskii, V.G. Koloshnikov, Yu.M. Loginov, and I.I. Smirenkina, *J. Anal. Chem. USSR* 41, 313 (1986).
102. M.A. Bolshov, S.A. Dashin, A.V. Zybin, V.G. Koloshnikov, M.A. Maiorov, and I.I. Smirenkina, *J. Anal. Chem. USSR* 41, 1301 (1986).
103. C.J. Molnar, R.D. Reeves, J.D. Winefordner, M.T. Glenn, J.R. Ahlstrom, and J. Savory, *Appl. Spectrosc.* 26, 606 (1972).
104. D.E. Goforth, Ph.D. Dissertation, University of Florida, Gainesville, FL (1986).
105. N. Omenetto and J.D. Winefordner, *Appl. Spectrosc.* 26, 555 (1972).

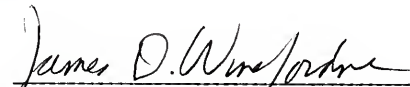


106. N. Omenetto and J.D. Winefordner, *Progress Anal. At. Spectrosc.* 1-2, 1 (1979).
107. W. Slavin, "Graphit Furnace AAS: A Source Book," The Perkin Elmer Corp., Norwalk, CT (1984).
108. J.C. Travis, G.C. Turk, J.R. DeVoe, P.K. Schenck, and C.A. van Dijk, *Progress Anal. At. Spectrosc.* 7, 199 (1984).
109. I. Magnusson, S. Sjoström, M. Lejon, and H. Rubinsztein-Dunlop, *Spectrochim. Acta* 42B, 713 (1987).
110. M.A. Bolshov, A.V. Zybin, V.G. Koloshnikov, and K.N. Koshelev, *Spectrochim. Acta* 32B, 279 (1977).


## BIOGRAPHICAL SKETCH

Moi Bon Leong was born in St. Louis, Missouri, on March 7, 1959. After learning that Tony Mellone was also born in the same city and was still living there, the Leong family moved to Brooklyn, New York, in 1961. There he attended and graduated elementary school (P.S. 48, 1970), junior high school (P.S. 227, 1973), and high school (New Utrecht, 1976) with a few honors which are too brief to mention. Pondering his future (well, not really), he decided to attend Pace University in Manhattan, New York (otherwise known as the city), in the fall of 1976. He graduated cum laude, but no one cared, in the summer of 1980. Faced with what to do, he made the big decision to leave home and attend graduate school at Iowa State University in Ames, Iowa, in 1980. After finishing a master's degree in 1984 with Dr. Velmar Fassel, but not graduating until 1985, he decided to come to Florida to thaw out and join Jim's group at the University of Florida in the fall of 1984. This is where he has spent the last three and one-half years of his life. He has had a great time here and would not trade it for anything in the world except fame and fortune, maybe just fortune.

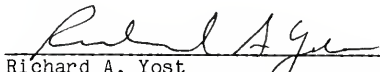
I certify that I have read this study and that in my opinion it conforms to acceptable standards of scholarly presentation and is fully adequate, in scope and quality, as a dissertation for the degree of Doctor of Philosophy.

  
James D. Winefordner, Chairman  
Graduate Research Professor of Chemistry

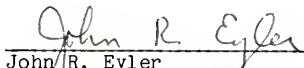
I certify that I have read this study and that in my opinion it conforms to acceptable standards of scholarly presentation and is fully adequate, in scope and quality, as a dissertation for the degree of Doctor of Philosophy.

  
John G. Dorsey  
Associate Professor of Chemistry

I certify that I have read this study and that in my opinion it conforms to acceptable standards of scholarly presentation and is fully adequate, in scope and quality, as a dissertation for the degree of Doctor of Philosophy.

  
Richard A. Yost  
Associate Professor of Chemistry

I certify that I have read this study and that in my opinion it conforms to acceptable standards of scholarly presentation and is fully adequate, in scope and quality, as a dissertation for the degree of Doctor of Philosophy.

  
John R. Eyler  
Professor of Chemistry

I certify that I have read this study and that in my opinion it conforms to acceptable standards of scholarly presentation and is fully adequate, in scope and quality, as a dissertation for the degree of Doctor of Philosophy.



---

Alex E. Green  
Graduate Research Professor of Nuclear  
Engineering Sciences

This dissertation was submitted to the Graduate Faculty of the Department of Chemistry in the College of Liberal Arts and Sciences and to the Graduate School and was accepted as partial fulfillment of the requirements for the degree of Doctor of Philosophy.

April, 1988

---

Dean, Graduate School

